UNIVERSITY OF BELGRADE
FACULTY OF MECHANICAL ENGINEERING

ABDULRAZAG ABDALLAH ELMILADI

STRESS ANALYSIS AND OPTIMIZATION OF LAMINATE LAYUP OF DEFINED COMPOSITE STRUCTURE GEOMETRY UNDER GIVEN LOADING CONDITIONS

DOCTORAL DISSERTATION

BELGRADE, 2021

УНИВЕРЗИТЕТ У БЕОГРАДУ
МАШИНСКИ ФАКУЛТЕТ

АБДУЛРАЗАГ АБДАЛАХ ЕЛМИЛАДИ

НАПОНСКА АНАЛИЗА И ОПТИМИЗАЦИЈА СЛАГАЊА ЛАМИНА КОМПОЗИТНЕ КОНСТРУКЦИЈЕ ДЕФИНИСАНЕ ГЕОМЕТРИЈЕ ЗА ЗАДАТЕ УСЛОВЕ ОПТЕРЕЋЕЊА

ДОКТОРСКА ДИСЕРТАЦИЈА

БЕОГРАД, 2021

SUPERVISOR:

Dr. Igor Balać, full time professor
University of Belgrade, Faculty of Mechanical Engineering
.....

BOARD OF COMMISSION:

Dr. Milorad Milovančević, full time professor
University of Belgrade, Faculty of Mechanical Engineering
.....

Dr. Aleksandar Grbović, full time professor
University of Belgrade, Faculty of Mechanical Engineering
.....

Dr. Nina Obradović, principal research fellow
Institute of Technical Sciences SASA
.....

DEDICATION

To my father's immaculate spirit, my mother, my wife, my daughters, son, to my brothers and sisters for their boundless support, and my teachers,
I dedicate this thesis

ACKNOWLEDGMENT

I would firstly to thank the God without whom nothing is possible.

I would like to express my sincere gratitude and fully thanks to my supervisor **Dr. Igor Balać**, full time professor for his offers continuous support to the thesis guides and revision of my research.

I would like to thank **Dr. Aleksandar Grbović**, full time professor for sharing his knowledge and experience.

I would also like to extend my gratitude to the staffs of Mechanical Engineering faculty and my friends whose help was very valuable in this research.

I would like to thank all those people who made this thesis possible.

Finally, my deep appreciation is addressed to whole my family my- mother, wife, daughters, and son for their patience and supporting me during the period of my study.

ABSTRACT

The main aim of this thesis is to obtain the methodology capable of optimizing the composite structure of defined geometry with defined laminate layup, under given loading conditions, where the goal is to achieve high levels of stiffness and strength and minimal weight. The composite structure of defined geometry is a tail boom (empennage) of a lightweight aircraft. The tail boom consists of different structural parts that are connected to the aircraft cabin. In order to achieve the desired requirements regarding stiffness, strength, and weight, the tail boom has been made from carbon fibre reinforced composite material.

Analytical and numerical methods have been used for estimating the strength and elastic constants of the carbon fibre /epoxy composite material. The analytical methods were mainly based on the Mechanics of material approach. At the same time well known Semi-Empirical models of Halpin-Tsai and Chamis, were also considered. Obtained results were compared to outcomes of finite element (FE) analysis.

After the estimation of the material properties, the typical layup configurations of the laminate composite structure were defined. A numerical FE model of tail boom has been made. All defined layup configurations were incorporated into tail boom structural parts and loaded by pre-defined aerodynamic loads. Coupling fluid/structure simulations have been used in this thesis for the accurate prediction of the external aerodynamic loads that act on composite tail boom structure. The one-way and two-way Fluid-Structure Interaction (FSI) simulations have been used for the evaluation of forces that act on tail boom composite structure. In order to obtain failure free laminate, the strength of each part of the tail boom structure has been checked by using the Tsai-Wu failure theory. The level of strength of each structural part of tail boom structure was estimated by a pre-defined parameter, called safety factor (*SF*) which was used as a key parameter in the optimization procedure. During the optimization procedure, design variables were: orientation angles, stacking sequences, lamina thickness, and the number of plies.

The influence of material low-level porosity on elastic properties of the matrix, used as fiber binder in carbon fibre composite material, has been studied through numerical analysis. In order to study the effect of micro-scale low-level porosity on the elastic properties of the matrix material, the FE analysis based on 3-D unit cell numerical model has been applied. The distribution of pores is idealized by new *multi pore unit cell* (MPUC) model. The comparison of the obtained values for the modulus of elasticity (E), shear modulus (G) and Poisson's ratio (ν_{12}), for different shapes, content, and size of the pores, with available experimental data published in the literature, has been performed. It was confirmed that material porosity, in form of closed pores, has a notable influence on the elastic properties of structural materials.

The effect of thermal load (extreme operating temperatures) on carbon fibre composite (CFC) structure, which results in thermal stresses, has been studied as well. The thermal stress analysis of CFC structure, exposed to different levels of low and high temperatures, has been performed. This analysis has been done using the FE method, where different temperature ranges between–50°C and +50 °C, have been applied. Obtained results showed that temperature load has a significant impact on the strength of composite structure.

Key words: Finite Element Analysis (FEA), Strength of Fiber Reinforced Composites, Failure Theory, Porosity of Structural Materials, Thermal Stresses.

UDK 66.018.9:539.216:519.6(043.3)

САЖЕТАК

Основни циљ ове дисертације је да се добије методологија која ће омогућити да се оптимизује композитна конструкција дефинисане геометрије са дефинисаним слагањем ламината, за задате услове оптерећења, где је циљ постизање високог нивоа крутости и чврстоће а минималне масе. Композитна конструкција дефинисане геометрије је репна део трупа лаког авиона. Репни део трупа се састоји од различитих конструктивних делова који су повезани са кабином авиона. Да би се постигли жељени захтеви у погледу крутости, чврстоће и тежине, репни део трупа је направљен од композитног материјала ојачаног угљеничним влакнима.

Аналитичке и нумеричке методе су коришћене за процену чврстоће и константи еластичности композитне ламине (угљенично влакно – епокси матрица). Аналитичке методе су се углавном заснивале на принципима Отпорности материјала. Истовремено, за процену константи еластичности разматрани су и добро познати полуемпиријски модели *Halpin-Tsai*-а и *Chamis*-а. Добијени резултати су упоређени са резултатима добијеним применом методе коначних елемената (МКЕ).

Након дефинисања карактеристика еластичности и чврстоће ламине, дефинисане су типичне конфигурације слагања ламината. Израђен је нумерички модел репног дела трупа. Све претходно дефинисане конфигурације слагања ламина у ламинат су додељене као материјал (угљенично влакно – епокси) од кога су направљени сви структурални делови репног дела трупа који је потом оптерећен унапред дефинисаним аеродинамичким оптерећењима. У овој дисертацији коришћене су симулације применом нумеричке анализе интеракције флуида и структуре - *спрегнуте анализе* (енг. *coupled analysis*), где се аеродинамичко оптерећење добијено коришћењем прорачунске динамике флуида (ПДФ) спреже са резултатима структурних анализа добијених применом МКЕ. Једносмерне и двосмерне спрегнуте анализе коришћене су за израчунавање аеродинамичких сила које делују на композитну конструкцију репног дела трупа. Чврстоћа сваког дела конструкције репног дела трупа, у смислу провере губитка носивости, проверена је коришћењем критеријума *Tsai-Wu*. Ниво чврстоће сваког конструктивног дела конструкције репног крака је процењен унапред дефинисаним параметром, названим фактор сигурности (*SF*) који је коришћен као кључни параметар у поступку оптимизације. Током поступка оптимизације, дизајнерске променљиве су биле: оријентацијски углови, начин слагања, дебљина ламине као и број слојева.

Нумеричким методама проучаван је утицај порозности ниског нивоа на карактеристике еластичности материјала матрице, која се користи као везиво угљеничних влакана у композитном материјалу. Нумеричка анализа заснована на примени МКЕ је примењена за проучавање утицаја структурне порозности ниског нивоа на карактеристике еластичности материјала матрице. Распоред пора је симулиран применом новог *multi-pore unit cell* (MPUC) 3-D нумеричког модела. Извршено је поређење добијених вредности за модул еластичности (E), модул смицања (G) и Поасонов однос (ν_{12}) за различите облике и различите запреминске уделе порозитета, са доступним експерименталним подацима, објављеним у доступној литератури. Потврђено је да порозност материјала, у облику затворених пора, има значајан утицај на карактеристике еластичности структуралних материјала.

Извршена је анализа утицаја температурског оптерећења на композитни материјал угљенично влакно / епокси, а која подразумева појаву тзв. „термичких напона“. Извршена је анализа термичког напрезања разматране композитне конструкције изложене различитим нивоима ниских и високих температура. Ова анализа је урађена применом МКЕ, при чему су примењени различити температурни распони између –50°C и +50°C. Добијени резултати показују да је утицај екстремних температура на чврстоћу композитне конструкције, знатан.

Кључне речи: метода коначних елемената (МКЕ), чврстоћа композитног материјала ојачаног влакнима, критеријуми губитка носивости, порозитет, термички напони.

УДК 66.018.9:539.216:519.6(043.3)

TABLE OF CONTENTS

LIST OF FIGURES:

LIST OF TABLES

CHAPTER ONE

1 Introduction and literature survey

1.1 Introduction

1.1.1 Background

Carbon fibre composite structures have been received much attention in recent decades because of their high strength/weight and stiffness/weight ratios. Therefore, the mechanical behaviour of composite structures has been studied intensively.

Composites provide enough flexibility to manufacture products with complex shapes. Due to these properties, they are capable of different applications such as aerospace, automobiles, wind turbine blades, constructions, electronics, and other industries. Laminated composites involve complex structures made of numerous layers, materials, thickness, and orientations. which provide many advantages such as: excellent mechanical properties, perfect damping properties, very good heat insulation, etc.. However, engineering challenge is to predict how the finished product will perform under real working conditions. This involves analysis of stresses and deformations as well as use of appropriate failure criteria.

Fibre reinforced composites consists of finite number of thin layers (laminas) which form a final structural form known as laminate. Each lamina in laminate has continuous fibres in different orientations in order to get the required strength and stiffness properties. Therefore, In Carbon Fibre/Epoxy composite materials, in aerospace industry, the orientation angles of laminas, needed for final laminate layup, are usually: $0^{\circ}, +45^{\circ}, -45^{\circ}$ and 90° [1].

1.1.2 Objectives of the research

This study aims to obtain the methodology capable of optimising composite structure of defined geometry with defined laminate layup, under given loading conditions, where the goal is to obtain a composite structure with high levels of stiffness and strength and minimal weight.

In this thesis, composite structure of defined geometry is an empennage for a lightweight aircraft. The empennage (Tail boom) consists of horizontal and vertical stabilizers and connecting boom. The structure has been made from Carbon Fibre/Epoxy composite material. Due to the complexity of empennage geometry, for designing and analyzing the structure of this model the Finite Element Method (FEM) has been used. In complex geometrical shapes, experimental methods involves many models to be tested under the destructive test. This methods cost a lot of time and money and should be minimized as much as possible. The analysis of complex structures could be quite demanding and difficult, so the use of FEM, in this cases, is proven to be very effective.

1.1.3 The influence of porosity on the elastic properties of composite materials

In the research presented in this thesis, the effect of void content on the elastic properties of fibre-reinforced composites (FRCs) was studied because void content influences the mechanical properties of the composite structure. The investigation of voids in composite materials started around half a century ago and is still progressive research field in the composites community. This is due to the still unknown influence of voids as well as difficulties in their control in modern manufacturing techniques like out-of-autoclave curing which are further complicated by using modified resins with high viscosity [2].

During the manufacturing process of fibre-reinforced composites (FRCs), defects or flaws can easily be introduced into the material, among which void is the most common one. Many factors lead to the formation of void among the curing pressure, resin system, orientation angles, environmental conditions, and so on, some of which are almost unavoidable. The existence of voids results in a reduction of the mechanical properties of carbon fibre reinforced materials, which have been the subject of many researchers for several decades [3].

However different defect types that can be identified during the manufacturing of FRCs. The void is the most important manufacturing defect since many of the other defects occur more rarely compared to void formation [4]. Porosities or voids are the most studied type of manufacturing defect, very often formed in the processing of fibre-reinforced composites. Due to their large influence on the physical and thermo-mechanical properties of composites, they have been widely studied, with the focus on three study paths: void formation, characteristics, and mechanical effects. Therefore, as many scientific studies reveal, it is critical to establish the acceptable level of voids in designing FRCs structures because of their detrimental effects on the mechanical performance of FRCs products [5]. The effect of voids on mechanical properties can be summarized as follows [6]:

1. Influences the inter-laminar shear strength.
2. Reduces tensile properties.
3. Causes a reduction of shear resistance.
4. Causes transverse cracking.
5. Reduces fatigue resistance.
6. Causes a reduction in impact resistance.
7. Causes a reduction of inter-laminar fracture toughness.

1.1.4 The fibre-reinforced composite material forms

The basic building block of fiber reinforced composites is lamina. The lamina is made of continuous fibers and matrix which binds fibers together as shown in Figure 1.1. Typical forms of FRCs are:

1. Unidimensional: unidirectional tows, yarns, or tapes.
2. Bidimensional: woven or non-woven fabrics (felts or mats).
3. Tridimensional: fabrics (sometimes called multidimensional fabrics with fibres oriented along with several directions (more than two).

For a single lamina, as it is shown in Figure 1.1, axes in the 1–2 coordinate system are called the local axes or principal material axes. The direction 1 is parallel to the fibers and the direction 2 is perpendicular to the fibers. Sometimes, direction 1 is called longitudinal while direction 2 is called transverse direction. Lamina stiffness and strength properties in the transverse direction (direction 2) are usually much lower than stiffness and strength properties in the longitudinal direction (direction 1).

Woven Fabrics: in this type, the fabrics are made of fibres oriented along with two perpendicular directions, the first one being known as the warp - direction 1 and the other being known as the fill (or the weft) direction - direction 2, as shown in Figure 1.2.

Figure 1.3a, shows a plain weave where each fill goes over a warp yarn then under a warp yarn and so on. In Figure 1.4b, each filling yarn goes over the fourth warp yarns before it continues under the fifth one. For this reason, it is called a 5-harness sat. In addition, Figure 1.5c shows a twill weave.

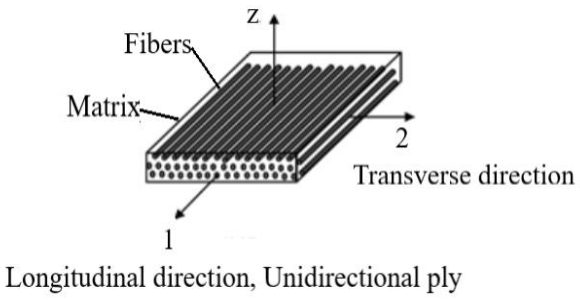

Figure 1.1: The Directions of Unidirectional Ply

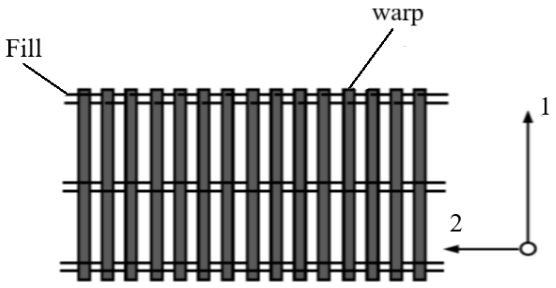

Figure 1.2: The Orientations in Composite Layers

Lamina stiffness in direction 1, obtained by a woven fabric is less than stiffness of unidirectional ply. This is because of the curvature of warp fibres, which is inevitable in these type of composites. This curvature makes the woven fabric more deformable than the two cross plies when subjected to the same loading, as shown in Figure 1.4. The unidirectional plies are held together by polymer matrix.

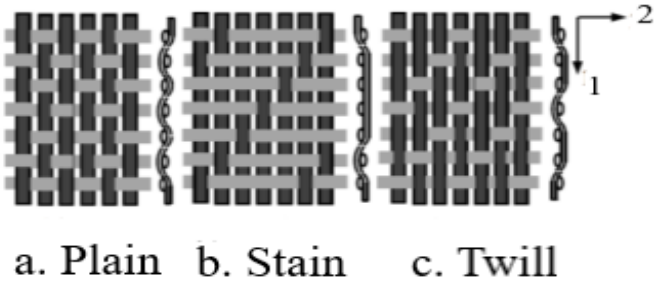

Figure 1.3: Forms of woven fabrics [1]

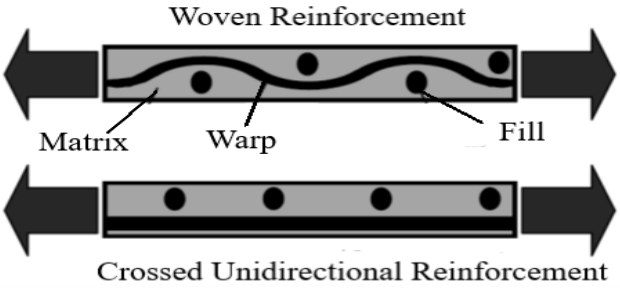

Figure 1.4: Cross-section of a layer with fibers crossed at 90° [1]

1.1.5 Mechanical properties of Carbon fibre/Epoxy composite material

As it is well known, when properly selected, composite materials offer several advantages over conventional structural materials (e.g. metals). Therefore, proper selection of fiber and proper selection of matrix in fiber reinforced composite material is very important issue. The selection is directly dependent on the type of application. In this study, materials which have been selected and used in the following analysis are carbon fibre (3K E13 (EPO3)) and Epoxy resin (MGS LR 285). Their mechanical properties are presented in Table 1.1 [7].

Table 1.1: Mechanical properties of Carbon fibre/Epoxy composite material used in the study

Description	Fibre	Epoxy	Units
Density (ρ)	1770	1200	kg/m^3
Young's Modulus E_1	2.37E+05	3E+03	MPa
Young's Modulus E_2	2.3E+04	3E+03	MPa
Shear Modulus G_{12}	9.875E+4	1.09E+3	MPa
Poisons Ratio (v)	0.2	0.38	
Ultimate Tensile Stress	4205	80	MPa
Ultimate Compressive Stress	4205	140	MPa
Ultimate Shear Strength	145	70	MPa

1.1.6 Thermal stresses

In laminated composite structures, during process of manufacturing, thermal loads are introduced when the composite is cooling down from processing temperatures. Stresses generated as a result of curing, during the manufacturing process, are called residual stresses. The mismatch of thermal expansion coefficients in different directions is the main cause of residual stresses that arise after the manufacturing process is finished [8].

The second source of thermal loads appears to be the environment (extreme operating temperatures) resulting in the appearance of thermal stresses. A typical example is an aircraft exposed to extremely low temperatures while flying at high altitudes. These conditions contribute to reducing composite structure strength by the fact that additional thermal stresses can significantly decrease the estimated composite structure strength, which is usually determined by the test data obtained by standard laboratory tests on the temperature of 23°C. Since operating temperatures can be quite different from standard laboratory tests temperature, it is clear that thermal stresses should not be neglected and must be involved in the composite structure design.

Several researchers investigated this phenomenon in several papers. Studies about the influence of the temperature generally can be divided into two groups. In the first group, the authors investigated thermally induced stresses on a micro-level scale, where they are generated locally in the vicinity of the contact surface of fibre and matrix due to the difference in the coefficient of thermal expansion between matrix and fibre [9]. The other group of authors was focused on a macro-level scale, where the mismatch of the coefficient of thermal expansion in different directions generates thermal stresses within a composite [10] [11] [12] [13].

1.1.7 Optimization methods

Optimization methods utilized in the variable stiffness design of composite materials are graded as follows:

1. If applicable, the optimality criterion methods and topology optimization with a local update rule are the best candidates for variable stiffness designs. These methods break down the complex design problem into a set of simple local problems with a simple updating rule.
2. When such optimality criteria cannot be easily established, multi-level optimization methods can be used. These methods decompose the original problem into several sub-problems, each with a smaller number of design variables. The possibility of such decomposition is the major concern when these methods are used. However, design problems of composite materials have been demonstrated to provide a good possibility for such decompositions in different situations.

In problems, where the optimality criterion and multi-level method cannot be used, depending on the availability of gradients, a genetic algorithm or gradient-based method or the combination of these two methods are recommended [14].

1.1.8 Coupling fluid/structure simulations

Coupling fluid/structure simulations are used in this thesis for the accurate prediction of the aerodynamic loads of the carbon fibre composite structure - tail boom. The aerodynamic loads acting on the tail boom result in deformations of its flexible structure, which in turn causes changes in the fluid flow, and thus the loads itself [15]. The aerodynamic loads are usually calculated using a Computational Fluid Dynamics approach (CFD) implemented in some FEM software. The structural responses of the model are determined by using Finite Element Analysis (FEA). To determine the dynamic characteristics of the tail boom, a steady-state computational fluid dynamics simulation must be carried out first, in order to determine the fluid pressure on the tail boom. This is used as a load or boundary condition for the simulation of configuration deformation. This approach is called a one-way coupled simulation, since no deflection is fed back into CFD. To determine the influence of the deformed tail on the aerodynamic performance, the deformations has to be brought back into the CFD solution, so that an improved solution can be found and the loop can be closed. This approach is called two-way coupled Fluid-Structure Interaction (FSI) simulation or multi-field simulation [16], [17], [18] which is used in this thesis.

1.1.9 Initial hypotheses of the thesis

The initial hypotheses of the thesis are as follows:

1. The starting hypothesis is that the Tsai-Wu failure criteria can be used for the calculation of fiber reinforced composite structure strength. This hypothesis is acceptable by the fact that the Tsai-Wu failure criterion is confirmed by a huge number of experiments.
2. FEM can be used to accurately calculate stresses in each lamina for the given loading conditions. This hypothesis is acceptable by the fact that in the past few decades FEM has been established as a numerical method that can be used as a tool for quite accurate predictions of stresses and strains in different composite structures under given loading conditions.

1.2 The structure of the thesis

The thesis is organized into seven main chapters, which are summarized below:

Chapter one consists of basic information of carbon fibre reinforced composite materials and literature survey, which covers the existing work in the area of fibre reinforced composite structure design regarding the strength and stiffness. In this chapter ingridients of composite material that is used for analysis will be defined (which fiber, which matrix, volume fraction etc.).

Chapter two describes analytical and numerical (based on FEM) methods which are used for strength and stiffness calculations of single lamina as well as for whole laminate. The use of Tsai-Hill and Tsai-Wu failure criteria are presented. Following this, the steps of analyzing a laminated composite under the applied forces and moments, as well as temperature load, are described. Finally at the end of the chapter, for adopted lamina, made from carbon fiber and epoxy matrix, estimated values of strength and elastic constants for principal material directions are obtained.

In **Chapter three** carbon fiber reinforced composite tail boom numerical model is defined. Evaluation of aerodynamical loads acting on the tail boom structure is performed through coupled FSI analysis. At the end of the chapter, the influence of structural porosity on the elastic properties of composite materials is analyzed.

Chapter four brings numerical methods, which are used for the optimisation of fibre reinforced composite parts of the tail boom. For defined aerodynamical loads of the tail boom structure, stresses of outer skin and stiffeners (main frame, formers, and stringers), having ten differently oriented symmetrical layers of carbon fiber reinforced matrix (epoxy), is analyzed by FEM. After optimization procedure (defined in chapter two), new laminate layup for each structural part of the tail boom with defined thickness, is introduced.

In **Chapter five** analytical and finite element methods are used for studying the effect of external applied temperature loads on the strength of laminated carbon-epoxy fiber composite structure. The evaluation of strength of final laminate configurations under combined external loads (aerodynamical and temperature loads) and comparison to the previous load case is given.

The tail boom manufacturing steps has been presented in **Chapter six**.

Chapter seven concludes the thesis with conclusions, and some recommendations for future research.

1.3 Literature survey

Number of publications have been studied different problems related to the carbon fibre composite materials and structures, as well as defining aerodynamic loads acting on aircraft structures.

In Ref. [19] an analytical and numerical evaluation of elastic models for composite structures has been studied. Elastic properties like Young's modulus (E_1 and E_2), Poisson's ratio (v_{12} and v_{21}), and In-plain shear modulus (G_{12}) for different volume fractions are evaluated using FEM. These investigated results were compared with the results obtained by analytical methods like the rule of mixture, Halpin-Tsai, Nielsen, and Chamis. The main goal of this paper is to compare analytical results with numerical results of elastic properties.

In Ref. [20], and [21] the mechanical properties of fibre-reinforced composites using FEM were investigated. The micromechanical analysis has been considered an important method in the investigations of composite material properties. This study focused on the determination of the properties of fibre-reinforced composite materials with different volume fractions under different

loading conditions. The estimation of engineering constants, such as the longitudinal Young's module (E_1), the transversal Young's module (E_2), the minor Poisson's ratio (v_{21}), have been done by using the numerical method and the micromechanical analysis. Thus, this work was useful for predicting the engineering constants in composites subjected to longitudinal and transverse loading by adopting the finite element method and micromechanics approach.

In Ref. [22], the optimization of automotive fibre composite material for driveshaft has been studied. The main target was decreasing the weight of a drive shaft in order to reduce the weight of vehicle. The replacement of composite structures for traditional metal structures has many advantages due to the higher specific stiffness and strength of composite materials. This study includes the analysis, carried out on the driveshaft, with different composite materials and concludes that the use of fibre composite materials are suited for a long driveshafts.

In Ref. [23], [24] and [25] an optimization procedure of variable stiffness composites is discussed. Improving structural performance can be achieved by adjusting the material properties in directions that are more convenient for carrying loads. The magnitude of a defective zone is usually controlled by two sets of parameters: design parameters and manufacturing parameters. These papers have investigated how the parameters, governing the defect formation, affect the set of optimal solutions for the problem of multiple optimisations, where at the same time the in-plane stiffness and load are increased.

In ref. [26], the authors have done an optimal design of fighter aircraft wing panels laminates under the Multi-Load case environment by Ply-Drop and Ply-Migrations. In this paper, the authors aimed to achieve the minimum weight of wing panels laminates. Ply drop (PD) operation in the study followed by ply-migrations (PM). The ply migration is required for ply-continuity and achieving a smooth external aerodynamic surface. The laminate weight minimization has been achieved as a target of multi-objective optimization (MOO), by applying excess design margins of Tasi-Wu first ply failure-index and wingtip side deflection. The optimization method was automated, which makes PD practically possible in the design stage.

In Ref. [27], the optimisation of a laminate composite plate was done for maximum safety factor using Tsai-Wu criteria for the optimization process and the authors have chosen fibre orientation angles and stacking sequence as design variables.

In Ref. [28], an optimization method to reduce thickness (or weight) of layered composite plates exposed to in-plane loading have been proposed. It has been stated that in general, the using of only two distinct fiber angles is enough to get the best possible design. For some other loading conditions, different stacking sequences with the same objective function value have been obtained with a big number of distinct fiber angles. They have concluded that, superior designs have been obtained by using three or four distinct angles, which have the similar thickness but a high safety factor.

In Ref. [29], [30],[31] A potential of FSI analysis of an aircraft wing at subsonic speeds has been studied. As stated, the interaction between a semi-rigid structure and the surrounding fluid environment is a serious problem within the evaluation of aircraft wing stability and the design of turbo machinery. The partially coupled analysis is figured out with the help of a FEM at different speeds in the subsonic Mach number range.

In Ref. [32] The authors have developed a Two-way fluid-structure coupling for studying power transformers, subjected to internal dynamic overpressures. At the same time, this paper highlights the quality of FSI simulation tools that can be improved by further research such as a precise damping characteristic consistent with the existence of fluid in a structure.

CHAPTER TWO

2 Strength and stiffness of laminate

Lamina is basic building block of fiber reinforced composite material. A typical lamina is a thin layer of composite material that is generally have thickness on the order of 0.125 mm. As mentioned before, typical composite structural part has a finite number of layers (laminas) forming a final structural form known as laminate. A laminate is constructed by stacking a finite number of such single lamina in the direction of the laminate thickness [33].

Failure of a structural component usually is defined as the inability of the component to carry load. Failure of fiber-reinforced composite materials is a complex and important topic. For polymer-matrix composites reinforced with unidirectional fibers, the fiber direction is much stronger than the other directions [34]. At the other hand, for laminate composite structure, the strength is related to the strength of individual lamina in laminate. Therefore, demand of safe design of fibre reinforced composite structures, initiated development of appropriate failure theory. All available failure theories were more or less verified by experiments. In mechanics of composite materials, the most widely used failure theories are: Tsai-Hill and Tsai-Wu failure theories. Both failure theories show a very good agreement with experimental results [35].

In mechanics of composite materials, methods that have been used for strength and stiffness calculations of fiber reinforced composite parts can be divided into analytical and numerical methods. In case of complex geometry shapes, the use of the finite element method is strikingly dominant.

2.1 Analytical method

For a simple geometrical shapes such as composite plates and beams, analytical methods defined in any book from Mechanics of composite materials can be successfully used for strength and stiffness analysis.

2.1.1 Lamina stress-strain relationship (Hook's law)

According to the Theory of elasticity, if a plate is thin and there are no out-of-plane loads, it can be considered to be under plane stresses. In this case, assuming that plate is positioned in plane 1-2, the stresses in direction 3, as shown in Figure 2.1, are equal to zero: $\sigma_3 = 0, \tau_{31} = 0$ and $\tau_{23} = 0$. The fact that lamina can be considered as very thin plate leads to an assumption that it is under plane stresses if there are no out-of-plane loads acting on it. [35].

As mentioned before, lamina stiffness and strength properties in the transverse direction (direction 2) are lower than stiffness and strength properties in the longitudinal direction (direction 1). Therefore, loads should be acting along direction of fibre. However, in some load cases lamina must be placed in such position when loads is acting at an angle to principal material directions 1 and 2 - Figure 2.1. The coordinate system used for showing so-called angle lamina is as given in Figure 2.2. The direction 1 is parallel to the fibres and the direction 2 is perpendicular to the fibres, while direction 3 is normal to 1-2 plane. The axes in the X-Y coordinate system are called the global axes or the off-axes. The angle between the local and global axes is denoted by an angle θ. The stress-strain Equations for the X-Y coordinate system, 1-2 coordinate system and the global and local stresses in an angle lamina are related as follows [35]. The global stresses $(\sigma_x, \sigma_y, \tau_{xy})$ and local stresses $(\sigma_1, \sigma_2, \tau_{12})$ in an angle lamina are related to each other through the transformation matrix $[T]$:

$$\begin{bmatrix}\sigma_1\\ \sigma_2\\ \tau_{12}\end{bmatrix} = [T]\begin{bmatrix}\sigma_x\\ \sigma_y\\ \tau_{xy}\end{bmatrix}, \tag{2.1}$$

$$\begin{bmatrix}\sigma_x\\ \sigma_y\\ \tau_{xy}\end{bmatrix} = [T]^{-1}\begin{bmatrix}\sigma_1\\ \sigma_2\\ \tau_{12}\end{bmatrix}. \tag{2.2}$$

where transformation matrix $[T]$ and inverted transformation matrix $[T]^{-1}$ are defined as:

$$[T] = \begin{bmatrix} c^2 & s^2 & 2sc \\ s^2 & c^2 & -2sc \\ -sc & sc & c^2 - s^2 \end{bmatrix}, \qquad [T]^{-1} = \begin{bmatrix} c^2 & s^2 & -2sc \\ s^2 & c^2 & 2sc \\ sc & -sc & c^2 - s^2 \end{bmatrix},$$

where: $c = \cos(\theta), s = \sin(\theta)$ (angle (θ) is the ply angle degree between the local and global axis).

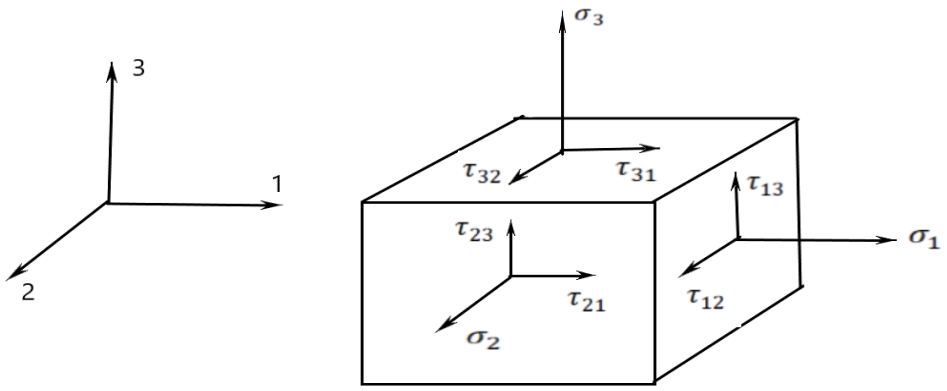

Figure 2.1: Stresses at some point in stressed body in orthogonal coordinate system 1-2-3.

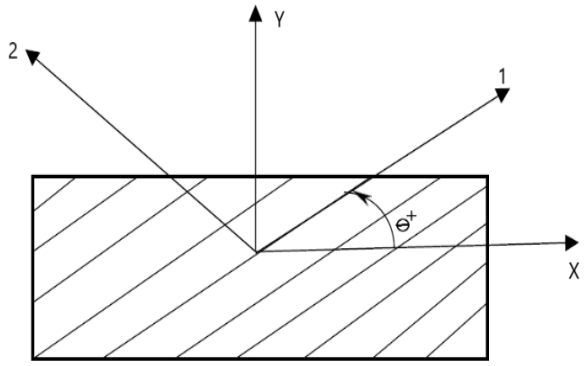

Figure 2.2: The global (X-Y) and local (1-2) coordinate systems of a lamina

In Equations (2.1), σ_1 and σ_2 are local normal stresses in directions 1 and 2, τ_{12} is shear stress in plane 1-2, while σ_x, and σ_y are global normal stresses in directions X and Y, τ_{xy} is shear stress in plane X-Y. In the same manner, the global strains $(\varepsilon_x\,, \varepsilon_y\,, \gamma_{xy})$ and local strains $(\varepsilon_1\,, \varepsilon_2\,, \gamma_{12})$ in an angle lamina are related to each other through the transformation matrix $[T]$:

$$\begin{bmatrix} \varepsilon_1 \\ \varepsilon_2 \\ \dfrac{\gamma_{12}}{2} \end{bmatrix} = [T] \begin{bmatrix} \varepsilon_x \\ \varepsilon_y \\ \dfrac{\gamma_{xy}}{2} \end{bmatrix}, \qquad \begin{bmatrix} \varepsilon_x \\ \varepsilon_y \\ \dfrac{\gamma_{xy}}{2} \end{bmatrix} = [T]^{-1} \begin{bmatrix} \varepsilon_1 \\ \varepsilon_2 \\ \dfrac{\gamma_{12}}{2} \end{bmatrix}, \tag{2.3}$$

where: ε_1 and ε_2 are local normal strains in directions 1 and 2, γ_{12} is the shear strain in plane 1-2, while ε_x and ε_y are global normal strains in directions X and Y and γ_{xy} is the shear strain in plane X-Y. According to Hook's law global strains can be expressed in terms of global stresses as:

$$\begin{bmatrix} \varepsilon_x \\ \varepsilon_y \\ \gamma_{xy} \end{bmatrix} = [\bar{S}] \begin{bmatrix} \sigma_x \\ \sigma_y \\ \tau_{xy} \end{bmatrix} = \begin{bmatrix} \bar{S}_{11} & \bar{S}_{12} & \bar{S}_{16} \\ \bar{S}_{12} & \bar{S}_{22} & \bar{S}_{26} \\ \bar{S}_{16} & \bar{S}_{26} & \bar{S}_{66} \end{bmatrix} \begin{bmatrix} \sigma_x \\ \sigma_y \\ \tau_{xy} \end{bmatrix}, \tag{2.4}$$

where matrix $[\bar{S}]$ is called transformed reduced compliance matrix:

$$[\bar{S}] = \begin{bmatrix} \bar{S}_{11} & \bar{S}_{12} & \bar{S}_{16} \\ \bar{S}_{12} & \bar{S}_{22} & \bar{S}_{26} \\ \bar{S}_{16} & \bar{S}_{26} & \bar{S}_{66} \end{bmatrix}. \tag{2.5}$$

Elements of the transformed reduced compliance matrix $\bar{S}_{ij}$ are given by [35]:

$$\begin{aligned}
\bar{S}_{11} &= S_{11}c^4 + (2S_{12} + S_{66})s^2c^2 + S_{22}s^4, \\
\bar{S}_{22} &= S_{11}s^4 + (2S_{12} + S_{66})s^2c^2 + S_{22}\,c^4, \\
\bar{S}_{16} &= (2S_{11} - 2S_{12} - S_{66})sc^3 - (2S_{22} - 2S_{12} - S_{66})s^3c, \\
\bar{S}_{26} &= (2S_{11} - 2S_{12} - S_{66})s^3c - (2S_{22} - 2S_{12} - S_{66})sc^3, \\
\bar{S}_{66} &= 2(2S_{11} + 2S_{22} - 4S_{12} - S_{66})s^2c^2 + S_{66}(s^4 + c^4)\,,
\end{aligned}$$

where the compliances S_{ij} and the engineering constants are related by the following relations:

$$S_{11} = \frac{1}{E_1}\,,\ S_{12} = -\frac{v_{12}}{E_1}\,,\ S_{22} = \frac{1}{E_2}\,,\ S_{66} = \frac{1}{G_{12}}.$$

In previous relations, the engineering constants are defined as follows:

$E_1 =$ The modulus of elasticity in direction 1,
$E_2 =$ The modulus of elasticity in direction 2,
$v_{12} =$ The major Poissons ratio,
$G_{12} =$ The shear modulus in plane $1-2$.

Thus, the stresses and strains in Equation (2.4) are related through the following four independent engineering constants: E_1, E_2, v_{12}, G_{12}.

By inverting transformed reduced compliance matrix in Equation (2.4) we define transformed reduced stiffness matrix $[\bar{Q}]$:

$$[\bar{Q}] = [\bar{S}]^{-1} .$$

Elements of transformed reduced stiffness matrix $[\bar{Q}]$ are given by:

$$[\bar{Q}] = \begin{bmatrix} \bar{Q}_{11} & \bar{Q}_{12} & \bar{Q}_{16} \\ \bar{Q}_{12} & \bar{Q}_{22} & \bar{Q}_{26} \\ \bar{Q}_{16} & \bar{Q}_{26} & \bar{Q}_{66} \end{bmatrix} , \tag{2.6}$$

where the transformed reduced stiffnesses $\bar{Q}_{ij}$ and the engineering constants are related by the following relations:

$$\begin{aligned}
\bar{Q}_{11} &= Q_{11}c^4 + 2(Q_{12} + 2Q_{66})s^2c^2 + Q_{22}s^4 , \\
\bar{Q}_{12} &= \bar{Q}_{21} = (Q_{11} + Q_{22} - 4Q_{66})s^2c^2 + Q_{12}(s^4 + c^4) , \\
\bar{Q}_{22} &= Q_{11}s^4 + 2(Q_{12} + 2Q_{66})s^2c^2 + Q_{22}c^4 , \\
\bar{Q}_{16} &= \bar{Q}_{61} = (Q_{11} - Q_{12} - 2Q_{66})sc^3 - (Q_{22} - Q_{12} - 2Q_{66})s^3c , \\
\bar{Q}_{26} &= \bar{Q}_{62} = (Q_{11} - Q_{12} - 2Q_{66})s^3c - (Q_{22} - Q_{12} - 2Q_{66})sc^3 , \\
\bar{Q}_{66} &= (Q_{11} + Q_{22} - 2Q_{12} - 2Q_{66})s^2c^2 + Q_{66}(s^4 + c^4) ,
\end{aligned}$$

where:

$$Q_{11} = \frac{E_1}{1 - \nu_{12}\nu_{21}} , \qquad Q_{22} = \frac{E_2}{1 - \nu_{12}\nu_{21}} ,$$

$$Q_{12} = \frac{\nu_{21}E_1}{1 - \nu_{12}\nu_{21}} = \frac{\nu_{12}E_2}{1 - \nu_{12}\nu_{21}} , \qquad Q_{66} = G_{12} .$$

Now global stresses in terms of global strains can be expressed through relationship, known as Hook's law for a generally orthotropic lamina, as following matrix Equation:

$$\begin{bmatrix} \sigma_x \\ \sigma_y \\ \tau_{xy} \end{bmatrix} = \begin{bmatrix} \bar{Q}_{11} & \bar{Q}_{12} & \bar{Q}_{16} \\ \bar{Q}_{12} & \bar{Q}_{22} & \bar{Q}_{26} \\ \bar{Q}_{16} & \bar{Q}_{26} & \bar{Q}_{66} \end{bmatrix} \begin{bmatrix} \varepsilon_x \\ \varepsilon_y \\ \gamma_{xy} \end{bmatrix} . \tag{2.7}$$

2.1.2 Analysis of a Laminate

In mechanics of composite materials a laminate is considered as a thin plate made of layers (laminas) having different orientations. Principles of Classical Lamination Theory (CLT) is used to develop relationships for a plate under in-plane loads, such as shear and axial forces, and bending and twisting moments - Figure 2.3.

If the global strains in k^{th} lamina are known the global stresses at any point along with the thickness of the k^{th} lamina (Figure 2.4), can be calculated from Equation (2.7):

$$\begin{bmatrix}\sigma_x\\ \sigma_y\\ \tau_{xy}\end{bmatrix}_k = \begin{bmatrix}\bar{Q}_{11} & \bar{Q}_{12} & \bar{Q}_{16}\\ \bar{Q}_{12} & \bar{Q}_{22} & \bar{Q}_{26}\\ \bar{Q}_{16} & \bar{Q}_{26} & \bar{Q}_{66}\end{bmatrix}_k \begin{bmatrix}\varepsilon_x\\ \varepsilon_y\\ \gamma_{xy}\end{bmatrix}_k . \tag{2.8}$$

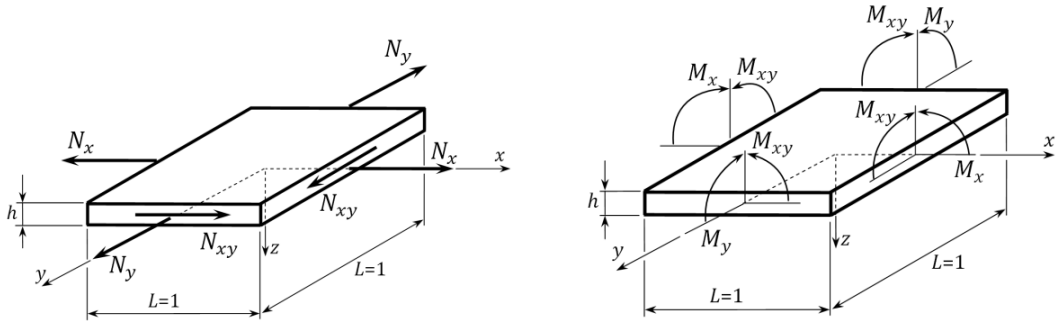

(a) (b)

Figure 2.3: Forces and moments acting on a laminate cross sections.

The basic hypothesis in CLT is Kirchhof hypothesis, which states that a straight line that is initially perpendicular to the midplane of the plate remains straight and perpendicular to the midplane of the plate after deformation. According to Kirchhof's hypothesis, the following expressions for the global strains induced at any point positioned at distance z from laminate middle surface can be easily obtained:

$$\begin{bmatrix}\varepsilon_x\\ \varepsilon_y\\ \gamma_{xy}\end{bmatrix} = \begin{bmatrix}\varepsilon_x^0\\ \varepsilon_y^0\\ \gamma_{xy}^0\end{bmatrix} + z\begin{bmatrix}k_x\\ k_y\\ k_{xy}\end{bmatrix} , \tag{2.9}$$

where: $\varepsilon_x^0, \varepsilon_y^0$ are global normal strains while γ_{xy}^0 is the in-plane shear strain at the middle surface (mid-plane) of the laminate (at z = 0). Curvatures k_x and k_y are mid-plane curvatures along the X and Y axis and k_{xy} is twisting curvature of mid-plane laying in the X-Y plane.

According to Equation (2.9) Equation (2.8) becomes:

$$\begin{bmatrix}\sigma_x\\ \sigma_y\\ \tau_{xy}\end{bmatrix}_k = \begin{bmatrix}\bar{Q}_{11} & \bar{Q}_{12} & \bar{Q}_{16}\\ \bar{Q}_{21} & \bar{Q}_{22} & \bar{Q}_{26}\\ \bar{Q}_{61} & \bar{Q}_{62} & \bar{Q}_{66}\end{bmatrix}_k \begin{bmatrix}\varepsilon_x^0\\ \varepsilon_y^0\\ \gamma_{xy}^0\end{bmatrix} + z\begin{bmatrix}\bar{Q}_{11} & \bar{Q}_{12} & \bar{Q}_{16}\\ \bar{Q}_{21} & \bar{Q}_{22} & \bar{Q}_{26}\\ \bar{Q}_{61} & \bar{Q}_{62} & \bar{Q}_{66}\end{bmatrix}_k \begin{bmatrix}k_x\\ k_y\\ k_{xy}\end{bmatrix} , \tag{2.10}$$

where coordinate z for k^{th} lamina is in range: $z_{k-1} \le z \le z_k$ (k=1,...,N).

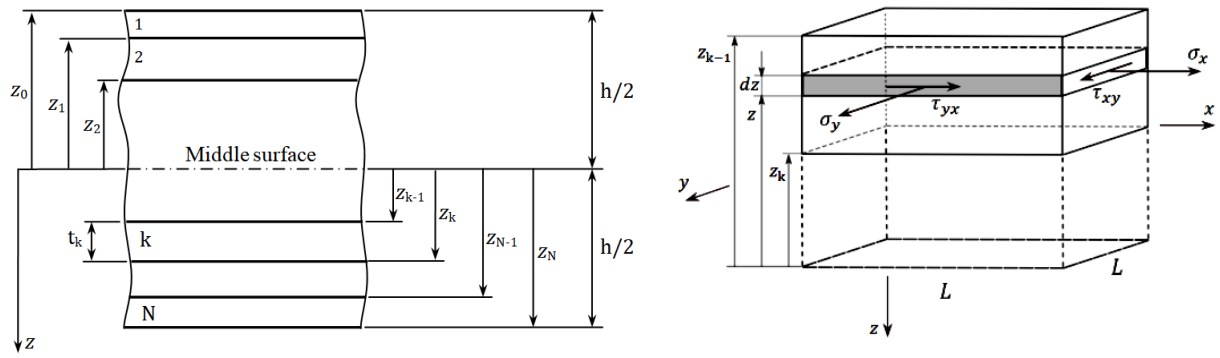

(a) (b)

Figure 2.4: (a) - Laminated plate geometry with numbering and (b) - stresses in the k^{th} lamina.

Force and Moment resultants:

As previously mentioned, a laminate is constructed by stacking a finite number of a single lamina in the direction of the laminate thickness – Figure 2.4a. The following assumptions are made in the CLT to develop relationship between Force and Moments and mid-plane strains and curvatures:

- Each lamina is homogeneous and orthotropic.
- A line straight and perpendicular to the middle surface remains straight and perpendicular to the middle surface during deformation ($\gamma_{xz} = \gamma_{yz} = 0$).
- Displacements($|u|, |v|, |w|$) in the three directions (X, Y, and Z) are continuous and small throughout the laminate ($|u|, |v|, |w| \ll h$), where h is the laminate thickness.
- Each lamina obeys according to Hook's law.
- No slip occurs between the lamina interfaces.

If laminated plate is loaded only with in-plane forces and moments (Figure 2.3) then from equilibrium of forces and moments in laminate cross-sections with stresses acting along laminate thickness (Figure 2.4b) we obtain equilibrium Equations [35]:

$$N_x = \int_{-h/2}^{h/2} \sigma_x \, dz \, , \qquad N_y = \int_{-h/2}^{h/2} \sigma_y \, dz \, , \qquad N_{xy} = \int_{-h/2}^{h/2} \tau_{xy} \, dz \, ,$$

$$M_x = \int_{-h/2}^{h/2} \sigma_x z \, dz \, , \qquad M_y = \int_{-h/2}^{h/2} \sigma_y z \, dz \, , \qquad M_{xy} = \int_{-h/2}^{h/2} \tau_{xy} z \, dz \, ,$$

where:

N_x, N_y – Normal forces per unit length along X and Y axis,
N_{xy} – Shear force per unit length in the X-Y plane,
M_x, M_y – Bending moments per unit length along X and Y axis,
M_{xy} – Twisting moment per unit length in the X-Y plane,

Previously defined equilibrium Equations can be written in matrix form:

$$\begin{bmatrix} N_x \\ N_y \\ N_{xy} \end{bmatrix} = \int_{-\frac{h}{2}}^{\frac{h}{2}} \begin{bmatrix} \sigma_x \\ \sigma_y \\ \tau_{xy} \end{bmatrix} dz \ , \tag{2.11a}$$

$$\begin{bmatrix} M_x \\ M_y \\ M_{xy} \end{bmatrix} = \int_{-h/2}^{h/2} \begin{bmatrix} \sigma_x \\ \sigma_y \\ \tau_{xy} \end{bmatrix} z \, dz \ . \tag{2.11b}$$

Having in mind that laminate is made of N laminas, previous equations can be written as:

$$\begin{bmatrix} N_x \\ N_y \\ N_{xy} \end{bmatrix} = \sum_{\mathrm{k}=1}^{\mathrm{N}} \int_{z_{\mathrm{k}-1}}^{z_{\mathrm{k}}} \begin{bmatrix} \sigma_x \\ \sigma_y \\ \tau_{xy} \end{bmatrix}_{\mathrm{k}} dz \ , \tag{2.12a}$$

$$\begin{bmatrix} M_x \\ M_y \\ M_{xy} \end{bmatrix} = \sum_{\mathrm{k}=1}^{\mathrm{N}} \int_{z_{\mathrm{k}-1}}^{z_{\mathrm{k}}} \begin{bmatrix} \sigma_x \\ \sigma_y \\ \tau_{xy} \end{bmatrix}_{\mathrm{k}} z \, dz \ . \tag{2.12b}$$

Since the global stresses in each lamina can be calculated by using Equation (2.10), with fact that $[\bar{Q}]_{\mathrm{k}}$ is constant through the thickness of k^{th} lamina, Equations (2.12a) and (2.12b) can be written in matrix form as following sum of integrals:

$$\begin{bmatrix} N_x \\ N_y \\ N_{xy} \end{bmatrix} = \left\{ \sum_{k=1}^{\mathrm{N}} \begin{bmatrix} \bar{Q}_{11} & \bar{Q}_{12} & \bar{Q}_{16} \\ \bar{Q}_{21} & \bar{Q}_{22} & \bar{Q}_{26} \\ \bar{Q}_{61} & \bar{Q}_{62} & \bar{Q}_{66} \end{bmatrix}_k \int_{z_{k-1}}^{z_k} dz \right\} \begin{bmatrix} \varepsilon_x^0 \\ \varepsilon_y^0 \\ \gamma_{xy}^0 \end{bmatrix} + \left\{ \sum_{k=1}^{\mathrm{N}} \begin{bmatrix} \bar{Q}_{11} & \bar{Q}_{12} & \bar{Q}_{16} \\ \bar{Q}_{21} & \bar{Q}_{22} & \bar{Q}_{26} \\ \bar{Q}_{61} & \bar{Q}_{62} & \bar{Q}_{66} \end{bmatrix}_k \int_{z_{k-1}}^{z_k} z \, dz \right\} \begin{bmatrix} k_x \\ k_y \\ k_{xy} \end{bmatrix} ,$$

$$\begin{bmatrix} M_x \\ M_y \\ M_{xy} \end{bmatrix} = \left\{ \sum_{k=1}^{\mathrm{N}} \begin{bmatrix} \bar{Q}_{11} & \bar{Q}_{12} & \bar{Q}_{16} \\ \bar{Q}_{21} & \bar{Q}_{22} & \bar{Q}_{26} \\ \bar{Q}_{61} & \bar{Q}_{62} & \bar{Q}_{66} \end{bmatrix}_k \int_{z_{k-1}}^{z_k} z \, dz \right\} \begin{bmatrix} \varepsilon_x^0 \\ \varepsilon_y^0 \\ \gamma_{xy}^0 \end{bmatrix} + \left\{ \sum_{k=1}^{\mathrm{N}} \begin{bmatrix} \bar{Q}_{11} & \bar{Q}_{12} & \bar{Q}_{16} \\ \bar{Q}_{21} & \bar{Q}_{22} & \bar{Q}_{26} \\ \bar{Q}_{61} & \bar{Q}_{62} & \bar{Q}_{66} \end{bmatrix}_k \int_{z_{k-1}}^{z_k} z^2 \, dz \right\} \begin{bmatrix} k_x \\ k_y \\ k_{xy} \end{bmatrix} .$$

By solving integrals in previous equations, we obtain:

$$\begin{bmatrix} N_x \\ N_y \\ N_{xy} \end{bmatrix} = \left\{ \sum_{k=1}^{\mathrm{N}} \begin{bmatrix} \overline{Q}_{11} & \overline{Q}_{12} & \overline{Q}_{16} \\ \overline{Q}_{21} & \overline{Q}_{22} & \overline{Q}_{26} \\ \overline{Q}_{61} & \overline{Q}_{62} & \overline{Q}_{66} \end{bmatrix}_k (z_k - z_{k-1}) \right\} \begin{bmatrix} \varepsilon_x^0 \\ \varepsilon_y^0 \\ \gamma_{xy}^0 \end{bmatrix} +$$

$$+ \left\{ \frac{1}{2} \sum_{\mathrm{k}=1}^{\mathrm{N}} \begin{bmatrix} \overline{Q}_{11} & \overline{Q}_{12} & \overline{Q}_{16} \\ \overline{Q}_{21} & \overline{Q}_{22} & \overline{Q}_{26} \\ \overline{Q}_{61} & \overline{Q}_{62} & \overline{Q}_{66} \end{bmatrix}_k (z_k^2 - z_{k-1}^2) \right\} \begin{bmatrix} k_x \\ k_y \\ k_{xy} \end{bmatrix} ,$$

$$\begin{bmatrix} M_x \\ M_y \\ M_{xy} \end{bmatrix} = \left\{ \frac{1}{2} \sum_{k=1}^{\mathrm{N}} \begin{bmatrix} \overline{Q}_{11} & \overline{Q}_{12} & \overline{Q}_{16} \\ \overline{Q}_{21} & \overline{Q}_{22} & \overline{Q}_{26} \\ \overline{Q}_{61} & \overline{Q}_{62} & \overline{Q}_{66} \end{bmatrix}_k (z_k^2 - z_{k-1}^2) \right\} \begin{bmatrix} \varepsilon_x^0 \\ \varepsilon_y^0 \\ \gamma_{xy}^0 \end{bmatrix} +$$

$$+ \left\{ \frac{1}{3} \sum_{k=1}^{\mathrm{N}} \begin{bmatrix} \overline{Q}_{11} & \overline{Q}_{12} & \overline{Q}_{16} \\ \overline{Q}_{21} & \overline{Q}_{22} & \overline{Q}_{26} \\ \overline{Q}_{61} & \overline{Q}_{62} & \overline{Q}_{66} \end{bmatrix}_k (z_k^3 - z_{k-1}^3) \right\} \begin{bmatrix} k_x \\ k_y \\ k_{xy} \end{bmatrix} .$$

Usually, in Mechanics of composite materials, the resultant forces and moments are written in terms of mid-plane strains and curvatures, in following matrix forms:

$$\begin{bmatrix} N_x \\ N_y \\ N_{xy} \end{bmatrix} = \begin{bmatrix} A_{11} & A_{12} & A_{16} \\ A_{12} & A_{22} & A_{26} \\ A_{16} & A_{26} & A_{66} \end{bmatrix} \begin{bmatrix} \varepsilon_x^0 \\ \varepsilon_y^0 \\ \gamma_{xy}^0 \end{bmatrix} + \begin{bmatrix} B_{11} & B_{12} & B_{16} \\ B_{12} & B_{22} & B_{26} \\ B_{16} & B_{26} & B_{66} \end{bmatrix} \begin{bmatrix} k_x \\ k_y \\ k_{xy} \end{bmatrix}, \tag{2.13a}$$

$$\begin{bmatrix} M_x \\ M_y \\ M_{xy} \end{bmatrix} = \begin{bmatrix} B_{11} & B_{12} & B_{16} \\ B_{12} & B_{22} & B_{26} \\ B_{16} & B_{26} & B_{66} \end{bmatrix} \begin{bmatrix} \varepsilon_x^0 \\ \varepsilon_y^0 \\ \gamma_{xy}^0 \end{bmatrix} + \begin{bmatrix} D_{11} & D_{12} & D_{16} \\ D_{12} & D_{22} & D_{26} \\ D_{16} & D_{26} & D_{66} \end{bmatrix} \begin{bmatrix} k_x \\ k_y \\ k_{xy} \end{bmatrix}. \tag{2.13b}$$

Equations (2.13a) and (2.13b) can be writen in short (compact) form by introducing following matrices:

$$[N] = \begin{bmatrix} N_x \\ N_y \\ N_{xy} \end{bmatrix}, \quad [M] = \begin{bmatrix} M_x \\ M_y \\ M_{xy} \end{bmatrix}, \quad [\varepsilon^0] = \begin{bmatrix} \varepsilon_x^0 \\ \varepsilon_y^0 \\ \gamma_{xy}^0 \end{bmatrix}, \quad [k] = \begin{bmatrix} k_x \\ k_y \\ k_{xy} \end{bmatrix},$$

$$[A] = \begin{bmatrix} A_{11} & A_{12} & A_{16} \\ A_{12} & A_{22} & A_{26} \\ A_{16} & A_{26} & A_{66} \end{bmatrix}, \quad [B] = \begin{bmatrix} B_{11} & B_{12} & B_{16} \\ B_{12} & B_{22} & B_{26} \\ B_{16} & B_{26} & B_{66} \end{bmatrix}, \quad [D] = \begin{bmatrix} D_{11} & D_{12} & D_{16} \\ D_{12} & D_{22} & D_{26} \\ D_{16} & D_{26} & D_{66} \end{bmatrix},$$

where, members of matrices $[A]$, $[B]$, and $[D]$ are defined as follows:

$$\begin{aligned} A_{\mathrm{ij}} &= \sum_{k=1}^{n} \left[\left(\bar{Q}_{\mathrm{ij}} \right) \right]_k (z_k - z_{k-1}), \qquad \mathrm{i} = 1, 2, 6; \quad \mathrm{j} = 1, 2, 6, \\ B_{\mathrm{ij}} &= \frac{1}{2} \sum_{k=1}^{n} \left[\left(\bar{Q}_{\mathrm{ij}} \right) \right]_k (z_k^2 - z_{k-1}^2), \qquad \mathrm{i} = 1, 2, 6; \quad \mathrm{j} = 1, 2, 6, \\ D_{\mathrm{ij}} &= \frac{1}{3} \sum_{k=1}^{n} \left[\left(\bar{Q}_{\mathrm{ij}} \right) \right]_k (z_k^3 - z_{k-1}^3), \qquad \mathrm{i} = 1, 2, 6; \quad \mathrm{j} = 1, 2, 6. \end{aligned} \tag{2.14}$$

Now the final relation between the resultant forces and moments and mid-plane strains and curvatures can be expressed in one matrix Equation:

$$\begin{bmatrix} N_x \\ N_y \\ N_{xy} \\ M_x \\ M_y \\ M_{xy} \end{bmatrix} = \begin{bmatrix} A_{11} & A_{12} & A_{16} & B_{11} & B_{12} & B_{16} \\ A_{12} & A_{22} & A_{26} & B_{12} & B_{22} & B_{26} \\ A_{16} & A_{26} & A_{66} & B_{16} & B_{26} & B_{66} \\ B_{11} & B_{12} & B_{16} & D_{11} & D_{12} & D_{16} \\ B_{12} & B_{22} & B_{26} & D_{12} & D_{22} & D_{26} \\ B_{16} & B_{26} & B_{66} & D_{16} & D_{26} & D_{66} \end{bmatrix} \begin{bmatrix} \varepsilon_x^0 \\ \varepsilon_y^0 \\ \gamma_{xy}^0 \\ k_x \\ k_y \\ k_{xy} \end{bmatrix}, \tag{2.15}$$

or, in short (compact) form as:

$$\begin{bmatrix} N \\ \cdots \\ M \end{bmatrix} = \begin{bmatrix} \mathrm{A} & \vdots & \mathrm{B} \\ \cdots & \vdots & \cdots \\ \mathrm{B} & \vdots & \mathrm{D} \end{bmatrix} \begin{bmatrix} \varepsilon^0 \\ \cdots \\ k \end{bmatrix}, \tag{2.16}$$

The matrices: [A], [B], and [D] are known as extensional, coupling, and bending stiffness matrices respectively. The extensional stiffness matrix [A] relates the resultant in-plane forces to the in-plane strains, whereas the coupling stiffness matrix [B] couples the force and moment to the mid-plane strains and mid-plane curvatures. The bending stiffness matrix [D] relates bending moments to the plate curvatures. In case when laminate has plies above the mid-plane which have same orientation, material, and thickness as the plies below the mid-plane, then such laminate is a *symmetric laminate*. In other words, a symmetric laminate has both geometric and material property symmetry about the mid-surface. Such a symmetry condition, when implemented in Equation (2.16), leads to the conclusion that in symmetric laminates coupling matrix must be equal to zero ([B]=0). This means that bending–stretching coupling will not be present in such laminates. Therefore, whenever it is possible, fiber reinforced composite structural parts should be always made of symmetric laminates.

2.1.3 Tsai-Hill failure theory

Implementation of Tsai-Hill failure theory implies conducted experiments which have the following strengths of a single lamina as known outputs:

$(\sigma_1^T)_{ult}$ - Ultimate longitudinal (in direction along fiber axis) tensile strength,
$(\sigma_1^C)_{ult}$ - Ultimate longitudinal (in direction along fiber axis) compression strength,
$(\sigma_2^T)_{ult}$ - Ultimate transverse (in direction normal to fiber axis) tensile strength,
$(\sigma_2^C)_{ult}$ - Ultimate transverse (in direction normal to fiber axis) compression strength,
$(\tau_{12})_{ult}$ - Ultimate in-plane shear strength (in plane1-2).

According to Tsai-Hill failure theory a lamina has failed if following Equation is violated:

$$\left[\frac{\sigma_1}{X_1}\right]^2 - \left[\left(\frac{\sigma_1}{X_2}\right)\left(\frac{\sigma_2}{X_2}\right)\right] + \left[\frac{\sigma_2}{Y}\right]^2 + \left[\frac{\tau_{12}}{S}\right]^2 \leq 1 \ , \tag{2.17}$$

where: $X_1 = (\sigma_1^T)_{ult}$ if $\sigma_1 > 0$,
$X_1 = (\sigma_1^C)_{ult}$ if $\sigma_1 \leq 0$,
$X_2 = (\sigma_2^T)_{ult}$ if $\sigma_2 > 0$,
$X_2 = (\sigma_2^C)_{ult}$ if $\sigma_2 \leq 0$,
$Y = (\sigma_2^T)_{ult}$ if $\sigma_2 > 0$,
$Y = (\sigma_2^C)_{ult}$ if $\sigma_2 \leq 0$,
$S = (\tau_{12})_{ult}$.

If the left side of Equation (2.17) is less than 1, the composite lamina is considered to be safe and there is an amount of so-called reserve of strength - *RS*, which means that loads can be increased until the left side of inequality approaches unity, while satisfying condition given in Equation (2.17) in every moment. According to the previous definition of *RS*, it can be expressed as:

$$RS = 1 - \left[\frac{\sigma_1}{X_1}\right]^2 - \left[\left(\frac{\sigma_1}{X_1}\right)\left(\frac{\sigma_2}{X_1}\right)\right] + \left[\frac{\sigma_2}{Y}\right]^2 + \left[\frac{\tau_{12}}{S}\right]^2 . \tag{2.18}$$

Obviously, the values of RS lie between 0 and 1. A hypothetical case, when *RS*=1 means that the lamina is in a stress-free state which represents the case when no external loads (mechanical or thermal) are applied. As the loads increase, less reserve of strength remains and the *RS* value approaches zero. This case means potential failure of the lamina. As obvious from Equation (2.18), linearly added loads, which result in a linear increase in stresses, lead to the nonlinear reduction of *RS*.

The reserve of strength can be used as parameter in laminate optimisation to determine optimal laminate configuration. Since failure of laminate is directly connected with failure of it's lamina with minimal value of *RS* (first ply failure), reserve of strength of the laminate can be defined as minimum value of *RS* for k^{th} lamina composing considered laminate. In case when *m* different laminate configurations is considered, optimal laminate configuration is the one with maximum value of the reserve of strength of all considered laminates. Therefore *RS* for a laminate is obtained as:

RS^n = minimum of RS^k , n= 1, 2, ….. m, k= 1, 2, 3,…, N,

while optimal laminate configuration is the one satisfying:

RS^{opt} = maximum of RS^n .

2.1.4 Tsai-Wu failure theory

Tsai and Wu developed their criterion by postulating that the strength of a unidirectional composite can be treated mathematically as a tensoral quantity. The Tsai-Wu failure theory is more general than the Tsai-Hill failure theory, [35]. The Tsai-Wu criterion predicts that failure will not occur if the following inequality is satisfied:

$$\frac{\sigma_1^2}{X_1|X_2|} + \frac{\sigma_2^2}{Y_1|Y_2|} + \frac{\tau_{12}^2}{S^2} - \frac{\sigma_1.\sigma_2}{\sqrt{X_1X_2Y_1Y_2}} + \left(\frac{1}{X_1} - \frac{1}{|X_2|}\right)\sigma_1 + \left(\frac{1}{Y_1} - \frac{1}{|Y_2|}\right)\sigma_2 < 1 . \tag{2.19}$$

Similarly as defined in Tsai-Hill failure theory, in order to find out whether the lamina is failed or not the same strengths must be known. In Equation (2.1) X_1, X_2, Y_1, Y_2 and S represents the following:

$X_1 = (\sigma_1^T)_{ult}$ − Ultimate longitudinal tensile strength in a direction along the fiber axis,
$X_2 = (\sigma_1^C)_{ult}$ − Ultimate longitudinal compression strength in a direction along the fiber axis,
$Y_1 = (\sigma_2^T)_{ult}$ − Ultimate transverse tensile strength in a direction normal to the fiber axis,
$Y_2 = (\sigma_2^C)_{ult}$ − Ultimate transverse compression strength in a direction normal to the fiber axis,
$S = (\tau_{12})_{ult}$ − Ultimate in − plane shear strength (in plane 1 − 2).

If the value of Equation (2.19) is less than one, the lamina is safe and the load can be increased. But, if the value is greater than one, the lamina fails. If the value is equal to one, the failure load is indicated. In this thesis, the Tsai-Wu failure criterion is used in the design optimization process.

The safety factor - SF for the lamina, based on the Tsai-Wu failure theory, is defined as the ultimate stress (failure stress) over the applied stress:

$SF = (\text{failure stress})/(\text{applied stress})$.

The safety factor is used as parameter in laminate optimisation to determine optimal laminate configuration. In this thesis SF of every ply in a laminate is checked during the optimisation procedure. Failure is predicted if the inequality in Equation (2.19) has been violated. As obvious from Equation (2.19), for a safe status of lamina, SF for the k^{th} lamina, must be greater than one: $SF_{TW}^{k} > 1$. If $SF_{TW}^{k} < 1$ the lamina is not safe and will fail under the applied loads.

By definition of SF for the k^{th} lamina, SF_{TW}^{k}, based on the Tsai-Wu criteria (TW) the stress components at k^{th} lamina in Equation (2.19) in case when the failure load is indicated ($f = \sigma_{ij} SF_{TW}^{k}$), which makes the left side of Equation (2.19) equal to 1, which leads to:

$$a\left(SF_{TW}^{k}\right)^{2} + b\left(SF_{TW}^{k}\right) - 1 = 0\,, \tag{2.20}$$

where:

$$a = \frac{\sigma_1^2}{X_1|X_2|} + \frac{\sigma_2^2}{Y_1|Y_2|} + \frac{\tau_{12}^2}{S^2} - \frac{\sigma_1.\sigma_2}{\sqrt{X_1X_2Y_1Y_2}}\ , \tag{2.21}$$

$$b = \left(\frac{1}{X_1} - \frac{1}{X_2}\right)\sigma_1 + \left(\frac{1}{Y_1} - \frac{1}{Y_2}\right)\sigma_2\ . \tag{2.22}$$

The square root of Equation (2.20), provides the safety factor for k^{th} lamina - SF_{TW}^{k} as the one with smallest positive value of the two values calculated from:

$$SF_{TW}^{k} = \left|\frac{-b \pm \sqrt{b^2 - 4a}}{2a}\right|\ . \tag{2.23}$$

Due to the fact that a negative safety factor has no physical meaning, if a negative square root of Equation (2.20) appears, logicaly it should be neglected. The safety factor of the laminate, SF_{TW}^{n}, is the minimum value of the safety factor of the k^{th} lamina in laminate:

SF_{TW}^{n} = minimum of SF_{TW}^{k} , n= 1, 2, ….. m, k= 1, 2, 3,…, N.

In case when m different laminate configurations is considered, optimal laminate configuration is the one with maximum value of SF_{TW}^{n} of all considered laminates.

2.1.5 Thermal stresses

As mentioned before thermal stresses usually occur due to the exposure of real composite structure to extreme temperatures, for instance, higher than 40°C or lower than - 20°C. In order to investigate possible effects of temperature loads, the thermal stress analysis of carbon fibre reinforced composite structure, exposed to extreme temperatures, should be performed. For simple geometrical shapes this analysis can be done analytically, using CLT or numerically, using the finite element method, which appears to be the most suitable for complex geometries of structural parts.

According to the principles of CLT, under temperature loads, each ply in a laminate gets stressed by the deformation differences of the adjacent lamina. These additional stresses appear when the actual strains of the lamina - $[\varepsilon]$ are in excess or less than the thermal strains - $[\varepsilon^T]$ in the unrestricted lamina (free thermal strains). These strain differences are called mechanical strains - $[\varepsilon^M]$ and the stresses caused by them are called mechanical stresses under temperature loads or so-called thermal stresses -

$[\sigma^T]$. The typical geometry of the laminated plate, used for stress analysis, is shown in Figure 2.4a. In laminate, with the N lamina (Figure 2.4b), the mechanical strains in the k^{th} ply are given by:

$$\begin{bmatrix} \varepsilon_x^M \\ \varepsilon_y^M \\ \gamma_{xy}^M \end{bmatrix}_k = \begin{bmatrix} \varepsilon_x \\ \varepsilon_y \\ \gamma_{xy} \end{bmatrix}_k - \begin{bmatrix} \varepsilon_x^T \\ \varepsilon_y^T \\ \gamma_{xy}^T \end{bmatrix}_k . \tag{2.24}$$

Using stress-strain relations, Equation (2.8), the thermal stresses in the k^{th} lamina are given by:

$$\begin{bmatrix} \sigma_x^T \\ \sigma_y^T \\ \sigma_{xy}^T \end{bmatrix}_k = \begin{bmatrix} \bar{Q}_{11} & \bar{Q}_{12} & \bar{Q}_{16} \\ \bar{Q}_{21} & \bar{Q}_{22} & \bar{Q}_{26} \\ \bar{Q}_{61} & \bar{Q}_{62} & \bar{Q}_{66} \end{bmatrix}_k \begin{bmatrix} \varepsilon_x^M \\ \varepsilon_y^M \\ \gamma_{xy}^M \end{bmatrix}_k = [\bar{Q}]_k \begin{bmatrix} \varepsilon_x^M \\ \varepsilon_y^M \\ \gamma_{xy}^M \end{bmatrix}_k . \tag{2.25}$$

Where the superscript M represents the mechanical effects, while T stands for thermal effects. Matrix $[\bar{Q}]_k$ is reduced transformed stiffness matrix, which corresponds to the k^{th} ply located at the defined distance from the middle surface, as shown in Figure 2.4a. Substituting mechanical strains from Equation (2.24) into (2.25), we obtain expression for thermal stresses:

$$\begin{bmatrix} \sigma_x^T \\ \sigma_y^T \\ \sigma_{xy}^T \end{bmatrix}_k = [\bar{Q}]_k \begin{bmatrix} \varepsilon_x \\ \varepsilon_y \\ \gamma_{xy} \end{bmatrix}_k - [\bar{Q}]_k \begin{bmatrix} \varepsilon_x^T \\ \varepsilon_y^T \\ \gamma_{xy}^T \end{bmatrix} . \tag{2.26}$$

Free thermal strains - $[\varepsilon^T]$ in the k^{th} ply are given by coefficients of thermal expansion along global axes x and y (α_x, α_y and α_{xy}), and temperature change (ΔT):

$$\begin{bmatrix} \varepsilon_x \\ \varepsilon_y \\ \gamma_{xy} \end{bmatrix}_k = \begin{bmatrix} \alpha_x \\ \alpha_y \\ \alpha_{xy} \end{bmatrix} \Delta T . \tag{2.27}$$

If coefficients of thermal expansion along local axes 1 and 2 (α_1, α_2) are known, then coefficients α_x, α_y and α_{xy} can be calculated by using the following Equation:

$$\begin{bmatrix} \alpha_x \\ \alpha_y \\ \alpha_{xy}/2 \end{bmatrix} = [T]^{-1} \begin{bmatrix} \alpha_1 \\ \alpha_2 \\ 0 \end{bmatrix}, \tag{2.28}$$

where matrix $[T]$ is the transformation matrix which were defined in Section 2.1.1 as:

$$[T] = \begin{bmatrix} c^2 & s^2 & 2sc \\ s^2 & c^2 & -2sc \\ -sc & sc & c^2 - s^2 \end{bmatrix} . \tag{2.29}$$

According to CLT, actual strains in the k^{th} ply are given by mid-plane strains and curvatures (see Equation (2.9)):

$$\begin{bmatrix} \varepsilon_x \\ \varepsilon_y \\ \gamma_{xy} \end{bmatrix}_k = \begin{bmatrix} \varepsilon_x^0 \\ \varepsilon_y^0 \\ \gamma_{xy}^0 \end{bmatrix} + z \begin{bmatrix} k_x \\ k_y \\ k_{xy} \end{bmatrix} . \tag{2.30}$$

After substituting actual strains from Equation (2.30) into Equation (2.26), we get:

$$\begin{bmatrix} \sigma_x^T \\ \sigma_y^T \\ \sigma_{xy}^T \end{bmatrix}_k = [\bar{Q}]_k \begin{bmatrix} \varepsilon_x^0 \\ \varepsilon_y^0 \\ \gamma_{xy}^0 \end{bmatrix} + z[\bar{Q}]_k \begin{bmatrix} k_x \\ k_y \\ k_{xy} \end{bmatrix} - [\bar{Q}]_k \begin{bmatrix} \alpha_x \\ \alpha_y \\ \alpha_{xy} \end{bmatrix}_k \Delta T \ . \tag{2.31}$$

The stresses in each lamina can be integrated through the laminate thickness to give resultant forces and moments (or applied external forces and moments in selected cross-sections):

$$\begin{bmatrix} N_x \\ N_y \\ N_{xy} \end{bmatrix} = \int_{-\mathrm{h}/2}^{\mathrm{h}/2} \begin{bmatrix} \sigma_x^T \\ \sigma_y^T \\ \sigma_{xy}^T \end{bmatrix}_k dz = \sum_{\mathrm{k}=1}^{\mathrm{N}} \int_{z_{\mathrm{k}-1}}^{z_{\mathrm{k}}} \begin{bmatrix} \sigma_x^T \\ \sigma_y^T \\ \sigma_{xy}^T \end{bmatrix}_k dz \ , \tag{2.32}$$

$$\begin{bmatrix} M_x \\ M_y \\ M_{xy} \end{bmatrix} = \int_{-\mathrm{h}/2}^{\mathrm{h}/2} \begin{bmatrix} \sigma_x^T \\ \sigma_y^T \\ \sigma_{xy}^T \end{bmatrix}_k z\, dz = \sum_{\mathrm{k}=1}^{\mathrm{N}} \int_{z_{\mathrm{k}-1}}^{z_{\mathrm{k}}} \begin{bmatrix} \sigma_x^T \\ \sigma_y^T \\ \sigma_{xy}^T \end{bmatrix}_k z\, dz \ . \tag{2.33}$$

The forces and moments applied to a laminate in Equations (2.22) and (2.33) are known. In case of the absence of external forces and moments, their values can be set to be zero. In this case, substituting thermal stresses in the k^{th} lamina from Equation (2.31) into Equations (2.32) and (2.33), lead to following two equations:

$$\begin{bmatrix} N_x \\ N_y \\ N_{xy} \end{bmatrix} = 0 = \sum_{k=1}^{\mathrm{N}} \int_{z_{k-1}}^{z_k} \left\{ [\bar{Q}]_k \begin{bmatrix} \varepsilon_x^0 \\ \varepsilon_y^0 \\ \gamma_{xy}^0 \end{bmatrix} + z[\bar{Q}]_k \begin{bmatrix} k_x \\ k_y \\ k_{xy} \end{bmatrix} - [\bar{Q}]_k \begin{bmatrix} \alpha_x \\ \alpha_y \\ \alpha_{xy} \end{bmatrix}_k \Delta T \right\} dz \ , \tag{2.34}$$

$$\begin{bmatrix} M_x \\ M_y \\ M_{xy} \end{bmatrix} = 0 = \sum_{k=1}^{\mathrm{N}} \int_{z_{k-1}}^{z_k} \left\{ z[\bar{Q}]_k \begin{bmatrix} \varepsilon_x^0 \\ \varepsilon_y^0 \\ \gamma_{xy}^0 \end{bmatrix} + z^2[\bar{Q}]_k \begin{bmatrix} k_x \\ k_y \\ k_{xy} \end{bmatrix} - z[\bar{Q}]_k \begin{bmatrix} \alpha_x \\ \alpha_y \\ \alpha_{xy} \end{bmatrix}_k \Delta T \right\} dz \ . \tag{2.35}$$

Since $[\bar{Q}]_{\mathrm{k}}$ is constant through the thickness of k^{th} lamina, previous equations become:

$$\begin{aligned} 0 = & \left\{ \sum_{k=1}^{\mathrm{N}} [\bar{Q}]_k \int_{z_{k-1}}^{z_k} dz \right\} \begin{bmatrix} \varepsilon_x^0 \\ \varepsilon_y^0 \\ \gamma_{xy}^0 \end{bmatrix} + \left\{ \sum_{k=1}^{\mathrm{N}} [\bar{Q}]_k \int_{z_{k-1}}^{z_k} z\, dz \right\} \begin{bmatrix} k_x \\ k_y \\ k_{xy} \end{bmatrix} \\ & - \left\{ \sum_{k=1}^{\mathrm{N}} [\bar{Q}]_k \begin{bmatrix} \alpha_x \\ \alpha_y \\ \alpha_{xy} \end{bmatrix}_k \int_{z_{k-1}}^{z_k} dz \right\} \Delta T \ , \end{aligned} \tag{2.36}$$

$$\begin{aligned} 0 = & \left\{ \sum_{k=1}^{\mathrm{N}} [\bar{Q}]_k \int_{z_{k-1}}^{z_k} z dz \right\} \begin{bmatrix} \varepsilon_x^0 \\ \varepsilon_y^0 \\ \gamma_{xy}^0 \end{bmatrix} + \left\{ \sum_{k=1}^{\mathrm{N}} [\bar{Q}]_k \int_{z_{k-1}}^{z_k} z^2 dz \right\} \begin{bmatrix} k_x \\ k_y \\ k_{xy} \end{bmatrix} \\ & - \left\{ \sum_{k=1}^{\mathrm{N}} [\bar{Q}]_k \begin{bmatrix} \alpha_x \\ \alpha_y \\ \alpha_{xy} \end{bmatrix}_k \int_{z_{k-1}}^{z_k} z dz \right\} \Delta T \ . \end{aligned} \tag{2.37}$$

Aftwer solving integrals in Equations (2.36) and (2.37) we obtain:

$$0 = \left\{\sum_{k=1}^{\mathrm{N}} [\bar{Q}]_k (z_k - z_{k-1})\right\} \begin{bmatrix} \varepsilon_x^0 \\ \varepsilon_y^0 \\ \gamma_{xy}^0 \end{bmatrix} + \left\{\frac{1}{2}\sum_{k=1}^{\mathrm{N}} [\bar{Q}]_k (z_k^2 - z_{k-1}^2)\right\} \begin{bmatrix} k_x \\ k_y \\ k_{xy} \end{bmatrix} - \left\{\sum_{k=1}^{\mathrm{N}} [\bar{Q}]_k \begin{bmatrix} \alpha_x \\ \alpha_y \\ \alpha_{xy} \end{bmatrix}_k (z_k - z_{k-1})\right\} \Delta T \ , \tag{2.38}$$

$$0 = \left\{\frac{1}{2}\sum_{k=1}^{\mathrm{N}} [\bar{Q}]_k (z_k^2 - z_{k-1}^2)\right\} \begin{bmatrix} \varepsilon_x^0 \\ \varepsilon_y^0 \\ \gamma_{xy}^0 \end{bmatrix} + \frac{1}{3}\left\{\sum_{k=1}^{\mathrm{N}} [\bar{Q}]_k (z_k^3 - z_{k-1}^3)\right\} \begin{bmatrix} k_x \\ k_y \\ k_{xy} \end{bmatrix} - \left\{\frac{1}{2}\sum_{k=1}^{\mathrm{N}} [\bar{Q}]_k \begin{bmatrix} \alpha_x \\ \alpha_y \\ \alpha_{xy} \end{bmatrix}_k (z_k^2 - z_{k-1}^2)\right\} \Delta T \ . \tag{2.39}$$

If we do the same as we did in Section2.1.2, by introducing the following members:

$$A_{ij} = \sum_{k=1}^{N} \left[\bar{Q}_{ij}\right]_k (z_k - z_{k-1}) \, , \; B_{ij} = \frac{1}{2}\sum_{k=1}^{N} \left[\bar{Q}_{ij}\right]_k \left(z_k^2 - z_{k-1}^2\right) , D_{ij} = \frac{1}{3}\sum_{k=1}^{N} \left[\bar{Q}_{ij}\right]_k \left(z_k^3 - z_{k-1}^3\right), \tag{2.40}$$

equations (2.38) and (2.39) become:

$$0 = \begin{bmatrix} A_{11} & A_{12} & A_{16} \\ A_{12} & A_{22} & A_{26} \\ A_{16} & A_{26} & A_{66} \end{bmatrix} \begin{bmatrix} \varepsilon_x^0 \\ \varepsilon_y^0 \\ \gamma_{xy}^0 \end{bmatrix} + \begin{bmatrix} B_{11} & B_{12} & B_{16} \\ B_{12} & B_{22} & B_{26} \\ B_{16} & B_{26} & B_{66} \end{bmatrix} \begin{bmatrix} K_x \\ K_y \\ K_{xy} \end{bmatrix} - \left\{\sum_{k=1}^{\mathrm{N}} [\bar{Q}]_k \begin{bmatrix} \alpha_x \\ \alpha_y \\ \alpha_{xy} \end{bmatrix}_k (z_{\mathrm{k}} - z_{\mathrm{k-1}})\right\} \Delta T \, , \tag{2.41}$$

$$0 = \begin{bmatrix} B_{11} & B_{12} & B_{16} \\ B_{12} & B_{22} & B_{26} \\ B_{16} & B_{26} & B_{66} \end{bmatrix} \begin{bmatrix} \varepsilon_x^0 \\ \varepsilon_y^0 \\ \gamma_{xy}^0 \end{bmatrix} + \begin{bmatrix} D_{11} & D_{12} & D_{16} \\ D_{12} & D_{22} & D_{26} \\ D_{16} & D_{26} & D_{66} \end{bmatrix} \begin{bmatrix} K_x \\ K_y \\ K_{xy} \end{bmatrix} - \left\{\sum_{k=1}^{\mathrm{N}} [\bar{Q}]_k \begin{bmatrix} \alpha_x \\ \alpha_y \\ \alpha_{xy} \end{bmatrix}_k \frac{1}{2}(z_k^2 - z_{k-1}^2)\right\} \Delta T \ . \tag{2.42}$$

Now we can define so-called fictitious thermal loads (forces and moments):

$$[N^T] = \begin{bmatrix} N_x^T \\ N_y^T \\ N_{xy}^T \end{bmatrix} = \left\{\sum_{k=1}^{\mathrm{N}} [\bar{Q}]_k \begin{bmatrix} \alpha_x \\ \alpha_y \\ \alpha_{xy} \end{bmatrix}_k (z_k - z_{k-1})\right\} \Delta T \, , \tag{2.43a}$$

$$[M^T] = \begin{bmatrix} M_x^T \\ M_y^T \\ M_{xy}^T \end{bmatrix} = \frac{1}{2}\left\{\sum_{k=1}^{\mathrm{N}} [\bar{Q}]_k \begin{bmatrix} \alpha_x \\ \alpha_y \\ \alpha_{xy} \end{bmatrix}_k (z_k^2 - z_{k-1}^2)\right\} \Delta T. \tag{2.43b}$$

By substituting Equations (2.43) and (2.44) into Equations (2.41) and (2.42) after simple re-arrangements we obtain:

$$\begin{bmatrix} N_x^T \\ N_y^T \\ N_{xy}^T \end{bmatrix} = \begin{bmatrix} A_{11} & A_{12} & A_{16} \\ A_{12} & A_{22} & A_{26} \\ A_{16} & A_{26} & A_{66} \end{bmatrix} \begin{bmatrix} \varepsilon_x^0 \\ \varepsilon_y^0 \\ \gamma_{xy}^0 \end{bmatrix} + \begin{bmatrix} B_{11} & B_{12} & B_{16} \\ B_{12} & B_{22} & B_{26} \\ B_{16} & B_{26} & B_{66} \end{bmatrix} \begin{bmatrix} K_x \\ K_y \\ K_{xy} \end{bmatrix}, \tag{2.44}$$

$$\begin{bmatrix} M_x^T \\ M_y^T \\ M_{xy}^T \end{bmatrix} = \begin{bmatrix} B_{11} & B_{12} & B_{16} \\ B_{12} & B_{22} & B_{26} \\ B_{16} & B_{26} & B_{66} \end{bmatrix} \begin{bmatrix} \varepsilon_x^0 \\ \varepsilon_y^0 \\ \gamma_{xy}^0 \end{bmatrix} + \begin{bmatrix} D_{11} & D_{12} & D_{16} \\ D_{12} & D_{22} & D_{26} \\ D_{16} & D_{26} & D_{66} \end{bmatrix} \begin{bmatrix} K_x \\ K_y \\ K_{xy} \end{bmatrix}. \tag{2.45}$$

Equations (2.44) and (2.45) can be expressed in short form notation as:

$$\begin{bmatrix} N^T \\ \cdots \\ M^T \end{bmatrix} = \begin{bmatrix} A & \vdots & B \\ \cdots & \vdots & \cdots \\ B & \vdots & D \end{bmatrix} \begin{bmatrix} \varepsilon^0 \\ \cdots \\ k \end{bmatrix}, \tag{2.46}$$

where natrices $[A]$, $[B]$, and $[D]$ are defined as:

$$[A] = \begin{bmatrix} A_{11} & A_{12} & A_{16} \\ A_{12} & A_{22} & A_{26} \\ A_{16} & A_{26} & A_{66} \end{bmatrix}, \; [B] = \begin{bmatrix} B_{11} & B_{12} & B_{16} \\ B_{12} & B_{22} & B_{26} \\ B_{16} & B_{26} & B_{66} \end{bmatrix}, \; [D] = \begin{bmatrix} D_{11} & D_{12} & D_{16} \\ D_{12} & D_{22} & D_{26} \\ D_{16} & D_{26} & D_{66} \end{bmatrix}.$$

The fictitious thermal loads introduced in Equations (2.43a) and (2.43b) are the loads one can apply mechanically to induce the same stresses and strains as by the thermal load. Thus, if both mechanical and thermal loads are applied, the external mechanical loads can be added to the fictitious thermal loads to find the ply-by-ply stresses and strains in the laminate.

However, these loads can be applied even separately and then added by producing resulting stresses and strains from the solution of the two problems. As obvious fictitious thermal loads can be calculated and are known.

Mid-plane strains and curvatures can be calculated by inverting Equation (2.46):

$$\begin{bmatrix} \varepsilon^0 \\ \cdots \\ k \end{bmatrix} = \begin{bmatrix} A & \vdots & B \\ \cdots & \vdots & \cdots \\ B & \vdots & D \end{bmatrix}^{-1} \begin{bmatrix} N^T \\ \cdots \\ M^T \end{bmatrix}. \tag{2.47}$$

The thermal stresses in the k^{th} ply are then calculated by using Equation (2.31):

$$\begin{bmatrix} \sigma_x^T \\ \sigma_y^T \\ \sigma_{xy}^T \end{bmatrix}_k = [\bar{Q}]_k \begin{bmatrix} \varepsilon_x^0 \\ \varepsilon_y^0 \\ \gamma_{xy}^0 \end{bmatrix} + z[\bar{Q}]_k \begin{bmatrix} k_x \\ k_y \\ k_{xy} \end{bmatrix} - [\bar{Q}]_k \begin{bmatrix} \alpha_x \\ \alpha_y \\ \alpha_{xy} \end{bmatrix}_k \Delta T \ , \qquad (2.48)$$

where coordinate z for k^{th} lamina (see Figure 2.5) is in range: $z_{k-1} \leq z \leq z_k$ (k=1,…,N).

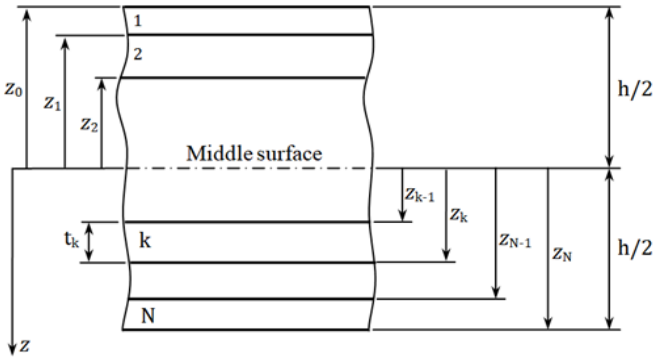

Figure 2.5: Coordinate locations of the top and bottom surfaces of plies in the laminate.

2.1.6 The steps of analyzing a laminated composite structure under the applied loads

The steps for analyzing a laminated composite subjected to applied forces and moments are as follows:

1. Calculate the values of the elements of transformed compliance stiffness matrix $[\bar{S}]$ for every ply using the four elastic moduli (engineering constants) as presented in Section2.1.1.
2. Find the values of the elements of transformed reduced stiffness matrix $[\bar{Q}]$ for each ply using the four elastic moduli (engineering constants) as presented in Section2.1.1.
3. Calculate the coordinate of the top and bottom surfaces z_k $(k = 1,2,\ldots,\text{N})$ for every ply as shown in Figure 2.6.
4. Find the three stiffness matrices [A], [B], and [D] using the Equation (2.14).
5. Substitute the values of stiffness matrices calculated in step four in Equation (2.15).
6. Apply forces and moments in Equation (2.15).
7. Solve the Equation (2.15) to find the mid-plane strains and curvatures.
8. Find global stresses in each lamina by using Equation (2.8)
9. Calculate the local stresses in each lamina by using Equation (2.1).

2.1.7 The failure criterion for a laminate

As mentioned before, laminate consists of layers of different orientations, as shown schematically in Figure 2.6. Unlike the strains which change linearly through the thickness of whole laminate, the stresses change linearly only through the thickness of single lamina, as it is shown in Figure 2.7. The stresses may jump from one lamina to another due to the transformed reduced-stiffness matrix changes from ply to ply because it depends on the material properties and orientation of the ply. These global stresses can then be transformed into local stresses through the transformation matrix – Equation (2.1).

In Section2.1.2 it was stated that if laminate is symmetric, coupling matrix does not exist and therefore the matrix $[B]$ is equal to zero:

$$[B] = 0. \tag{2.49}$$

In this case, relationships between the resultant forces and moments and mid-plane strains and curvatures, expressed through Equations (2.13a) and (2.13b) can be decoupled as follows:

$$\begin{bmatrix} N_x \\ N_y \\ N_{xy} \end{bmatrix} = \begin{bmatrix} A_{11} & A_{12} & A_{16} \\ A_{12} & A_{22} & A_{26} \\ A_{16} & A_{26} & A_{66} \end{bmatrix} \begin{bmatrix} \varepsilon_x^0 \\ \varepsilon_y^0 \\ \gamma_{xy}^0 \end{bmatrix}, \tag{2.50}$$

$$\begin{bmatrix} M_x \\ M_y \\ M_{xy} \end{bmatrix} = \begin{bmatrix} D_{11} & D_{12} & D_{16} \\ D_{12} & D_{22} & D_{26} \\ D_{16} & D_{26} & D_{66} \end{bmatrix} \begin{bmatrix} k_x \\ k_y \\ k_{xy} \end{bmatrix}. \tag{2.51}$$

This shows that the force and moment terms are uncoupled. So, if a laminate is subjected only to forces, it will have zero mid-plane curvatures. Also, if it is subjected only to moments, it will have zero mid-plane strains. The uncoupling between extensions and bending in symmetric laminates makes analysis of laminated composite plates to be quite simple.

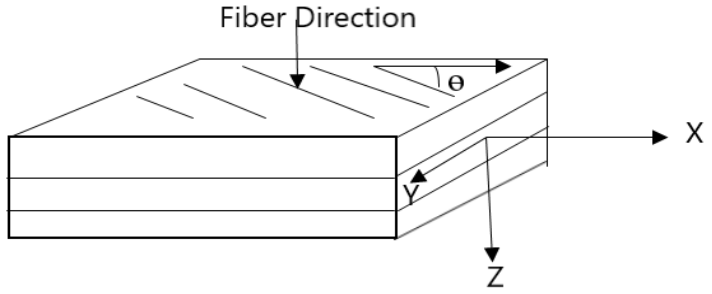

Figure 2.6: Schematic presentation lamina geometry.

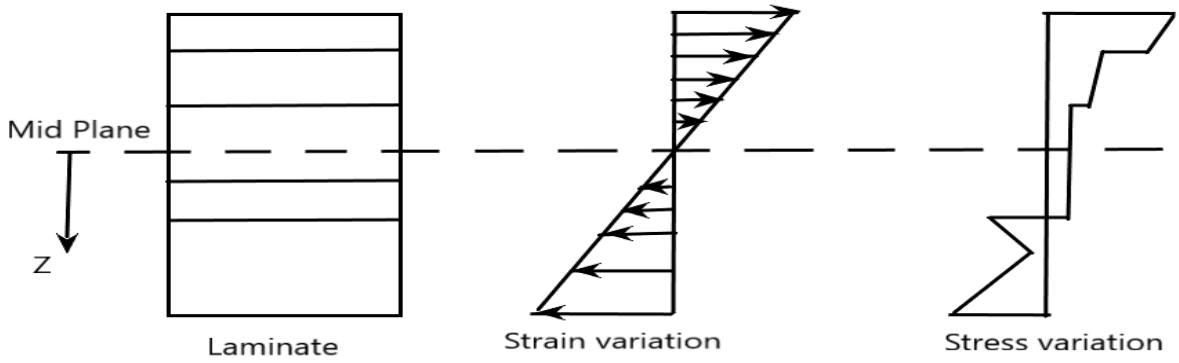

Figure 2.7: Stress and strain variation through the thickness of the laminate.

As it is known in laminated composite structural parts, due to the increase of mechanical loads, some lamina may fail, but the composite structure is still capable to take more loads until the moment all laminas fail. However, in this thesis it will be assumed that first ply failure leads to total failure of considered laminate. To determine potential failure of laminate, use the Tsai-Hill or Tsai-Wu failure criterion for each ply is aplied.

From previous discussion it is obvious that each lamina in cosidered laminate should be checked out by using Tsai-Hill or Tsai-Wu failure criterion in order to find it's the reserve of strength (RS) or safety factor (SF). If Tsai-Wu failure criterion is implemented, safety factor of the laminate is equal to the minimum value of SF of all laminas in the laminate. The SF for all laminate plies can be found as shown in Section2.1.4 (Equation (2.23). However, safety factor of the laminate is equal to the minimum value of SF of all laminas in the laminate:

$$SF = \text{minimum } (SF_{TW}^{1}, SF_{TW}^{2}, \dots, SF_{TW}^{n}) \ . \tag{2.52}$$

For an example, let us consider case when only unidirectional load in X, or Y, direction exists. In this case the first ply failure occurs at a lamina, which has a minimum safety factor at a load N_f defined as:

$$N_f = \text{N(MPa.mm)} * (SF) \ , \tag{2.53}$$

where:

- N is the component of applied axial load in X or Y directions (Figure 2.6),
- N_f is the maximum applied load before the first ply failure.

In this case, average normal stress of the laminate - $\overline{\sigma}$ is defined as:

$$\overline{\sigma} = \text{N(MPa.mm)/h} \ , \tag{2.54}$$

where h is the lamina thickness.

Now, the average normal stress before the first ply failure - $\overline{\sigma}_{ult}$ can be found, as follows:

$$\overline{\sigma}_{ult} = N_f/\text{h (MPa)}. \tag{2.55}$$

2.1.8 Optimization procedure

In optimization of laminated composite structure, the goal is to determine the optimum angle of each ply (lamina), the stacking sequence of the laminate and number of plies in order to reach maximal possible value of reserve of strength (RS) or safety factor (SF) as well as minimal weight. In this thesis the Tsai-Wu criteria were used to determine value of safety factor of laminate in order to check strength reserve prior to static first ply failure.

The optimisation steps of the laminate under defined loading conditions are summarized as follows:

1. The design variables are orientation angles and the thickness of the ply. Defined loads are used in the optimisation procedure in order to evaluate the maximum value of $SF$of all considered laminates. Initial laminates consists of 10 symmetric plies of reinforced carbon fibre composite material with six different orientation angles, as shown in Table 2.1.
2. The local stresses and strains are calculated by following the steps of analyzing the laminate, as presented in Section2.1.6.

3. The safety factor for the k^{th} lamina - SF^k, is calculated by using Equation (2.23). The safety factor of the laminate of constant thickness, SF^n, is the minimum value of the safety factor of the k^{th} lamina in laminate:

$$SF_{TW}^n = \text{minimum of } SF_{TW}^k \text{ , where: } k = 1, 2, 3, \ldots, 10. \quad (2.56)$$

The optimal laminate configuration is the one with the highest value of the safety factor:

$$SF^{opt} = \text{maximum of } SF^n \text{ , where: } n = 1, 2, \ldots.. 6. \quad (2.57)$$

4. If the selected laminate, which have been selected in step number three, has quite high value of SF then this laminate can be considered as a candidate for reduction of number of plies in order to minimize the thickness. In other words, when the laminate structure has a quite high safety factor, it can carry significantly more load, thus the number of plies can be reduced without jeopardizing safety. After reduction of number of the plies, the safety factor of the new laminate will be checked again in order to confirm that lamina is safe.

Table 2.1: Laminate configurations used in the optimization process

Laminate number	Laminate orientation angles	Number of plies	Lamina thickness (mm)	Laminate orientation angles	Number of plies	Lamina thickness (mm)
1	$[0/+45/90/-45/0]_s$	10	0.375	$[0/+45/90/-45/0]_s$	10	0.25
2	$[0/+30/90/-30/0]_s$	10	0.375	$[0/+30/90/-30/0]_s$	10	0.25
3	$[0/+30/90/-45/0]_s$	10	0.375	$[0/+30/90/-45/0]_s$	10	0.25
4	$[0/+60/90/-60/0]_s$	10	0.375	$[0/+60/90/-60/0]_s$	10	0.25
5	$[0/+45/-45/90/0]_s$	10	0.375	$[0/+45/-45/90/0]_s$	10	0.25
6	$[0/+30/90/+30/0]_s$	10	0.375	$[0/+30/90/+30/0]_s$	10	0.25
1	$[0/+45/90/-45/0]_s$	10	0.125			
2	$[0/+30/90/-30/0]_s$	10	0.125			
3	$[0/+30/90/-45/0]_s$	10	0.125			
4	$[0/+60/90/-60/0]_s$	10	0.125			
5	$[0/+45/-45/90/0]_s$	10	0.125			
6	$[0/+30/90/+30/0]_s$	10	0.125			

2.2 Evaluation of lamina's mechanical properties

In previous sections, the stress–strain relationships, engineering constants, and failure theories for an angle lamina were presented using four elastic moduli, five strength parameters, two coefficients of thermal expansion (CTE). Usually, these 11 parameters can be found experimentally by conducting several tension, compression, shear, and thermal tests on unidirectional lamina (laminates). However, unlike in isotropic materials, experimental evaluation of these parameters is quite costly and time consuming because they are functions of several variables: the individual constituents of the composite material, fiber volume fraction, packing geometry, processing, etc. Thus, if conduction of experiments is unavailable, there is the need for developing analytical models to somehow 'predict' these parameters. In this section, simple analytical as well as numerical models for 'predicting' these parameters in terms of the stiffnesses and strengths are presented.

As stated before it is assumed that the lamina is homogeneous by focusing on it's average response to mechanical loads. The lamina is simply looked at as a anisotropic material whose properties are different in various directions, but not different from one location to another.

In mechanics of composite materials, different analytical approaches or methods have been used for estimating elastic constants of fiber reinforced composite material. As already mentioned, these constants imply: Young's modulus (E_1 and E_2), Poisson's ratio (ν_{12}), and In-plain shear modulus (G_{12}). Some of approaches (methods) that have been used for their evaluation are: strength of the material approach, Semi-Empirical model (Halpin-Tsai), and Chamis model. At the end of this section, obtained results for E_1, E_2, ν_{12} and G_{12} were compared to the results obtained by the FEM.

By consideration of possible fiber packing geometry it can be easily shown that hexagonal fiber packing, shown in Figure 2.8, allows a maximum fiber volume fraction of 90.69%. In this thesis, the hexagonal packing geometry array of the carbon fibre composite material is adopted for further calculations.

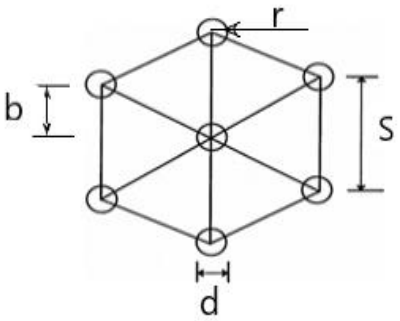

Figure 2.8: Fiber to fiber spacing in a hexagonal packing geometry.

2.2.1 Analytical methods

As mentioned before, if elastic constants of constituents of the composite material (fibre and matrix) are known, there are several approaches used for predicting values of the following elastic constants: E_1, E_2, ν_{12} and G_{12}. Usually, in all of these approaches, values of the elastic constants are expressed as function of fibre volume fraction - V_f.

i. Strength of material approach

In this approach simple analytical Equations for predicting elastic constants are developed, where the following assumptions are adopted:

1. The bond between fibres and matrix is perfect.
2. All fibres have same diameter and same distance from first neighboring fibre.
3. The fibres are continuous and parallel.
4. The fibre and the matrix follow Hooke's law (have linearly elastic behaviour).
5. The fibres possess uniform strength.
6. The fibres and the matrix are free of voids.

According to this approach, if elastic constants of fibre (E_f, v_f, G_f) and elastic constants of matrix (E_m, v_m, G_m) are known, for 'predicting' values of unidirectional lamina elastic constants, the following Equations can be used:

A. Longitudinal modulus of elasticity (E_1):

$$E_1 = E_f V_f + E_m(1 - V_f)\,. \tag{2.58}$$

B. Major Poisson's Ratio (ν_{12}):

$$\nu_{12} = v_f\, V_f + \nu_m(1 - V_f)\,. \tag{2.59}$$

C. Transverse modulus of elasticity (E_2):

$$E_2 = \left[\frac{E_f E_m}{E_m V_f + E_f(1 - V_f)}\right]\,. \tag{2.60}$$

D. In-Plane Shear Modulus (G_{12}):

$$G_{12} = \left[\frac{G_f G_m}{G_m V_f + G_f(1 - V_f)}\right]\,. \tag{2.61}$$

ii. Semi-Empirical Model (Halpin-Tsai)

Halpin Tsai Semi-Empirical Model propose that the elastic properties of unidirectional lamina can be estimated by using the following Equations**:**

(a) Longitudinal modulus of elasticity (E_1):

$$E_1 = E_f V_f + E_m(1 - V_f)\,. \tag{2.62}$$

(b) Major Poisson's Ratio (ν_{12}):

$$\nu_{12} = \nu_f V_f + \nu_m(1 - V_f)\,. \tag{2.63}$$

(c) Transverse modulus of elasticity (E_2):

$$E_2 = E_m\left[\frac{1+\zeta\eta V_f}{1-\eta V_f}\right], \tag{2.64}$$

where: $\eta = \frac{(E_f/E_m)-1}{(E_f/E_m)+\zeta}$.

(d) In-Plane Shear Modulus (G_{12}):

$$G_{12} = G_m\left[\frac{1+\xi\eta V_f}{1-\eta V_f}\right], \tag{2.65}$$

where: $\eta = \frac{(G_f/G_m)-1}{(G_f/G_m)+\xi}$.

In previous equations the term "ξ" is called the 'reinforcing factor' and depends on the following: fibre geometry, packing geometry, loading condition. For hexagonal array and circular fibre geometry for the transverse modulus of elasticity (E_2): ξ = 2(a/b). If same geometry and the same array of fibres is considered, for the In-Plane Shear Modulus (G_{12}): $\xi = \sqrt{3}Log_e(\mathrm{a/b})$, where: a is the length of the cross-section while b is the width of the cross-section in the direction of loading as shown in Figure 2.9 [35].

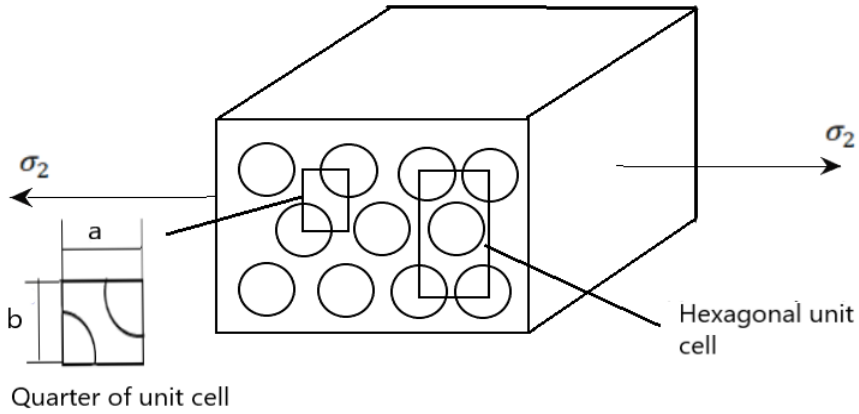

Figure 2.9: Transverse stress applied on a unidirectional lamina.

iii. Chamis Model

Chamis model, is widely used in Mechanics of composite materials for estimation of Transverse modulus of elasticity (E_2) and In-Plane Shear Modulus (G_{12}). According to Chamis model the elastic properties of unidirectional lamina can be estimated by using the following Equations**:**

(a) Longitudinal modulus of elasticity (E_1):

$$E_1 = E_f V_f + E_m(1 - V_f). \tag{2.66}$$

(b) Major Poisson's Ratio (ν_{12}):

$$\nu_{12} = \nu_f V_f + \nu_m(1 - V_f). \tag{2.67}$$

(c) Transverse Modulus (E_2):

$$E_2 = E_m\left[1 - [\sqrt{V_f}\left[1 - (E_m/E_f)\right]\right]^{-1}. \tag{2.68}$$

(d) In-Plane Shear Modulus (G_{12}):

$$G_{12} = G_m\left[1 - [\sqrt{V_f}\left[1 - (G_m/G_f)\right]\right]^{-1}. \tag{2.69}$$

2.2.2 Numerical method - FEM

Number of experimental results confirmed that proposed equations for estimating values of the elastic constants E_1 and ν_{12} are quite accurate and can be used as a quick tool for predicting these elastic constants. On the other hand, proposed Equations for predicting values of the elastic constants E_2 and G_{12} appear to be inaccurate. Therefore, numerical methods must be implemented in case when accurate estimation for elastic constants E_2 and G_{12} is required.

Here, a FEM technique has been used in order to accurately estimate values of the elastic constants E_2 and G_{12}. The properties of chosen carbon fibre and Epoxy resin materials have been presented in Table 1.1.

In numerical evaluation of the elastic properties it is assumed that:

- the fibres are arranged in a hexagonal array, as shown in Figure 2.9,
- the fibre and matrix are considered to be linear elastic materials,
- the fibre and matrix are considered to be homogenous, non-porous materials.

As shown in Figure 2.9, in hexagonal fibre array, unit cell, where b there is the half spacing between two fibres and r, is fibre radius. Then the area of the unit cell will be: $A = 2\sqrt{3}b^2$. Fibre volume fraction is defined as: $V_f = \pi r^2/\left(2\sqrt{3}b^2\right)$. The maximum achievable volume fraction is when $r = b$, and for this case: $V_f = \frac{\pi}{2\sqrt{3}} = 90.69\%$. However, this maximal theoretical limit is not achievable in practice. Geometry of unit cell is defined through dimensions of a and b when volume fraction is pre-defined. In this case these lengths a and b are defined as:

$$b = \sqrt{\pi r^2/\left(V_f 2\sqrt{3}\right)}\ , \qquad a = 2\sqrt{3}\, b. \tag{2.70}$$

The X, Y, Z coordinate system, shown in Figure 2.10, is used as reference coordinate system. The direction Z is along the fibre axis, the X direction is in the plane of the unit cell and normal to the fibres and the Y direction is normal to the plane of the unit cell and perpendicular on the fibres. It is assumed that the geometry, material, and loading of the unit cell are symmetrical concerning the X, Y, Z coordinate system. Therefore, a one-fourth portion of a unit cell is sufficient to carry out the analysis. The 3D FE mesh on the one-fourth portion of the unit cell is shown in Figure 2.11.

- **Geometry**

  The dimensions of the finite element model are taken as follows:

  $L_x = a$, $L_y = b$, and L_z= 0.01mm, are the lamina dimensions in (X, Y, and Z) directions.

- **Boundary conditions**

For evaluation the longitudinal modulus (E_1) and Poisson's ratio (ν_{12}) the load is applied, as a displacement of 0.1 μm along the fibre axis (Z-direction) as shown in Figure 2.12. Whereas, for evaluation of the transverse modulus (E_2) the load applied, as a displacement of 1μm normal to the direction of fibres (X-direction), as shown in Figure 2.13. For evaluation of the In-plane shear modulus (G_{12}) the model is created as a 3D geometry which represents a cube. The load is applied as a displacement in the right side parallel to the fibre axis in the (X-Y) plane with the value (2.7μm), and a rotation about (Y-axis) is applied, which is equal to 0.01°, as shown in Figure 2.14.

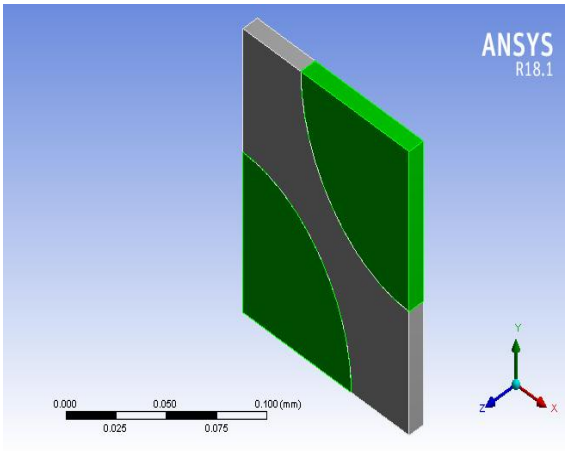

Figure 2.10: A one-fourth portion of the unit cell.

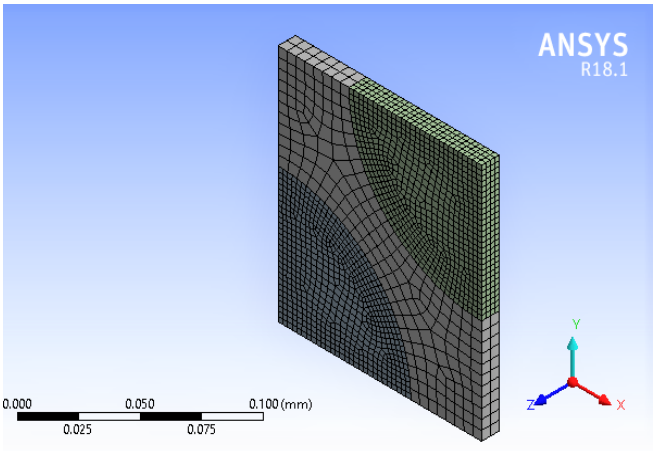

Figure 2.11: 3D Finite Element mesh on one-fourth portion of the unit cell.

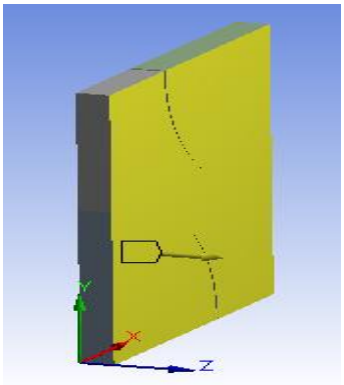

Figure 2.12: Displacement applied on the 3D model along the fiber axis for evaluating E_1 and v_{12}.

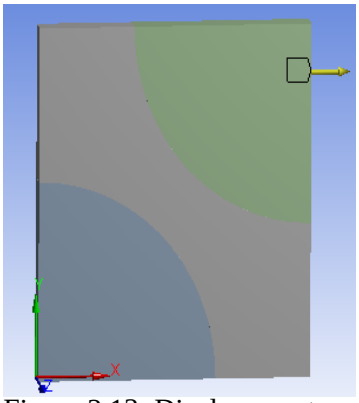

Figure 2.13: Displacement applied to the 3D model for evaluating E_2.

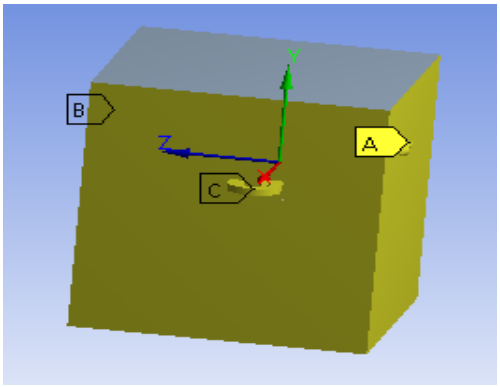

Figure 2.14: A 3D model for evaluating G_{12}.

Using a load in form of displacement (ΔL = 0.1μm) in the Z-the direction of the nodes positioned at the front the surface of the model (z= 0.01 mm), after deformation the displacement in direction X is marked by ΔL_2 (see Figure 2.12), with a condition that side surfaces have to remain parallel to their original directions, values for E, and v were obtained using following Equations:

$$E = \frac{FL}{\Delta L\, A}, \tag{2.71}$$

$$v = -\frac{\Delta L_2}{\Delta L}, \tag{2.72}$$

Where the surface area is calculated by using Equation (2.70):

$$A = 2\sqrt{3}b^2\ . \tag{2.73}$$

In previous equations, force F is obtained by summing reactions on the constrained surface, opposite to the loaded surface, area A, while: $L = L_z$ = 0.01 mm is initial length dimension.

Values for G were determined from the following Equations:

$$G = \frac{\tau}{\gamma}, \tag{2.74}$$

where: τ is the shear stress while γ is the shear strain calculated as:

$$\tau = \frac{F}{A}, \quad \gamma = 1.745 * 10^{-4}. \tag{2.75}$$

Obtained FEM results are compared with the results obtained by the strength of the material approach, Semi-Empirical model (Halpin-Tsai) and Chamis model.

- **Evaluation of longitudinal modulus (E_1)**

The results of the longitudinal modulus values, obtained by the analytical methods for varying fibre volume fractions (V_f), are compared with the FEM results as presented in Figure 2.15.

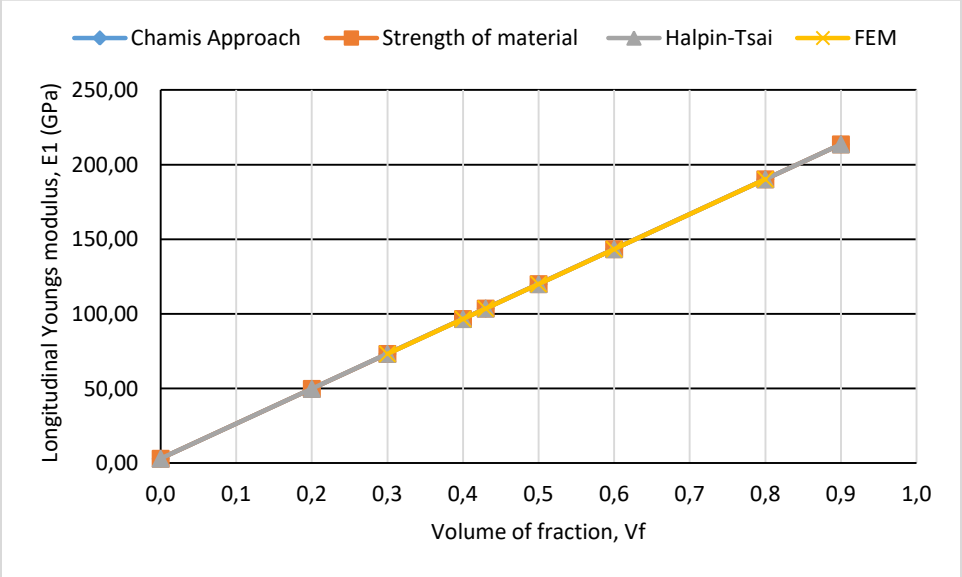

Figure 2.15: Change of longitudinal modulus E_1 with fiber volume fraction V_f.

The graph presented in Figure 2.15 clearly shows that the E_1 of the composite material is increasing linearly with varying fibre volume fraction V_f. From Figure 2.15 it is clear that FEM results for longitudinal modulus E_1 perfectly match the values obtained by analytical approaches.

- **Evaluation of Major Poisson's Ratio (ν_{12})**

The values of Poisson's ratio obtained by FEM for varying volume fractions are plotted with results, obtained by analytical methods, and are presented in Figure 2.16. The values of Poisson's ratio are decreased linearly as fibre volume fraction increases. The obtained FEM results perfectly match the values obtained by the analytical methods.

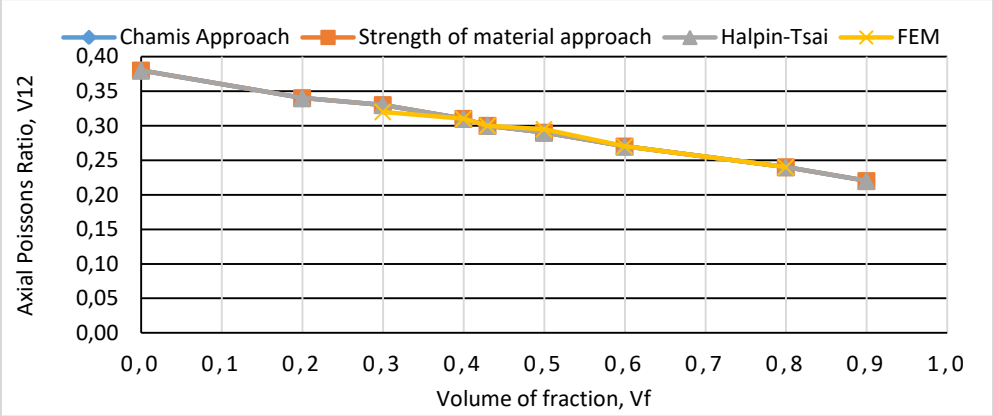

Figure 2.16: Change of Poisson's ratio ν_{12} with fiber volume fraction V_f.

- **Evaluation of Transverse Modulus of Elasticity (E_2)**

The values of the Transverse Modulus of Elasticity, obtained by FEM for different volume fractions, are plotted together with values, obtained by the analytical methods and presented in Figure 2.17. A non-linear relationship has been observed between the transverse modulus and fibre volume fraction. The values of E_2 increase by increasing fibre volume fraction. The Halpin-Tsai results are close to results of Chamis approach. Whereas, the FEM results are higher than the Halpin-Tsai results, while the strength of the material approach results is lower than the other method results.

- **Evaluation of Shear Modulus (G_{12})**

The values of effective shear modulus G_{12}, obtained by FEM, and values, obtained by the analytical methods for different fibre volume fractions, are presented in Figure 2.18. The graph presented in Figure 2.18 shows non-linear relationships between effective shear modulus and fibre volume fraction. The values of effective shear modulus G_{12} increase with increasing fibre volume fraction. It is shown that the Halpin-Tsai and Chamis are very close to FEM results.

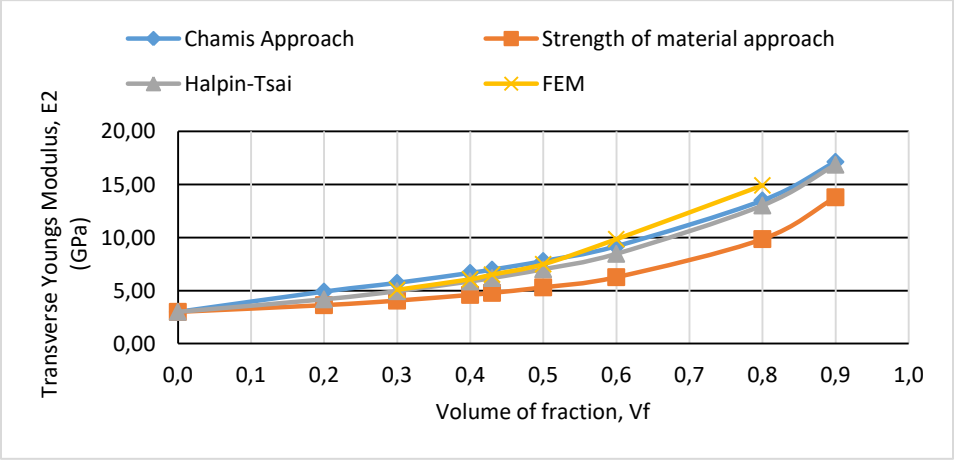

Figure 2.17: Transverse modulus E_2 with fiber volume fraction V_f.

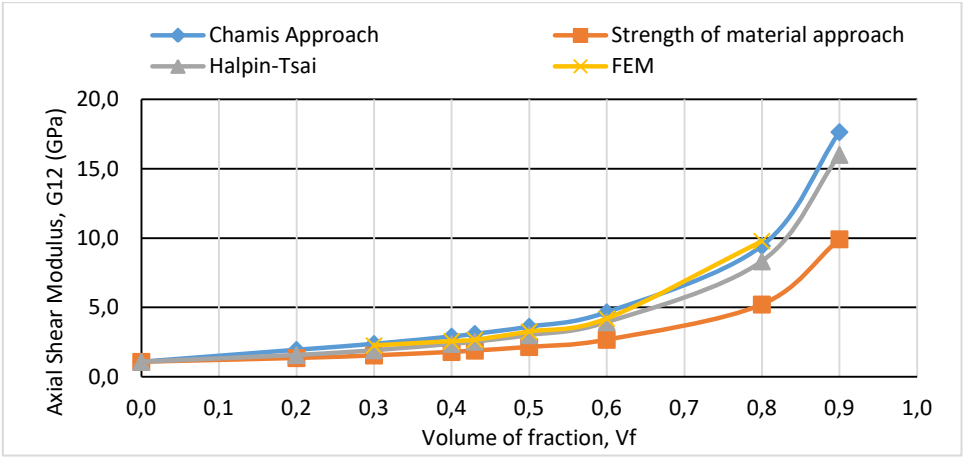

Figure 2.18: Change of Shear modulus G_{12} with fiber volume fraction V_f.

2.2.3 Strength of Unidirectional Lamina

Lamina strength parameters can be estimated based on the strength properties of fibres and matrix using principles of the mechanics of materials. The prediction of unidirectional lamina strength parameter is more difficult than a prediction of stiffness parameters since strengths are more sensitive to the material and geometry inhomogenity, the fibre-matrix interface, the manufacturing process, and the environment. Finally, the experimental evaluation is crucial in strength evaluation since it is direct and reliable.

1. **Longitudinal Tensile Strength-$\left(\sigma_1^T\right)_{ult}$**

As assumed earlier, the fibre and the matrix follow Hooke's law (have linearly elastic behaviour). Figure 2.19 shows the stress-strain curve for a unidirectional composite under uniaxial tensile load along fibres, where:

$\left(\sigma_f\right)_{ult}$ - the ultimate tensile strength of the fiber;
$(\sigma_m)_{ult}$ - the ultimate tensile strength of the matrix;
$\left(\varepsilon_f\right)_{ult}$ - the ultimate tensile strain of the fiber;
$(\varepsilon_m)_{ult}$ - the ultimate tensile strain of the matrix;

The fiber ultimate strain failure is:

$$\left(\varepsilon_f\right)_{ult} = \frac{\left(\sigma_f\right)_{ult}}{E_f} \ . \tag{2.76}$$

The matrix ultimate strain failure is:

$$(\varepsilon_m)_{ult} = \frac{(\sigma_m)_{ult}}{E_m} \ . \tag{2.77}$$

In previous Equations E_f is the modulus of elasticity of the fiber and E_m is the modulus of elasticity of the matrix. The composite tensile strength is presented by the following Equation:

$$(\sigma_1^T)_{ult} = \left(\sigma_f^T\right)_{ult} * V_f + \left(\varepsilon_f^T\right)_{ult} * E_m \left(1 - V_f\right) \ . \tag{2.78}$$

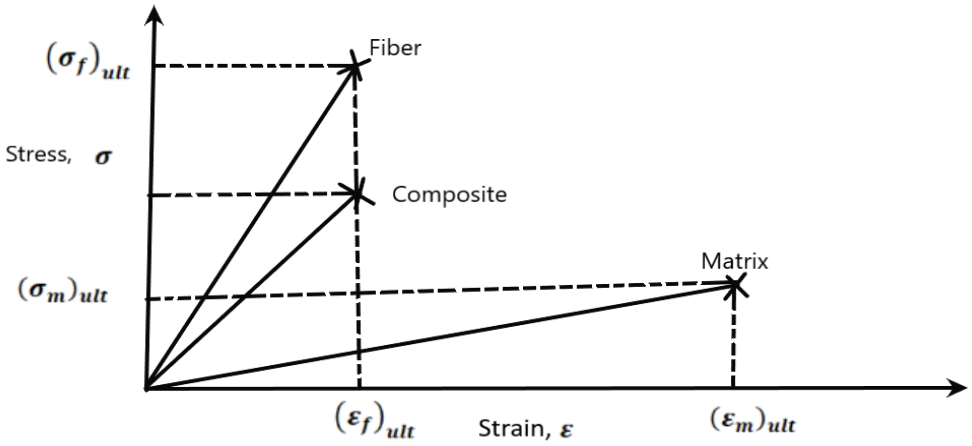

Figure 2.19: Stress–strain curve for a unidirectional composite under uniaxial tensile load along fibers.

At the moment when the fibres have been broken, the following question is arised: is the composite able to take more load? The stress, when the matrix can take a load, is given under the term: $(\sigma_m)_{ult}(1 - V_f)$. In that case only, if this stress is larger than $(\sigma_1^T)_{ult}$, in the Equation (2.78), it can have a potential for the composite to carry more load. The fibres volume fraction, possible to happen in this case, is called the minimum fibre volume fraction - $(V_f)_{min}$. This value can be calculated from the following Equation:

$$(V_f)_{min.} = \frac{(\sigma_m)_{ult} - E_m(\varepsilon_f)_{ult}}{(\sigma_f)_{ult} - E_m(\varepsilon_f)_{ult} + (\sigma_m)_{ult}} \ . \tag{2.79}$$

2. Longitudinal Compressive Strength-$(\sigma_1^C)_{ult}$

Longitudinal compressive strength cannot be expressed in the same manner as the longitudinal tensile strength, because the failure modes are different. When lamina is compressed along the direction of fibres, then failure due to tensile strains in the matrix and/or bond is dominant type of failure. Assuming that longitudinal compressive stress σ_1 is applied, the longitudinal compressive strain magnitude is presented by [35]:

$$|\varepsilon_1| = \frac{|\sigma_1|}{E_1} \ . \tag{2.80}$$

The transverse strain, which is the tensile, is presented by:

$$|\varepsilon_2| = \nu_{12} \frac{|\sigma_1|}{E_1} \ . \tag{2.81}$$

By using the maximum strain failure theory, when the transverse strain overtakes the ultimate transverse tensile strain $(\varepsilon_2^T)_{ult}$, the lamina can be considered to have failed in the transverse direction. Therefore, from Equation (2.81) we can obtain $(\sigma_1^C)_{ult}$ as:

$$(\sigma_1^C)_{ult} = \frac{E_1(\varepsilon_2^T)_{ult}}{\nu_{12}} \tag{2.82}$$

The value of $(\varepsilon_2^T)_{ult}$, can be calculated by using the mechanics of materials formula [35]:

$$(\varepsilon_2^T)_{ult} = (\varepsilon_m^T)_{ult}\left[\frac{d}{s}(\frac{E_m}{E_f} - 1) + 1\right], \quad (2.83)$$

where:

$(\varepsilon_m^T)_{ult}$ - represents the ultimate tensile strain of the matrix;
d - is diameter of the fibers;
s - is center to center spacing between the fibers.

The ratio d/s in Equation (2.83) can be related to volume fraction of fibers - V_f by following expression (see Equation (2.70)):

$$\frac{d}{s} = \sqrt{\frac{V_f 2\sqrt{3}}{\pi}}, \quad (2.84)$$

As it is known from number of scientific publications, unidirectional composite may also fail due to direct shear failure of fibers. In this case, the rule of mixtures gives the shear strength of the unidirectional composite as:

$$(\tau_{12})_{ult} = \left[\left(\tau_f\right)_{ult} V_f + (\tau_m)_{ult} V_m\right].$$

The lamina maximum shear stress under a longitudinal compressive load of magnitude σ_1 is $\sigma_1/2$ at 45° to the loading axis, thus:

$$(\sigma_1^c)_{ult} = 2\left[\left(\tau_f\right)_{ult} V_f + (\tau_m)_{ult} V_m\right]. \quad (2.85)$$

3. Transverse Tensile Strength -$\left(\sigma_2^T\right)_{ult}$

The estimation of the transverse tensile strength of a unidirectional lamina is given here with the following assumptions:

- The bond of fibre-matrix is perfect.
- Fibres have uniform spacing
- Hooke's law is applied to the fibre and matrix
- There are no residual stresses
- The stress is the same in the fibre and the matrix.

With the assumption that the lamina transverse failure depends on the matrix failure, the ultimate transverse failure strain is presented by:

$$(\varepsilon_2^T)_{ult} = (\varepsilon_m^T)_{ult}\left[\left(\frac{d}{s}\right)\left(\frac{E_m}{E_f} - 1\right) + 1\right],$$

where: $(\varepsilon_m^T)_{ult}$ is the ultimate tensile failure strain of the matrix, while ratio d/s is defined by Equation (2.84). The ultimate transverse strength is presented by:

$$(\sigma_2^T)_{ult} = E_2\,(\varepsilon_2^T)_{ult} = (\varepsilon_m^T)_{ult}\left[\left(\frac{d}{s}\right)\left(\frac{E_m}{E_f} - 1\right) + 1\right]. \quad (2.86)$$

4. Transverse Compressive Strength-$\left(\sigma_2^C\right)_{ult}$

The transverse compressive strength is usually defined as follows [35]:

$$(\sigma_2^c)_{ult} = E_2(\varepsilon_2^c)_{ult}\,, \tag{2.87}$$

where:

$$(\varepsilon_2^c)_{ult} = (\varepsilon_m^c)_{ult}\left[\left(\frac{d}{s}\right)\left(\frac{E_m}{E_f}-1\right)+1\right]. \tag{2.88}$$

In previous equations $(\varepsilon_m^c)_{ult}$ is the ultimate compressive failure strain of the matrix, while ratio d/s is defined by Equation (2.84).

5. In-Plane Shear Strength-$(\tau_{12})_{ult}$

The estimation of the ultimate shear strength for a unidirectional lamina using a mechanics of materials approach is given by [35]:

$$(\tau_{12})_{ult} = G_{12}(\gamma_{12})_{ult} = G_{12}\left[\left(\frac{d}{s}\right)\left(\frac{G_m}{G_f}-1\right)+1\right] * (\gamma_{12\mathrm{m}})_{ult} \tag{2.89}$$

Knowing the mechanical properties of selected fibre and selected matrix, presented in Table 1.1, the expected strengths of the lamina can be calculated by Equations (2.78), (2.85), (2.87), (2.88) and (2.89) while elastic properties (E_1, E_2, ν_{12} and G_{12}) were obtained numerically by FEM (see Section2.2.2). Calculated mechanical properties of the lamina material for 50% fibre volume fraction ($V_f = 0.50$) have been presented in Table 2.2.

Table 2.2: Calculated mechanical properties of the carbon fiber composite material for $V_f = 0.50$.

Discribtion	Value	Unit
Longitudinal Modulus, E_1	1.20E+05	MPa
Transverse Modulus, E_2	9.94E+03	MPa
In-plane Shear modulus, G_{12}	3.17E+03	MPa
Major Poisson's Ratio, (ν_{12})	0.30	
Ultimate tensile stress, $(\sigma_1^T)_{ult}$	2.1291E+03	MPa
Ultimate tensile stress, $(\sigma_2^T)_{ult}$	7.4221E+02	MPa
Ultimate compressive stress, $\left(\sigma_1^C\right)_{ult}$	2.10E+03	MPa
Ultimate compressive stress, $\left(\sigma_2^C\right)_{ult}$	4.0611E+02	MPa
Ultimate shear stress, $(\tau_{12})_{ult}$	8.00 E+01	MPa

CHAPTER THREE

3 Tail boom numerical model

The aim of this chapter is to define the numerical model (based on FEM) of a tail boom of lightweight aircraft, made of laminas of different orientation angles. The numerical tail boom model will be used for stress analysis and layup optimisation according to define external loads. These loads can be divided into three groups: aerodynamic loads generated due to the airflow around the tail during the flight, inertia loads, and temperature loads due to external extreme operating conditions.

3.1 Initial Tail boom specifications

The Tail boom of initial specifications are presented in Table 3.1, and the 3D drawing model is shown in Figure 3.1.

Table 3.1: Tail boom specifications

Tail boom length (mm)	3587	Vertical stabilizer length (mm)	1450
Tail boom cross-section (mm)	438x538	Vertical stabilizer width (mm)	200
Horizontal stabilizer length (mm)	1340	Maximum aircraft speed (Km/h)	180
Horizontal stabilizer width (mm)	200		

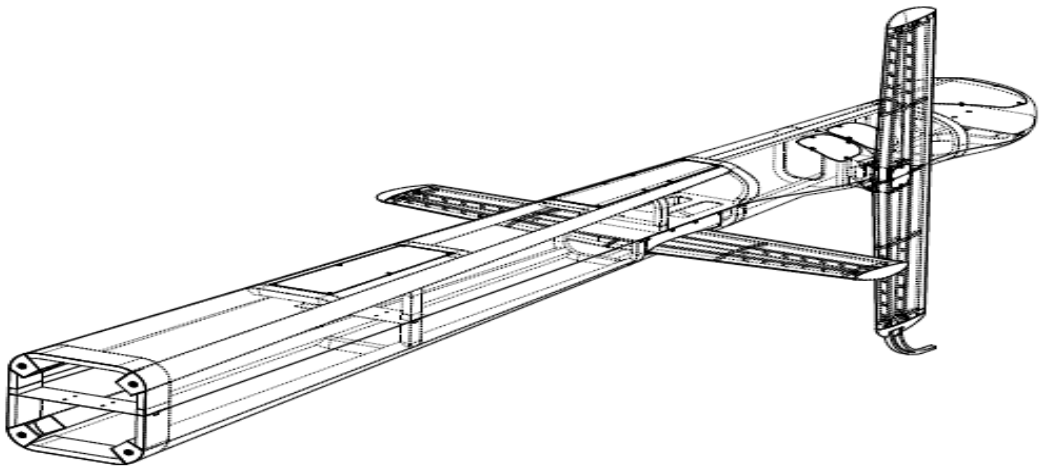

Figure 3.1: Tail boom 3D drawing.

3.2 Defining aerodynamical and inertial loads

The tail boom of the lightweight aircraft must be designed according to the desired specifications of the aircraft that include payload, size, flight range, and altitude. Nowadays, parts of flying vehicles are being built using composite materials in order to get a lightweight and strong structure. A numerical analysis of the tail boom must be carried out for the purpose of determining aerodynamic loads that will be acting on the model during the flight and finding stresses and elastic deformations as a result of these loads. Inertial loads must be considered too, and then based on maximum values of stresses and displacements of the tail boom, optimized composite structure might be suggested.

Once the 3D structure of the tail boom is defined according to defined requirements, the solution methods and boundary conditions are set for the numerical analysis. In the case of the structure shown in Figure 3.1, evaluation of aerodynamic loads acting during the flight had been carried out using classical engineering methods (not shown in this thesis) and obtained values were used to define reaction forces of the tail boom model. Besides that, the one-way and two-way FSI methods were employed for the purpose of confirmation of previously defined aerodynamic loads and easier transfer of resulting pressures to the tail boom finite element model. In past decade, FSI modeling have been widely used for analysing different types of structural parts such as: wind turbine blades, parafoils, hydrofoils, etc. (see [36], [37], [38], [39]). In the next sections, a complete procedure is presented.

3.2.1 Determination of reaction forces in a case of the classical approach

As said above, aerodynamic loads acting on the tail boom were firstly obtained using the classical approach which is not presented in this thesis since it is used only for confirmation of numerically obtained results. Loads acting on the tail boom body included the structure weight and weight of the instruments fixed on the tail boom in the case when acceleration is a=5g (requirement defined by regulations for the light aircraft). Additionally, aerodynamic forces acting on the horizontal and vertical stabilizer (see Figure 3.1) due to airflow were estimated and considered. The idea was to get the force reactions in the tail boom supports and then to compare these values with values of reactions obtained in the case of 1-way and 2-way CFD analysis of the same structure.

Forces that act on the model of the tail boom are presented in Figure 3.2 and shown in Table 3.2, and they are as follows: the first five forces represent inertial loads (weights) of different equipment attached to the tail boom. Points of action of these forces are determined according to the CG positions of the equipment. Thus, inertial force number one (F1) is acting in Z-direction at a point (A) on the structure, which is the position of the front main frame of the tail boom. The force number two (F2) is acting at a point (B) of the tail boom in the Z-direction; force number three (F3) is acting in Z-direction at a point (C) in the middle of the tail boom near the horizontal stabilizer. The force number four (F4) is acting on a point (D) on the rear side of the tail boom in the Y-direction; finally, force number five (F5) is acting in the Z-direction on the tail boom body near the vertical stabilizer.

Next six forces are aerodynamic forces that act on the horizontal (HR) and vertical (VR) stabilizer of the tail boom and they are numbered as follows: F6 (HR), F7 (HR), and F8 (HR) act in the Z-direction. while F9 (VR), F10 (VR), F11 (VR) act in the Y-direction. Magnitudes of these forces are presented in Table 3.2.

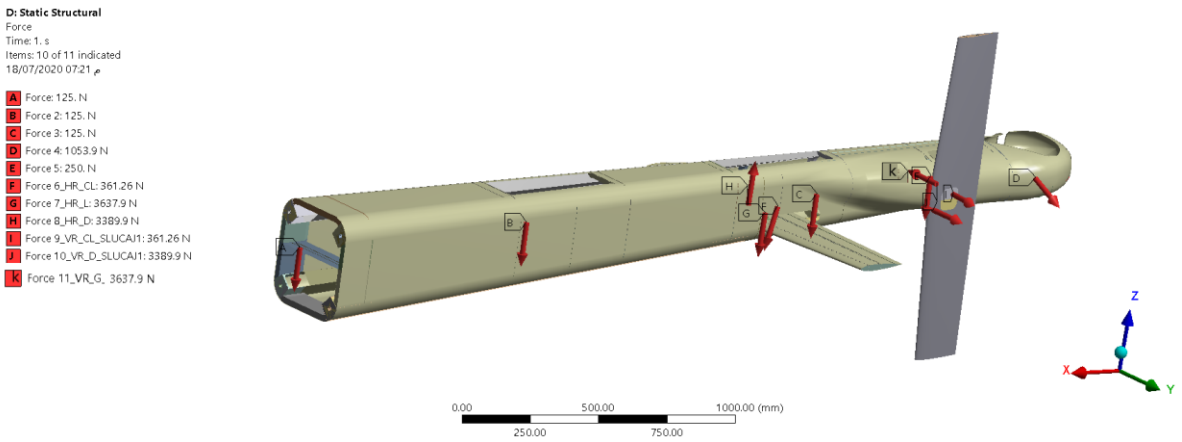

Figure 3.2: Forces acting on the tail boom body**.**

Table 3.2: Forces acting on the tail boom model (obtained in the weight and aerodynamical analysis)

Force number	Value (N)	Acting direction
F1	-125.00	Z-direction
F2	-125.00	Z-direction
F3	-125.00	Z-direction
F4	+1053.90	Y- direction
F5	-250.00	Z-direction
F6 (HR)	-361.26	Z-direction
F7 (HR)	-3637.70	Z-direction
F8 (HR)	+3389.90	Z-direction
Total force (HR)	-600.10	Z-direction
F9 (VR)	+361.26	Y-direction
F10 (VR)	-3389.90	Y-direction
F11 (VR)	+3637.90	Y-direction
Total force (VR)	+600.10	Y-direction

3.2.2 Values of reaction forces in a case of the classical approach

The tail boom is attached to the aircraft body by four joints, at positions 1-4 shown in Figure 3.3 and they are as follow: joint number (1) is the top left joint; joint number (2) is the top right joint; joint number (3) is the bottom left joint, and joint number (4) is the bottom right joint. Loads shown in Figure 3.2 and Table 3.2 caused force reactions at the positions of four joints (fixed supports). The values of the total force reactions are presented in Table 3.3.

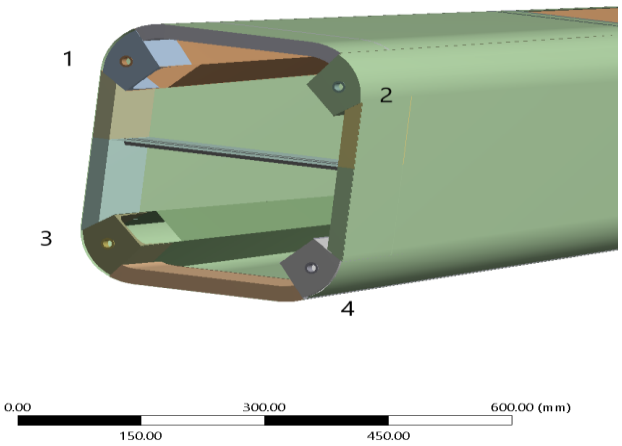

Figure 3.3: Tail boom connecting joints.

- **Finite element analysis (FEA)**

The defined model shape which used in the analysis to determine the values of the force reactions that acting on the Tail boom model fixing joints has presented in Figure 3.4.

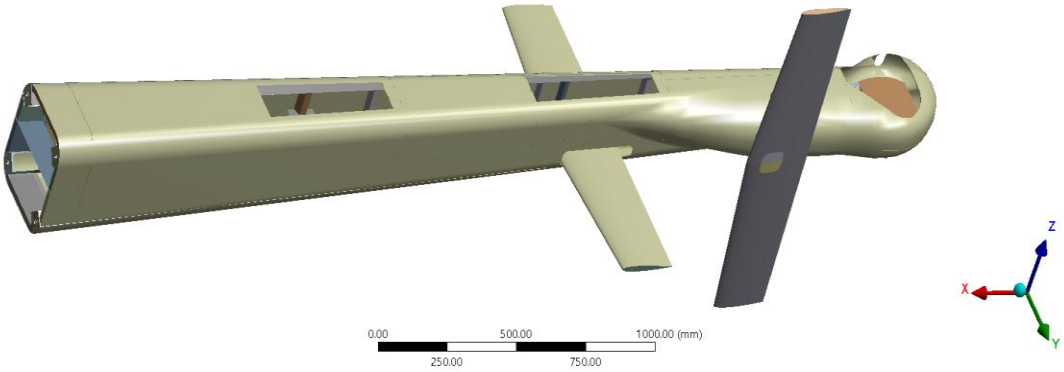

Figure 3.4: Tail boom model used in the analysis.

- **Boundary conditions**

The given load forces have been used in this analysis as presented in Table 3.2, the geometry was imported in a finite element software Workbench, the model's material has set as default material which was structural aluminium. Then, the model has been meshed as follows: the meshing size of the four fixing joints was chosen as a body sizing with 2mm due to the important parts of the analysis for determining the force and moment reactions that acting on these joints. Whereas, the meshing size of the tail body has been chosen as a face meshing sizing with 4mm in order to save meshing and analyzing time. After meshing procedure the number of meshing nodes obtained was 677419, while the number of elements was 541656 as shown in Figure 3.5. Then, fixed supports were applied on to the four connecting tail joints, and the output results were set as force reactions for the four fixing joints.

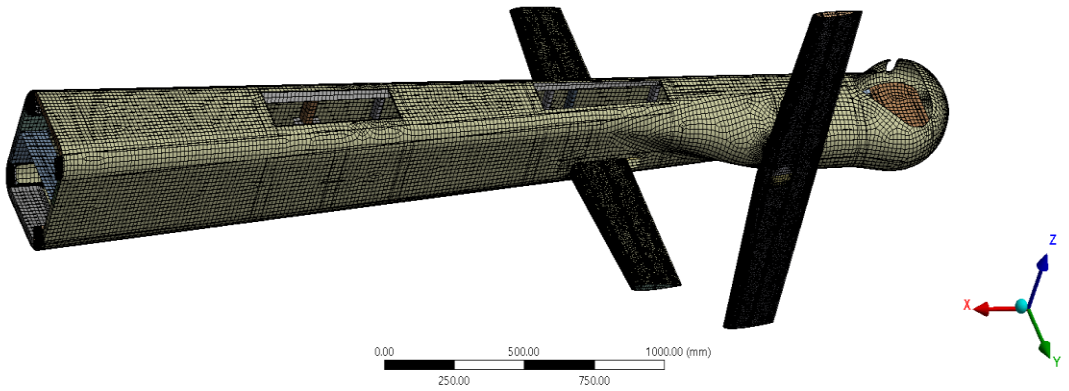

Figure 3.5: Tail boom meshed model.

- **Results**

Once the geometry is imported into the finite element method, the boundary condition have set, and the output results have been chosen as mentioned above. The results of the maximum total force and moment reactions which have been evaluated in this analysis were presented in Table 3.3.

From the results presented in Table 3.3, the maximum total force reaction was 16,030.00 N on joint number (4). The joints (1) and (2) are subjected to tension forces, whereas the joints (2) and (4) are subjected to compression forces. These values will be later compared to reactions in obtained after transferring loads from CFD analysis.

Table 3.3: Values of maximum total force and moment reactions acting on the Tail model

Joint number	Maximum total force reactions (N)	Acting direction
1	+14,847.00	X-axis
2	-1,729.80	X-axis
3	+2,467.80	X-axis
4	-16,030.00	X-axis

3.3 Numerical evaluation of aerodynamic loads using one-way and two-way FSI analysis

In this section aerodynamic loads are evaluated analyzing interaction of deformable structure with movable surrounding fluid through Fluid-Structure Interaction (FSI) coupling, using so-called one-way and two-way FSI modeling. As mentioned before, the aim of Coupling fluid/structure simulations is to obtain accurate prediction of the external aerodynamic loads acting on composite tail boom structure. In brief, short description of FSI modeling is given below.

3.3.1 One-Way FSI

In a one-way FSI analysis, the results of the CFD (Computational Fluid Dynamics) analysis at the fluid-structure intersection are transmitted and applied as loads to the mechanical analysis, but the results of the mechanical analysis are not returned back to fluid analysis. One-way transmit is suitable when the aerodynamic loads generate deformations which are not large and therefore will not produce a large affect on fluid analysis.

3.3.2 Two-Way FSI

In a two-way FSI modelling, the results of the CFD analysis at the fluid-structure intersection are moved and used as loads to the mechanical model, whereas the latest computed displacements at the intersection are returned back to the CFD analysis. Two-way FSI is suitable when the aerodynamic loads can generate such deformation that, when implemented in the fluid analysis, would largely affect results.

3.3.3 Modelling procedure

In the FSI analysis, the primary applied loads are calculated from the previous CFD model, which is transmitted to the transient structural model as first loads. Initial material properties of structural model (tail boom) is chosen to be classical material usually used in aircraft industry - aluminium. After that, the mechanical results have transmitted to the coupling model, which is connected to an additional CFD model in order to transfer the data between them to compute the results. The fluid region is solved until the force convergences are obtained. The calculated forces at the structure boundaries are then translated to the structure side. The structured side is calculated until the convergence criterion is reached. After that, the fluid flow for the next time step is calculated to convergence. The solution is finished when the maximum number of time steps is attained.

3.3.4 Coupling

In one-way and two-way coupling procedures, the results based on the individual method, where single solutions for the different physical fields, are obtained. One field that has to be solved is fluid dynamics, the other one is structure dynamics. At the boundary between fluids and solids, the fluid-structure intersection, the data of the results is shared between the fluid solver and structure solver. The information exchanged depends on the coupling procedure. To ensure that the steady-state of the model has reached, the number of iterations that has been used in the analysis is set as let us say 1200, so the time steps are 10 seconds, and sub-time steps are 0.012 seconds.

- **One-way system coupling**

The system coupling component was utilized to execute coupling between the CFD and FEA. The system coupling setup was defined to be the same for the CFD Fluent transient and FE modules. Two files of data transfers were formed for the two-way FSI analysis with a fluid-solid interface included of the whole model surfaces as the region of contribution from the FEA. In the data transfer procedure, the fluid force (pressure force) was transmitted from the CFD model at the structure region to the fluid-solid interface region of FEA. The sequence of data transfer was accountable for transferring the incremental displacement at the fluid-solid interface region in the FEA to the structure region as mesh displacement in the CFD. In the Fluent (Pressure load) simulation of the CFD model is solved to provide the initial pressure force on the structure's support, which is transferred to the specified fluid-solid interface in the structural model as the initial load on the support region. Then the

system coupling is started by transferring the displacement data, which occurred by the initial pressure load in FEA through the specified fluid-solid interface region in the structural model is transferred to the CFD of a transient. The system coupling implements mesh deformation with the selection mesh deformation settings. The process is repeated for the number of defined coupling iterations until the accomplishment of all the coupling steps. Figure 3.6, represents the flowchart of the one-way system coupling [40].

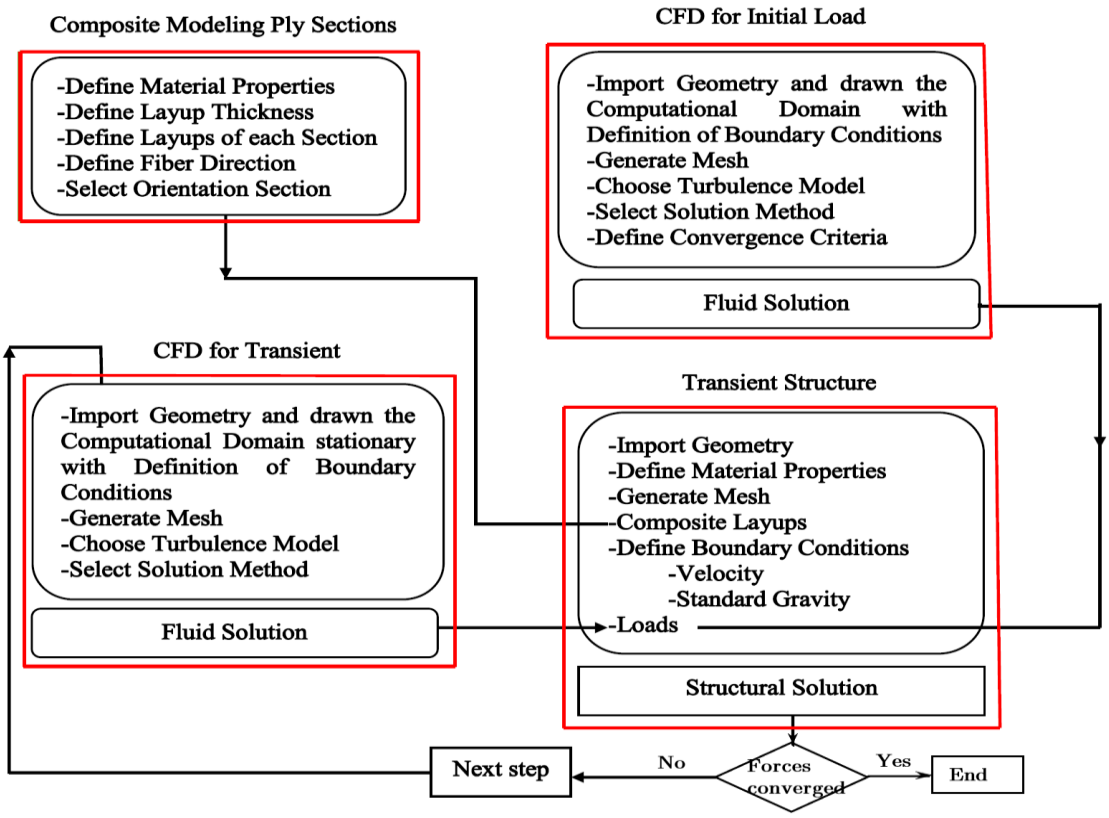

Figure 3.6: One-way system coupling flowchart.

- **Two-way system coupling**

The two-way system coupling runs by transferring displacement data created by the initial pressure load of fluent in the FEA to the CFD of the transient analysis. The deformations of the structure which have occurred in the maximum air speed according to results of one-way FSI, which drives us to execute an extra simulation for two-way FSI. The simulation configurations of two-way system coupling consist of the two main steps:

Step one, the time step size, finishing time, and the minimum/maximum of coupling iterations number at each step. In general, aside from coupling iterations at each step, the required information is automatically transferred to system coupling as soon as the solvers have been coupled.

Step two, data transfer is the most important part of the system coupling, because of incorporation and managing the data transfer sequence between the two numerical solvers, which are the Fluent to Mechanical and Mechanical to Fluent.

The process is repeated for the number of defined coupling iterations until the completed all of the coupling steps. Two-way system coupling simulation was performed for obtaining the more accurate results. Figure 3.7 describes the two-way system coupling flowchart [40].

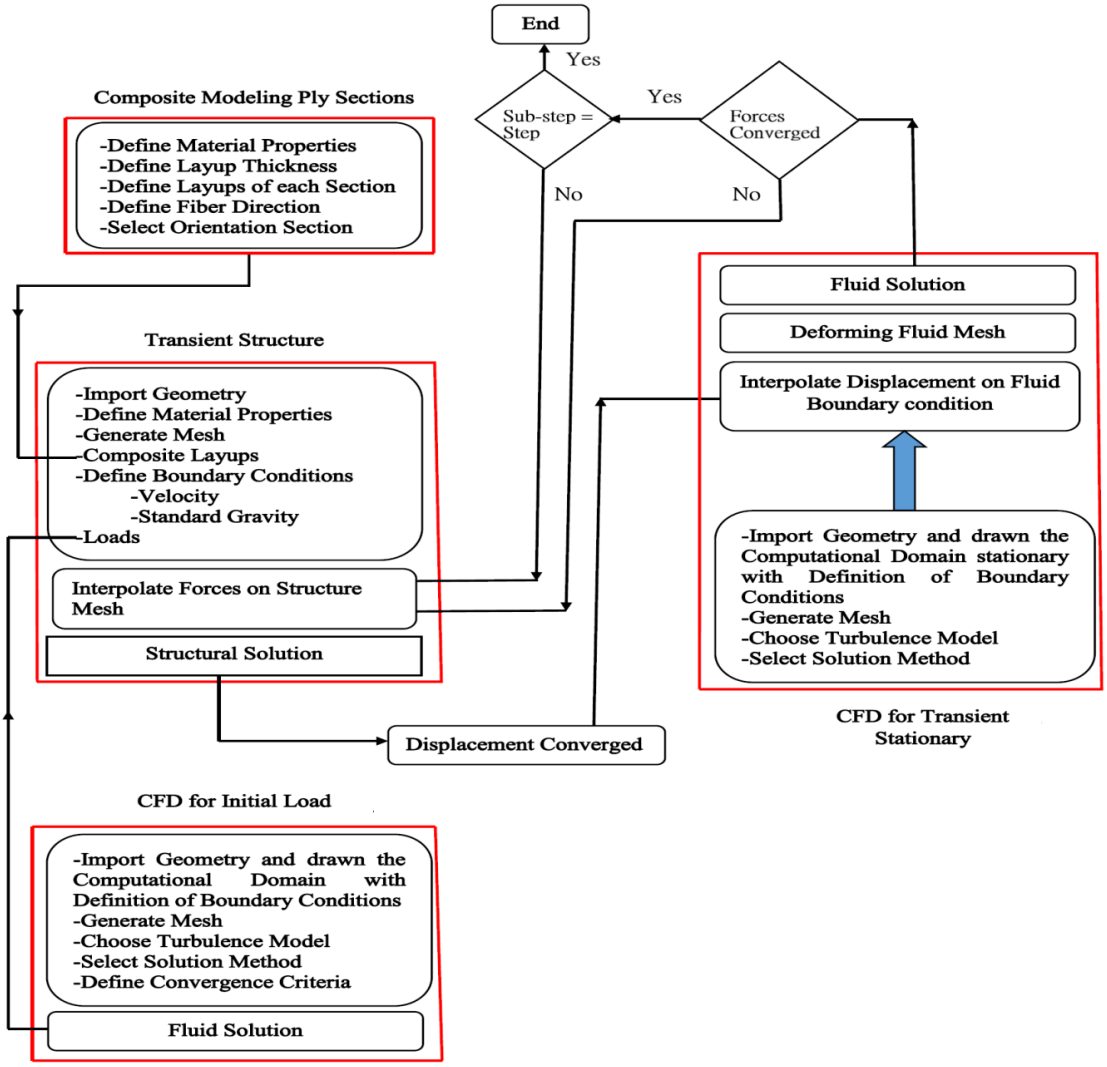

Figure 3.7: Two-way system coupling flowchart.

3.3.5 Applied methodology for obtaining the aerodynamic loads on stabilizers

The following steps have been done in the investigation of the aerodynamic loads that act on the tail boom stabilizers.

i. Modeling of the fluid field around the tail boom stabilizers

The modelling of the tail boom stabilizers, shown in Figure 3.1, includes making a solid model over its exterior surface. For a CFD analysis, the body should be enclosed in a continuum (field) which is representing fluid, wherein the boundary conditions are applied. This field around the stabilizers is made in CAD/CAM software and is importing into Ansys Workbench. In the case of the tail boom, the enclosed space is made around stabilizers since we want to evaluate aerodynamic loads on them only, and then to compare reactions at joints with previously estimated values (given in Table 3.3). If the difference between reactions is satisfactory small, we can consider CFD analysis to be well carried out.

The length of the enclosure around the stabilizers (Figure 3.8) is eight times the length of the vertical stabilizer, which is in total 12 meters, with a frontal distance between the enclosure inlet and the centre of the stabilizers about one-fourth the total enclosure length. The distance between the stabilizers and the outlet of the enclosure is then three-fourths the total enclosure length. The width and the height of the enclosure make a square with dimensions two times the stabilizer length, which is 3x3 meters. As can be seen in Table 3.3, this provides enough space for the airflow around the stabilizers by keeping them away from the enclosure surfaces to achieve steady-state flow.

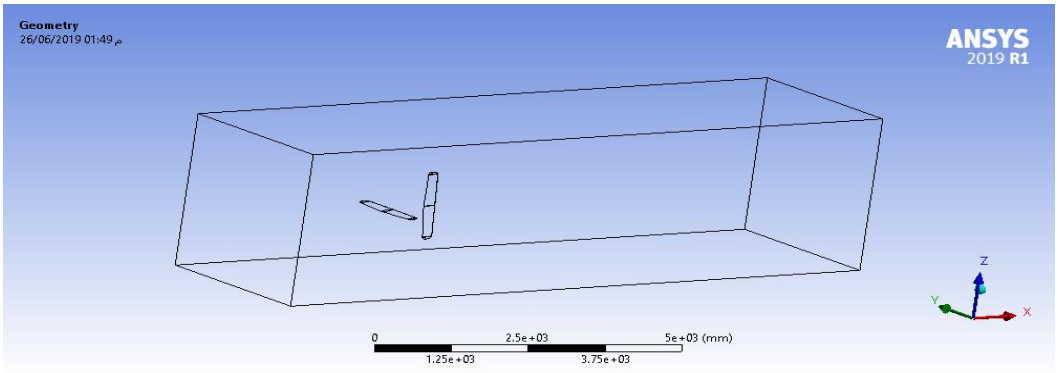

Figure 3.8: Enclosed space around the horizontal and vertical stabilizer.

Then, the bodies of stabilizers must be subtracted from the enclosure (using Boolean algebra) to get the continuum of fluid. After that, continuum must be meshed, as shown in Figure 3.9. The mesh in the area where fluid is in the contact with stabilizers must be refined (thus, an average size of 5 mm was used) since this is the most critical area for fluid-structure influence analysis, while the rest of the continuum can be meshed with coarse mesh (average size of element 15mm) to save computational time. The difference between the element sizes can be clearly seen in Figure 3.10, which gives a cross-sectional view of the mesh around "the holes" in the airfield that represent positions of vertical and horizontal stabilizers.

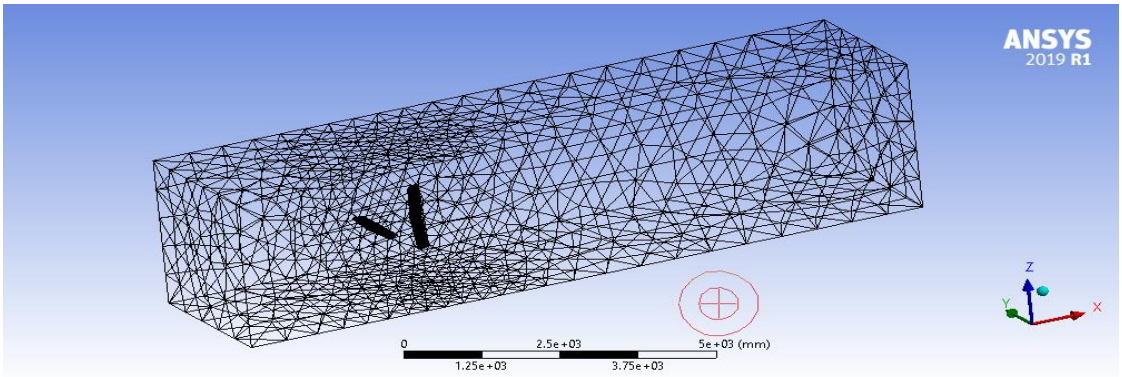

Figure 3.9: Meshing of the enclosure around stabilizers.

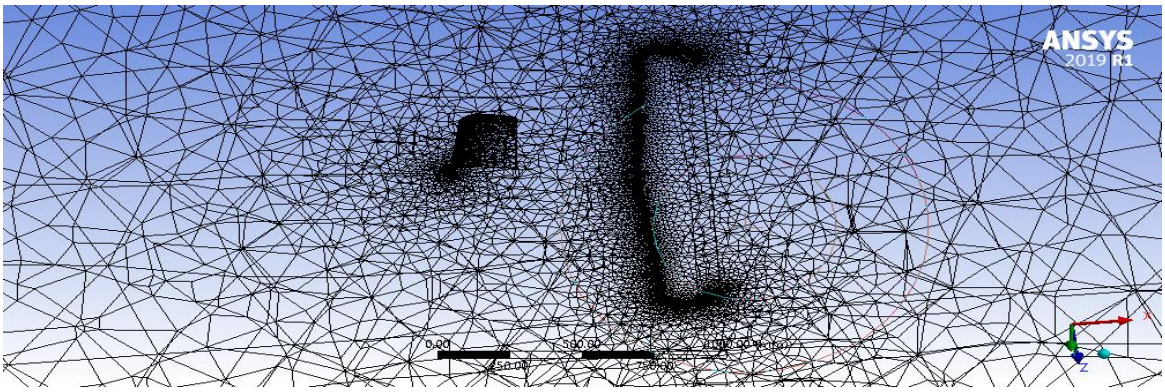

Figure 3.10: A cross-section in the continuum shows the element size difference between the area around stabilizers and the rest of continuum.

After the continuum is meshed, surfaces representing inlet, outlet, the plane of symmetry, walls, and wetted surfaces of stabilizers must be defined. Then, the next step is to define the properties of a fluid, i.e. appropriate model for fluid flow simulation.

ii. Model for CFD simulations

The (k- ω) model has been used for this kind of simulation. This is a two-equation model in which one equation matches the turbulent kinetic energy (k) and the other is the specific dissipation rate (ω). Two CFD simulations have been used in the fluent analysis, in the first CFD, only the imported pressure has been used as a primary load for the structural model in static structure models. The second CFD has been used with the transient structural model connected by system coupling in the Two-way FSI analysis.

iii. Material for CFD simulation

The working fluid in this simulation is air and is considered to flow around the stabilizers through the continuum. Only the density (ρ=1.225 kg/m^3) was taken as the material property of the air.

iv. Boundary Conditions

The boundary conditions that must be defined in an external flow analysis are velocity at the inlet of the continuum and pressure at the outlet of the continuum. According to the requirements for the light aircraft with the geometry of tail boom shown above, the cruising speed in flight is 180 km/h, while the maximum speed is 270 km/h, or approximately 75 m/s. Thus, at the inlet, the velocity of 75 m/s was defined, as well as the direction of fluid flow (normal to the inlet surface). On the other side of the continuum, outlet pressure with gauge pressure 0 Pa was defined representing the fact that the airflow is simulated at the absolute pressure of 1atm (the purpose of the light aircraft is surveillance of inaccessible terrain, so it will fly closer to the ground, at maximum altitude H=1000 m). The other faces of the continuum are named as wall or symmetry, which means that these faces are under no-slip condition i.e. there is zero velocity on them.

3.3.6 Results of CFD simulations (evaluated forces on stabilizers)

The results obtained using the one-way and two-way FSI analysis are presented in Table 3.4. Values in Table 3.4 indicate that these two analyses gave significantly different results. In the case of one-way analysis total force in the negative Z-direction on the horizontal stabilizer is 337 N, which is

around 50% less than the value obtained in two-way simulation (684 N). If we compare these two values with values obtained in the classical aerodynamical approach (presented in Table 3.2), we can see that two-way analysis gives a much better prediction (684 N compared to 600 N). On the other hand, the one-way analysis produced a total force of 250 N in the positive Y-direction on the vertical stabilizer, while two-way analysis gave 507 N in the same direction. Comparing these values with value in Table 3.2 (600 N), it is clear that two-way analysis again gives a better prediction. Anyhow, the conclusion that can be drawn is that two-way analysis should be used in simulations but let us not forget that this kind of analysis is computationally expensive and time-consuming.

Table 3.4: Forces acting on the tail boom stabilizers obtained in one-way and two-way FSI analyses

Force number	Value (N)		Acting direction
	One-way	Two-way	
F6 (HR)	+76.00	+153.00	Z-direction
F7 (HR)	-136.22	- 284.07	Z-direction
F8 (HR)	-156.64	-337.00	Z-direction
Total force (HR)	-337.00	-684.00	Z-direction
F9 (VR)	+51.20	+ 102.00	Y-direction
F10 (VR)	+152.74	+ 335.53	Y-direction
F11 (VR)	+72.20	+ 146.43	Y-direction
Total force (VR)	+250.20	+507.00	Y-direction

3.3.7 Evaluation of reactions on tail boom under loads imported from CFD analysis

Similar to calculations carried out with loads obtained in classical aerodynamical analysis and presented in Section 3.2.2, the FE model of tail boom was used to calculate the force reactions at joints shown in Figure 3.3 using values from CFD analysis. Loads were imported from the two-way analysis since it gave predictions closer to the classical approach. Results are presented in Table 3.5.

Table 3.5: Force reactions obtained for loads imported from CFD analysis

Joint number	Maximum total force reactions (N)
1	+13,702.0
2	- 823.00
3	+ 3,778.30
4	-16,795.00

Comparing values in Table 3.5 with values in Table 3.3, it can be seen that the force reactions at 4 joints, are similar and that no significant difference occurs. This justifies the use of CFD simulations in evaluation of loads acting on the tail boom and proves that all boundary conditions in fluid flow analysis have been defined well. Therefore, in the next steps (and chapters of this thesis) only results from CFD will be used as inputs.

3.4 The influence of porosity in composite material on elastic properties

As mentioned before porosities or voids are the most studied type of manufacturing defect [41], [42], [43]. This section aims to present the study the influence of void content on the elastic properties of matrix materials used as a binder in Fibre-Reinforced Composites (FRCs), by using the FEM.

3.4.1 The effects of the manufacturing defects on the mechanical properties

Manufacturing defects are one of the main factors that affect the mechanical properties of FRCs. Defects can be classified, based on their location, into the matrix, fibre, and interface defects. Fibre defects include fibre waviness, misalignment, and broken fibres, whereas the interface defects include initial fibre/matrix de-bonding and inter-laminar delamination, and matrix defects include incomplete matrix cure and voids. Voids are one of the most important defects.

3.4.2 Void formation

Void content is defined as the volume fraction of the voids in the composite material (mainly in matrix), usually reported in percent (%). The pecentage of voids in FRCs is influenced by the manufacturing process, reinforcement structure, stacking sequence (i.e. different stacking sequences, caused not only different void content, but also different shapes, sizes, and distributions of void, [44]).

3.4.3 Modelling procedure

In order to simulate such a microstructure fully, a three-dimensional (3D) model of a random distribution of particles and pores is required. A comparative evaluation of newly developed three-dimensional (3D) multi-pore numerical model (MPUC) versus two-phase unit cell (FCC) models, which were used for predicting porous material elastic constants (E, G, and ν) is carried out. The distribution of pore is idealized by random distribution and orientation of approximately 30 to 150 pores of the same size, which are represented here by the MPUC model. The irregular shape of porosity, appearing in real microstructure, is idealized as cylinder geometry shape with randomly chosen orientation, while intersecting of pores is not allowed, as shown in Figure 3.12a, 3.12b, and 3.12c. The aspect ratio length to diameter - L/D of the cylinder (Figure 3.12d) was chosen to be 1,2,5, and 10 respectively, while the diameter of pores was chosen to be D=1μm [45].

In the two-phase FCC porosity cell, there is one-spherical porosity at each corner and one-spherical porosity in each face of the cube cell, as shown in Figure 3.11. A model, consisting of a multi-pore in the unit cell (MPUC), differs from the previously mentioned one, by the fact that the number of pores with a fixed aspect ratio of L/D and pores orientation is randomly chosen. This fact contributes to as close as possible real microstructure representation. The assumptions for both models are: (1) the elastic properties of the material are linear; (2) the material is isotropic; (3) all spherical and cylinder-like pores are of the same size; and (4) the material will not fail at the prescribed loads. Due to the symmetry of the unit cell and the applied loads, as well as adopted isotropic material properties, the models were reduced to one-eighth of the unit cell, as shown in Figures 3.13(a) and 3.13 (b).

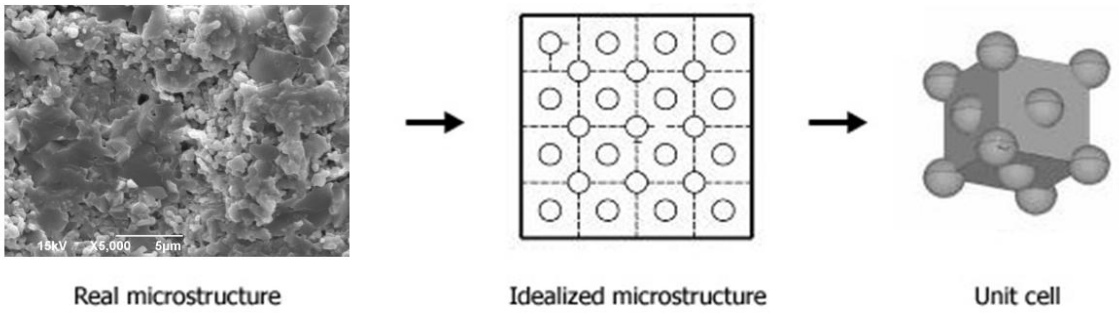

Figure 3.11. The idealization of the random pore distribution, shape, and size by arranging the pores on a FCC packing array [45]

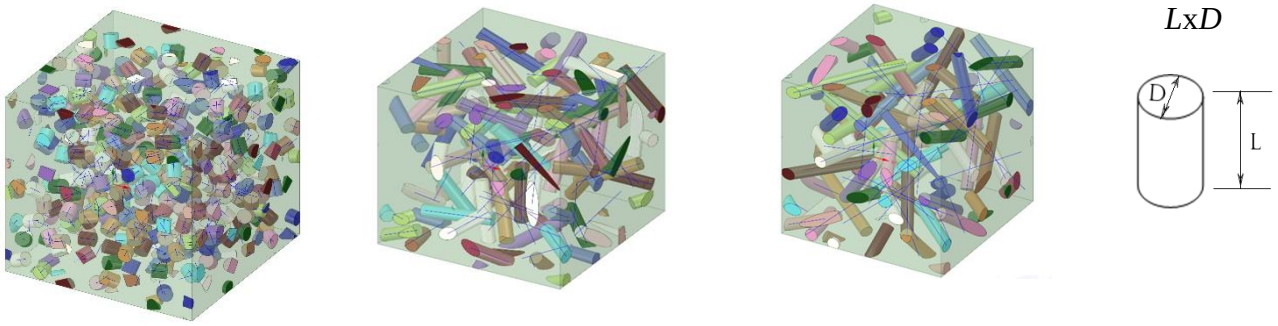

(a) (b) (c) (d)

Figure 3.12. MPUC model with 10% of porosity volume fraction (V_p): (a) L/D=1, (b) L/D=5, (c) L/D=10 and (d) dimensions of cylinder [45].

The different percentages and shapes of voids with different aspect ratios were considered in creating the models, as shown in Figures 3.12(b) and 3.12(c). The models are considered by introducing boundary conditions, which constrain the unit cell to remain in its original shape (cube). After loading, the sides remain parallel and orthogonal, but change in length. The unit cell is loaded in compression along the vertical y-direction with the adequate displacement steps. The local coordinate system aligns with the global one. The dimensions of reduced unit cells, presented in Figure 3.12, are 30×30×30μm. All (3D) FE models were produced using Ansys Workbench. The elements used are 10-node tetrahedral structural solid elements (an option of 20-node solid brick elements). A representative FE grid for evaluation of compressive stiffness with the porosity volume fraction V_p =0.134, shown in Figure 3.13a, contains 67453 elements and 95764 nodes. Each node has three degrees of freedom corresponding to the three degrees of translation. The material properties used in FE analyses, adopted from literature [45] and [46], were: E = 16,04GPa, ν = 0.124. It should be noticed that numerical simulations for MPUC models with aspect ratio L/D=10 were restricted to an upper level of $V_P = 0.17$, since the intersection of pores dramatically increases, which directly influences the major condition when the intersection of cylinders (pores) was not allowed. For other aspect ratios: 1, 2, and 5, numerical simulations for MPUC models were restricted to an upper level of $V_p = 0.2$.

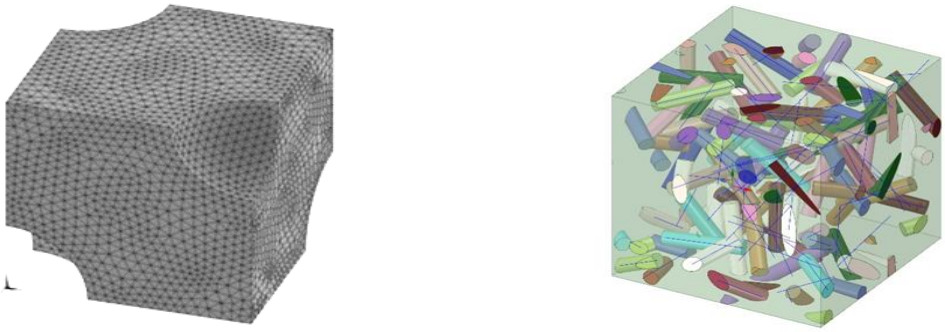

(a) (b)

Figure 3.13: FE grid of unit cell with 13,4% of porosity volume fraction (V_p): (a) FCC model and (b) MPUC model [45].

3.4.4 Numerical solution

The void formation was simulated by creating 28 different models of three-dimensional multi-pore unit cell model versus two-phase unit cell models which were used for predicting elastic constants (E, G, and ν) of porous material. Again, FEM has been used in order to investigate the effect of void content on the elastic properties of composite material. The void content was introduced in the models and is defined as the volume fraction of the pores V_p in the composite in percentage, shown in Figure 3.12a.

Using a load in form of displacement Δ=0,3 μm in the y-direction of the nodes positioned at the upper surface of the cube (y=30μm) Figures 3.12a and 3.12b, with such a condition that side surfaces have to remain parallel to their original directions, values for E and ν were obtained using following equations:

$$E = \frac{FH}{\Delta A} \tag{3.1}$$

$$\nu = -\frac{\Delta^{side}}{\Delta} \tag{3.2}$$

Force F is obtained by summing reactions on the constrained surface, opposite to the loaded surface, area A is 900 μm^2, H=30 μm represents a cube dimension, and Δ is displacement in the y-direction. After deformation, lateral displacement is marked by Δ^{side}.

Values for G have been determined from the following equation:

$$G = \frac{E}{2(1+\nu)} \tag{3.3}$$

Numerical solutions for different volume fractions of pores of compressive Young's modulus of elasticity (E), shear modulus (G), and Poison's ratio (ν) obtained by the MPUC model for different aspect ratios, are presented in Figure 3.14, Figure 3.16, and Figure 3.17.

3.4.5 Results and discussion

The values of elastic properties, obtained by the MPUC model for different aspect ratios and porosity volume fraction V_p(%), are presented in Table 3.6.

- **Young's modulus of elasticity (E)**

A variation of the Young's modulus has been observed and the results have shown that the values of Young's modulus have gradually decreased as the values of the void content have increased, whereas a slight decrease in the Young's modulus has noticed as the aspect ratios have increased as shown in Figure 3.14.

Table 3.6: Mechanical constants with different aspect ratios and pores content

L/D = 1				
Porosity volume fraction V_p(%)	5.65	10	13.4	17
Modulus of elasticity E (MPa)	14180	12873	11924	10968
Shear modulus G (MPa)	6279	5676	5233	4795
L/D = 2				
Porosity volume fraction V_p(%)	5.65	10	13.4	17
Modulus of elasticity E (MPa)	14166	12844	11884	10886
Shear modulus G (MPa)	6265	5651	5203	4747
L/D = 5				
Porosity volume fraction V_p(%)	5.65	10	13.4	17
Modulus of elasticity E (MPa)	14100	12733	11784	10869
Shear modulus G (MPa)	6221	5581	5147	4679
L/D = 10				
Porosity volume fraction V_p(%)	5.65	10	13.4	17
Modulus of elasticity E (MPa)	14086	12671	11676	10822
Shear modulus G (MPa)	6209	5541	5081	4661

Numerical solutions for the different volume fractions of pores of the compressive Young's modulus of elasticity (E), obtained by FCC and MPUC models, were compared in Figure 3.15. The normalized values for modulus of elasticity presented for MPUC have averaged values, obtained for all aspect ratios considered. From the presented results it is obvious that the MPUC model slightly underestimates values for the modulus of elasticity when comparing to the values obtained by the FCC model.

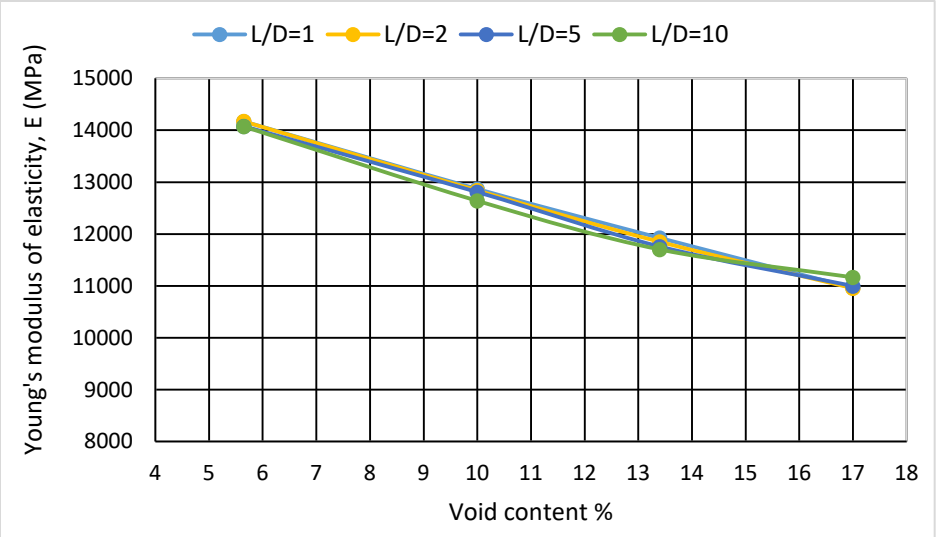

Figure 3.14 The variation of modulus of elasticity (E) with different values of void contents and aspect ratios.

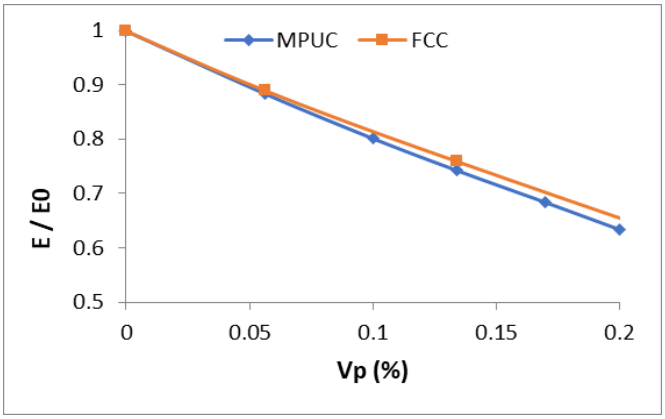

Figure 3.15. A comparison between compressive Young's modulus of elasticity (E) obtained by FCC and MPUC models.

- **The shear modulus (G)**

The values of shear modulus (G) obtained are plotted in a graph. The values of shear modulus (G) have decreased by increasing the void volume fraction, and a slight decrease in the shear modulus has been found as the aspect ratio has increased, as shown in Figure 3.16.

- **Poisson's ratio (v)**

The values of Poison's ratio (ν), which have been evaluated with different aspect ratios and porosity volume fractions as well, are presented in Figure 3.17. A gradual increment relationship has been observed between the Poisson's ratio (ν) and porosity content. The Poisson's ratio values have increased by increasing the void content whereas a slight increment has been observed by increasing the aspect ratio.

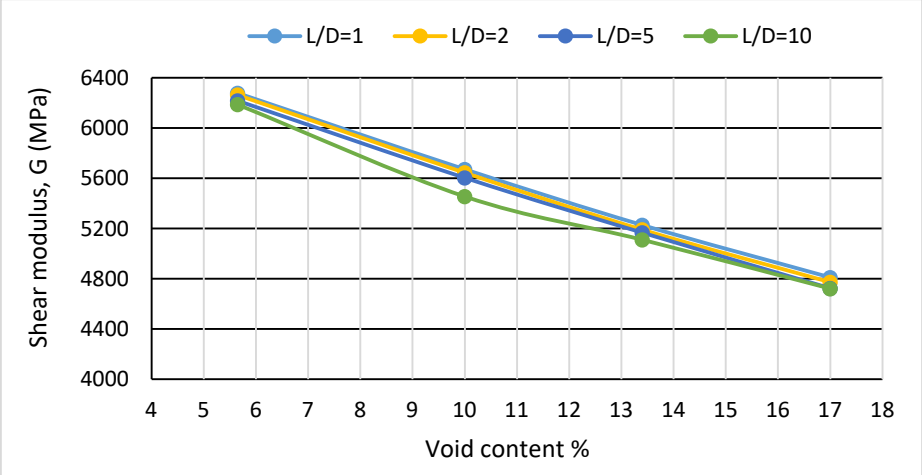

Figure 3.16: The variation of shear modulus with different values of void contents and aspect ratios.

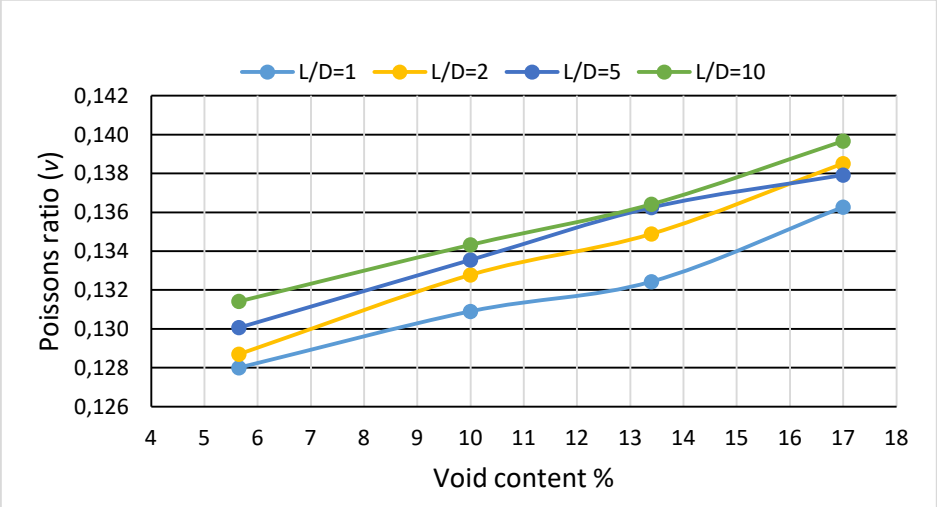

Figure 3.17: The variation of Poisson's ratio with different values of void contents and aspect ratios.

Conclusion that can be drawn is that the low-level porosity has noticeable influence on the composite material elastic properties while the shape of porosity has a low level impact on elastic properties. For fixed volume fraction, changing shape of pores by increasing aspect ratio (L/D) slightly decreases values of E, G and ν. Therefore it has no significant influence on elastic properties of matrix material. Volume fraction of porosity has a significant impact on elastic properties of matrix material. As it is evident from results presented in Figure 3.15, with the increase in porosity content, compressive modulus significantly decreases. For an example, porosity level of 10% leads to a modulus of elasticity decrease of approximately 20%. Contrary, less porosity in the material microstructure generally leads to noticeable higher values of E, G and ν.

Obtained values of compressive modulus of elasticity and shear modulus, for different values of void contents, predicted by MPUC model are in excellent agreement with several sets of previously published experimental data [47].

Comparisons with another existing numerical model - FCC have also shown particularly good agreement.

Finally, presented MPUC model are capable to simulate microstructure irregularity of pores shape and size regarding the influence of porosity volume fraction to elastic properties of wide range of structural materials.

CHAPTER FOUR

4 Optimization of tail boom structure

In this chapter analytical and numerical methods which are going to be used for optimization of layups of composite tail boom structure, will be presented. For defined aerodynamical loads of the tail boom structure (Section 3 – Table 3.4.) safety factors (based on Tsai-Wu failure theory) of stiffeners (main frame, formers, and stringers) and outer skin, having ten differently oriented symmetrical layers of carbon fiber reinforced matrix (epoxy), are evaluated by commercial FEM software Ansys. The properties of the carbon fibre/Epoxy composite material used in optimization procedure have presented in Table 2.2.

As described in Section 2.1.4, according to Tsai-Wu failure criteria, the failure is expected if the inequality in Equation (2.19) is violated. The optimization steps for the laminate under given loading conditions are presented in Section 2.1.8. In optimization procedure of tail boom skin, the design variables are orientation angles of the plies and ply thickness. The initial plies thicknesses are 0.125 mm, 0.250 mm, and 0.375 mm due to the manufacturing limitation of the closed molding process with two-sided mold sets. The selected laminates, shown in Table 2.1, have been used in the optimization procedure. Plies have been organized in way of symmetric laminates consisting of 10 layers with different orientation angles.

The safety factor for each lamina in the laminate is calculated according to the Tsai-Wu failure theory (SF_{TW}^{k}) using the Equation (2.21), and the safety factor of the laminate according to the Tsai-Wu failure theory (SF_{TW}^{n}) is the minimum of SF_{TW}^{k} obtained for all laminas:

SF_{TW}^{n} = minimum of SF_{TW}^{k} , k= 1, 2, 3,…, m.

Number m represents the maximum number of laminas.

Geometry model of the tail boom, used in further analysis is shown in Figure 4.1. The FE mesh of the tail boom, consisting of 351006 nodes, is shown in Figure 4.2. The FE mesh of frames and stringers is shown in Figure 4.3, while the mesh of additional elements (main frame, formers, and stringers) shown in Figure 4.4.

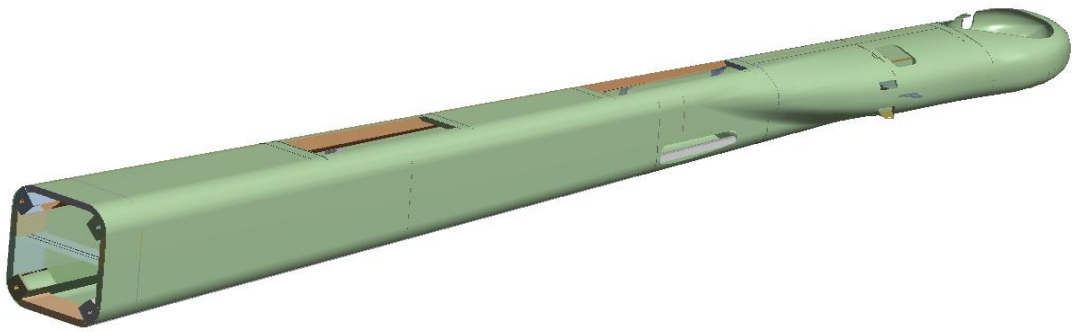

Figure 4.1 Geometry model of the tail boom.

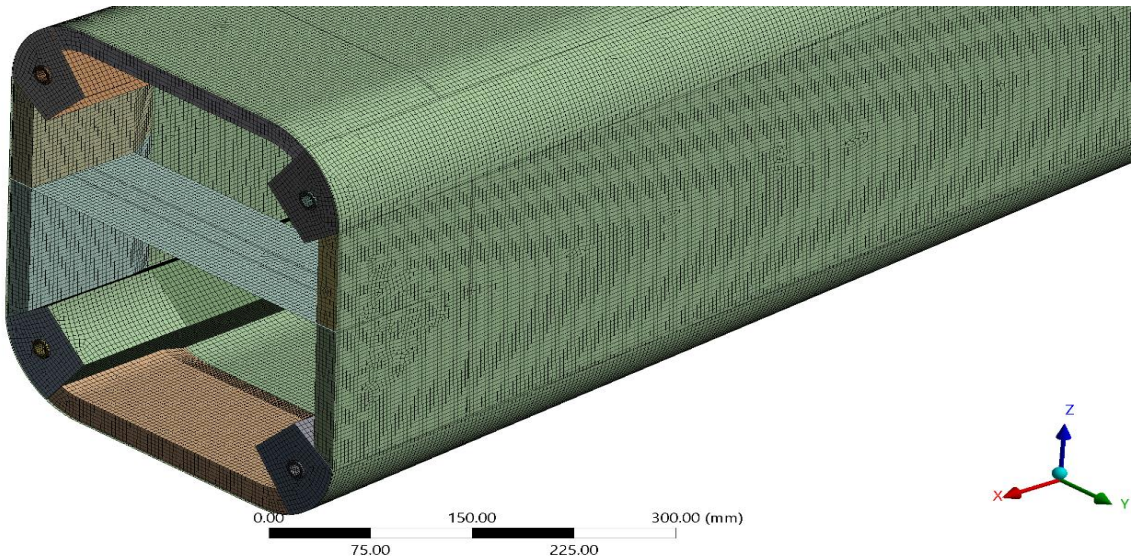

Figure 4.2 The FE mesh of the tail boom used in calculations (351006 nodes).

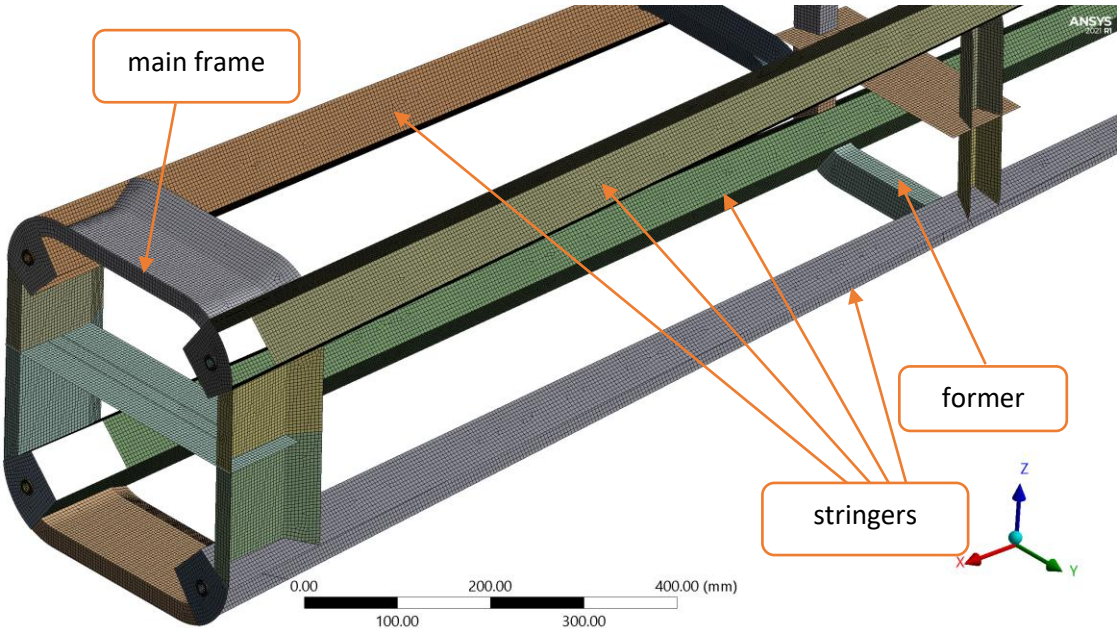

Figure 4.3 The mesh of frames and stringers.

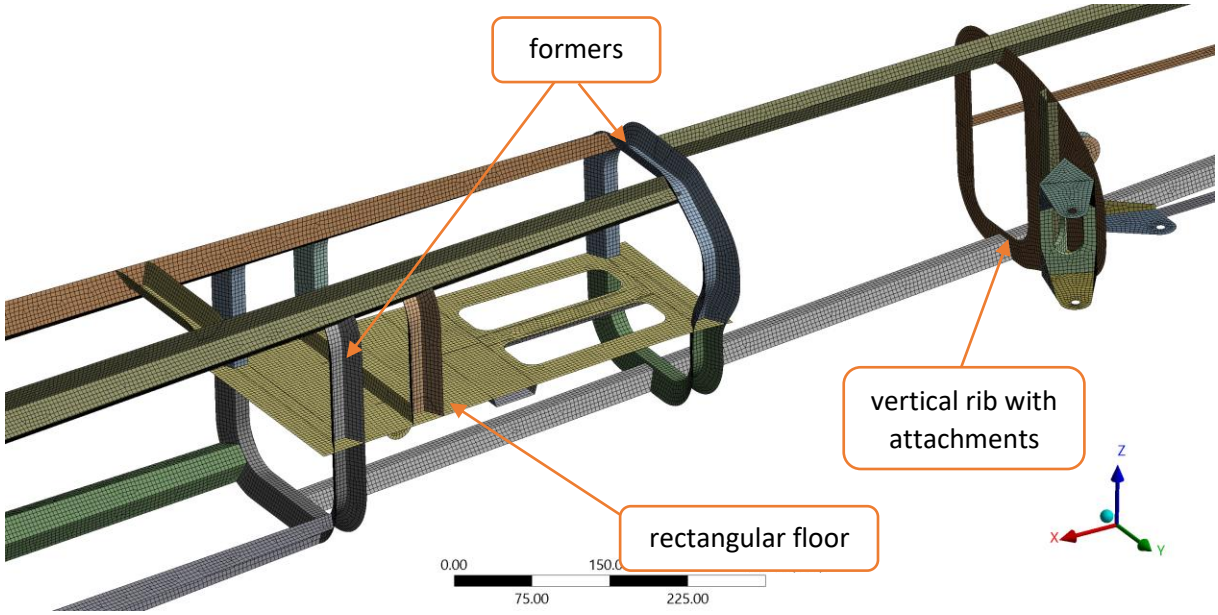

Figure 4.4 The mesh of additional elements.

After FE mesh has been defined, the next step is to define stack-ups that will determine the thickness of the tail boom parts.

Before defining properties of the material, a whole FE model was divided into 4 segments as presented in Figures 4.5 – 4.8. Later, plies are attached to each segment of the tail boom.

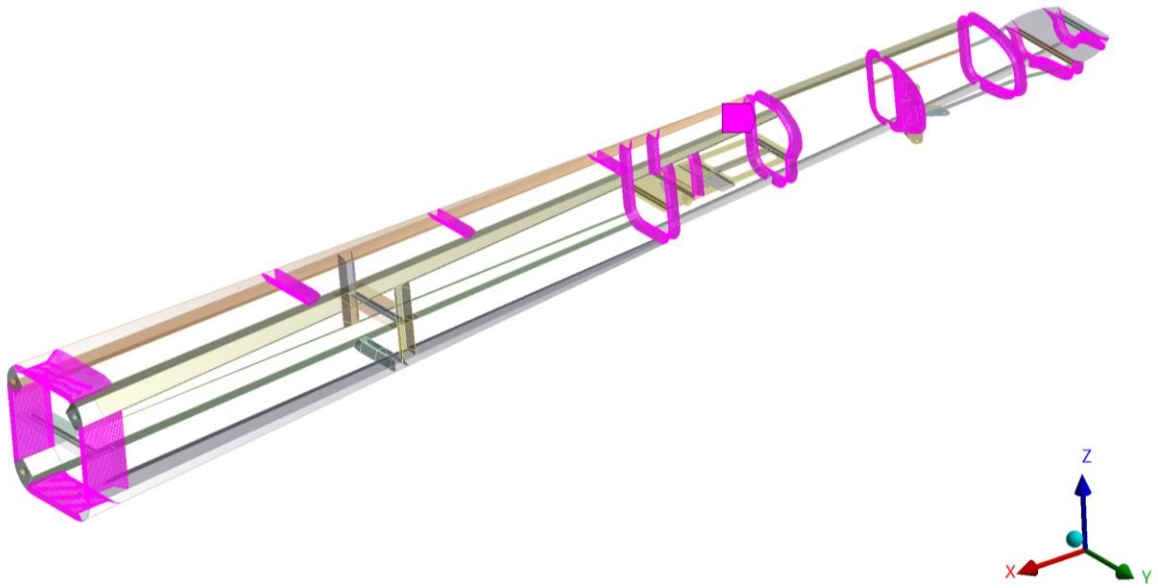

Figure 4.5 The first segment consisting mostly of frames.

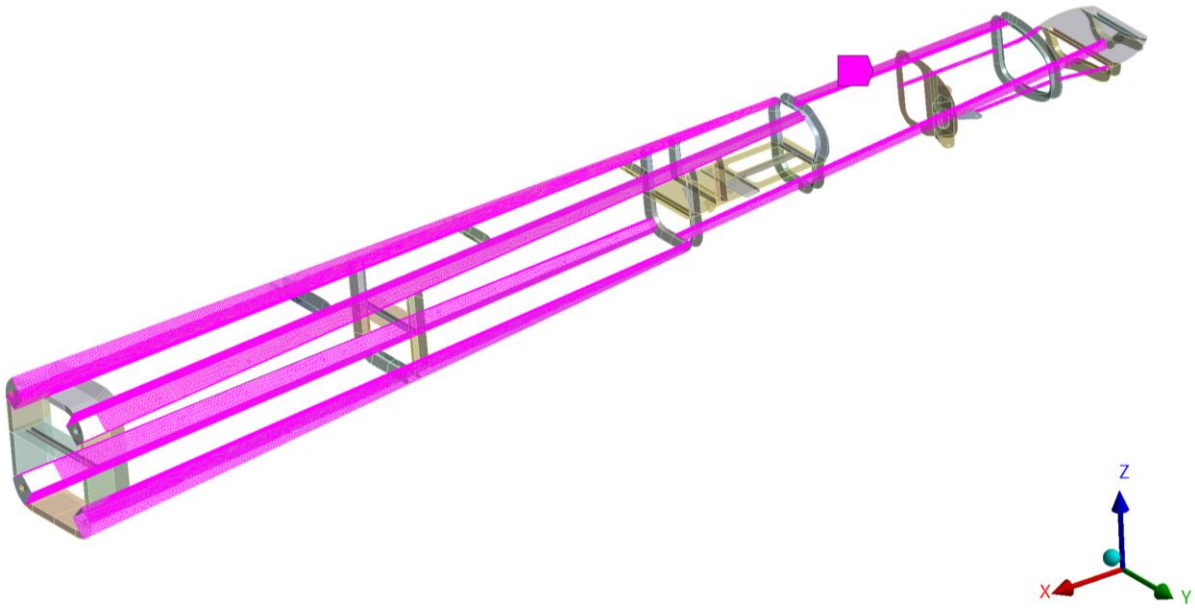

Figure 4.6 The second segment consisting of stringers.

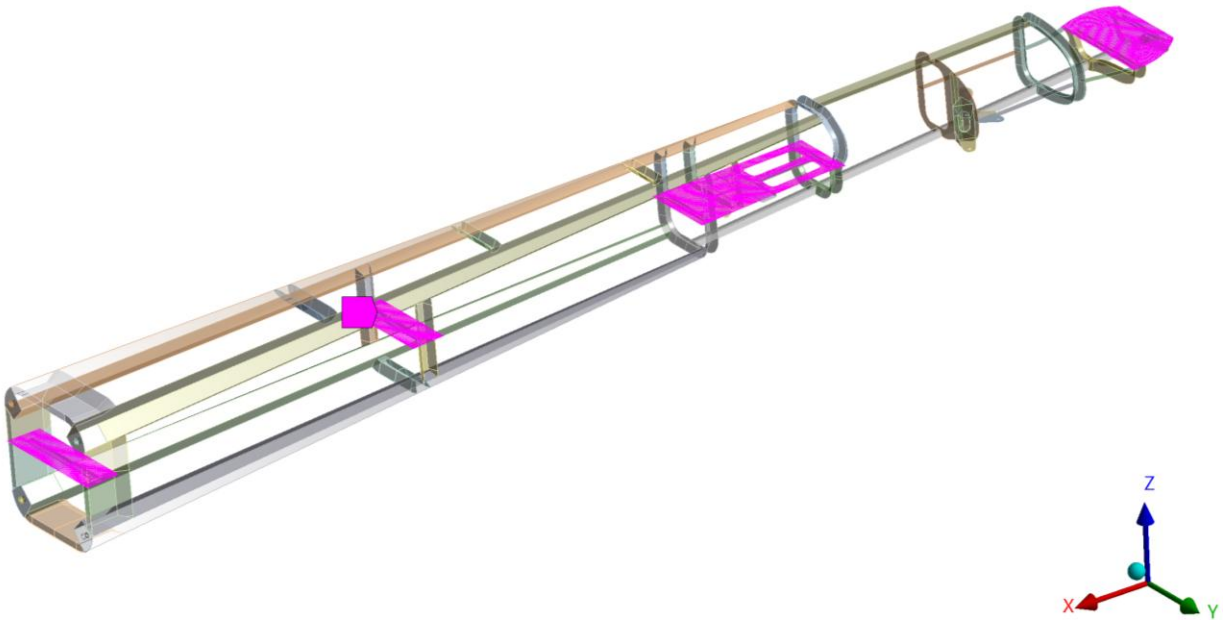

Figure 4.7 The third segment consisting of floor elements mostly.

All segments presented in the previous figures will be considered in the tail boom optimization. The mechanical properties of composite material used in all FE analyses are presented in Table 2.2.

Figure 4.8 The fourth segment consisting of outer skin.

As mentioned before, in Section 3, inertial loads (weights) representing different payloads on the tail boom structure are applied manually, while aerodynamic loads are transferred from CFD analysis. Since the main frame is used to connect the tail boom to the rest of the light aircraft structure through four joints (see Figure 3.3) and should be firmly attached, fixed supports are used as boundary conditions at 4 faces shown with letters A, B, C and D in Figure 4.9.

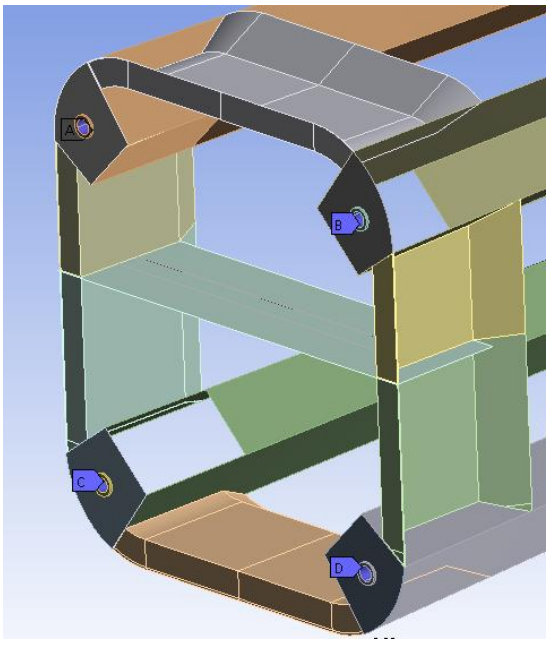

Figure 4.9 Boundary conditions (fixed supports) used in FE analysis.

Configurations of laminates having different stacking sequences for all structural parts, used in initial FE analysis, with calculated factors of safety SF_{TW} are presented in Table 4.1.

Table 4.1: Factors of safety for laminates of lamina thickness 0.125 mm

Ply thickness (mm)	0.125	Number of the plies	10
Laminate number	Laminate orientation angles	Tsai-Wu safety factor SF_{TW}	Laminate thickness (mm)
1	$[0/+45/90/-45/0]_s$	1.52	1.25
2	$[0/+30/90/-30/0]_s$	0.91	1.25
3	$[0/+30/90/-45/0]_s$	0.92	1.25
4	$[0/+60/90/-60/0]_s$	1.30	1.25
5	$[0/+45/-45/90/0]_s$	1.43	1.25
6	$[0/+30/90/+30/0]_s$	0.98	1.25

From results presented in Table 4.1, since laminate number 1 with orientation angles and stacking sequences $[0/+45/90/-45/0]_s$, has the highest safety factor of all considered lamina orientation angles, this laminate configuration, is addopted to be reference laminate configuration that will be used in further analysis.

4.1 Optimization of tail boom main frame, formers, and stringers

As mentioned before, the tail boom structure analyzed in this thesis is a semi-monocoque structure consisting of stiffeners (main frame, formers, and stringers) and outer skin. In this section focus is on the definition of composite material that can provide satisfactory strength of: main frame, formers, and stringers. All of these elements carry pre-defined loads (inertial and aerodynamic),and are made of carbon/epoxy composite material.

Structural elements of the tail boom should have a variable thickness because not all of them carry the same load. Therefore, the composite layup of the tail boom 30 different stack-ups have been made in Ansys Workbench. This considerable number of stack-ups was necessary since there were many areas where thickness could be varied. In this manner, simple and fast modification of composite layup and composite designs are possible, allowing researchers to examine different combinations and find the optimum solution.

Besides previously mentioned 30 stack-ups, 49 different oriented selection sets were defined. In Ansys Workbench oriented selection sets contain information about the layup area, the layup direction, and the reference direction for the fiber orientations. Layers of the composite design are then placed on the oriented selection set. Oriented selection set must also contain information about the direction in which the layers are placed on the mold surface (the orientation direction is either going in the normal direction of the elements or opposite to the normal direction). When fabrics are placed on the oriented

selection set angles can be defined too. These angles refer to the reference direction specified by the rosette related to the selected oriented selection set. Finally, the composite layup is defined by selecting the oriented selection set, defining the ply material, ply angle (with respect to the reference direction), and a number of layers. The ply material might consist of the fabric itself (where orientation angle must be defined) or the previously defined stack-up can be used. This provides the opportunity "to play" with distinct characteristics of applied material in the search for the best solution.

As stated before, in the case of the tail boom, the manufacturing limitation was that only fabrics with thicknesses of: 0.125mm, 0.250mm and 0.375mm (obtained in closed molding process with two-sided mold sets) were available. The initial structure of the tail boom (Figure 4.10) has been set up considering above mentioned limitations. The maximum thickness defined was 1.5mm (red-coloured parts of skin in Figure 4.10), while the smallest thickness 0.125mm was applied in the area where joints are used (blue colour).

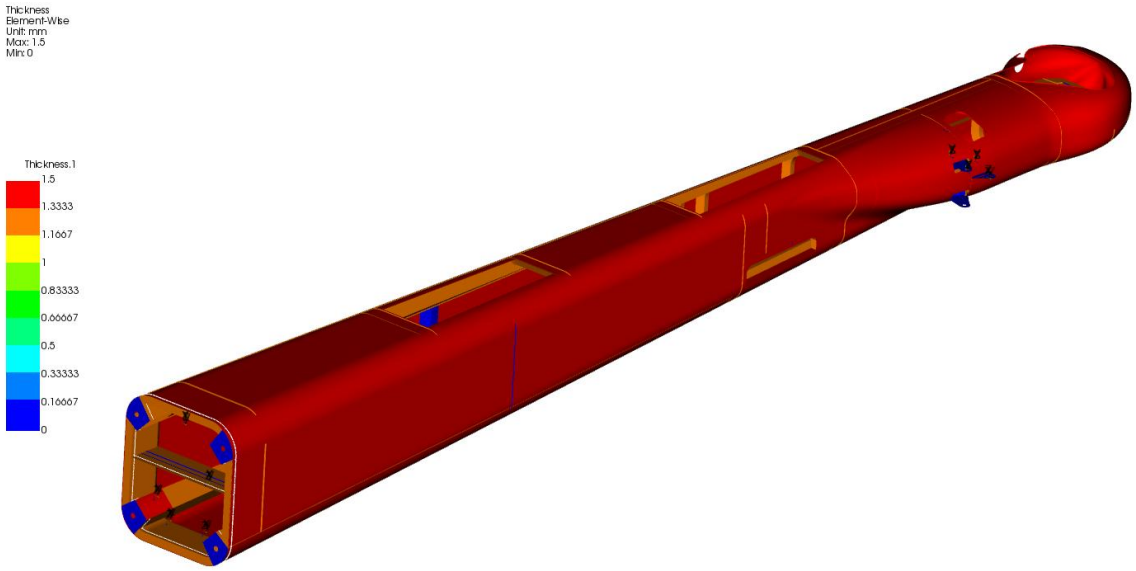

Figure 4.10 Initial composite layup of the tail boom.

- **Approach used in initial optimization of the tail boom**

Since tail boom has differently shaped parts like stringers, formers, floor, vertical rib, outer skin, etc., for each of them stacking sequences (the laminate thickness, a number of plies, orientation angles) must be properly defined. Since there are too many variables to analyse, it was decided to carry out optimization of the tail boom through one stage which should save calculation time. In the first, initial stage lamina thickness and the number of plies are varied for segments one, two, and three (Figures 4.5 – 4.7), with only one group of orientation angles used, previously addopted configuration $[0,+45,90,-45,0]_s$. It is the fact that laminate configuration with angles: $[0,+45,90,-45,0]_s$ is the most used orientation angles in the aircraft industry. The stringers and the mainframe parts expected to carry majority of external loads and therefore these parts are expected to be thicker than other ones (e.g. skin). Different orientation angles and stacking sequences (as presented in Figure 4.11), are analysed for the all structural parts of the tail boom to define the optimum orientation angles and stacking

sequences. Propoused procedure with parameter set between ACP (Pre) module (composite pre-modelling) and Static Structural is presented in Figure 4.11.

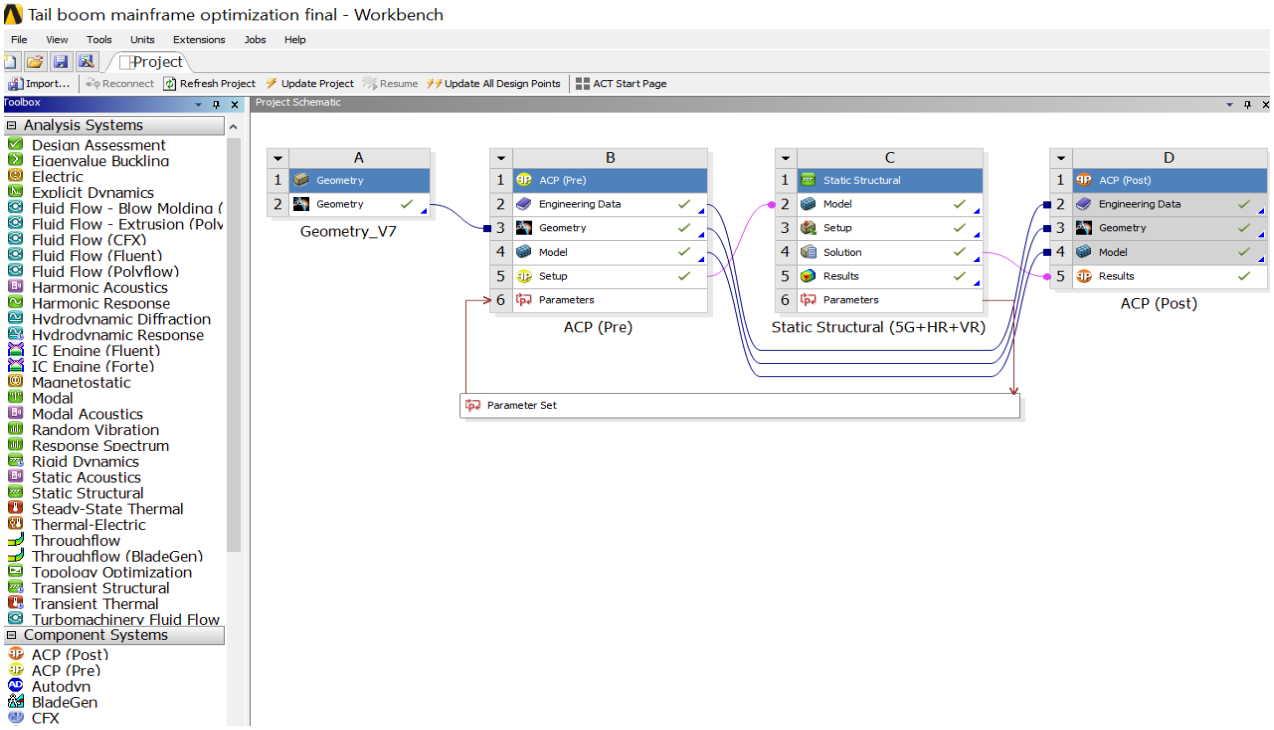

Figure 4.11 Parameter set between ACP (pre) and static structural.

In the Static Structural setup, the forces are applied to the model directly, or imported from the module for CFD analysis named Fluent if one-way or two-way analysis was performed before. Since the tail boom is attached to the aircraft cabin, fixed supports were applied at the four fixing joints, as shown in Figure 4.9. The analysis is then carried out and the solution results (total deformation and reference value of SF_{TW}) are extracted from the solution database. Selected parameters which are varied, namely lamina thickness and number of laminates, make the connection between the ACP (Pre) and the Static Structural (as shown in Figure 4.11). Thus, after each calculation, the update of design points is made, and Ansys Workbench starts new solution procedure. The software automatically changes the design variables and calculates the output results for all parts of the tail boom. After finishing the complete solution procedure the total number of design points (different combinations of laminates' thicknesses and a number of layers) was 21. All results (deformations and values of SF_{TW}) are sorted and presented in Table 4.2.

- **Results**

The total number of outputs named as design points (DP) were 21 and for each DP, the maximum total deformation and reference value of SF_{TW} were calculated, as shown in Table 4.2. It should be emhasized that thickness of the skin in this stage was fixed to 0,25mm with orientation angles of $[0/+45/90/-45/0]_s$.

Table 4.2 The tail boom structure thickness optimization through the definition of design points

Design point		Number of laminates			Orientation angles $[0/+45/90/-45/0]_s$	
	Lamina thickness (mm)	Frames and vertical rib	Stringers	Mainframe and floor	Maximum total deformation (mm)	SF_{TW}
1	0.375	2	3	3	14.04	10.56
2	0.375	3	2	4	14.27	10.06
3	0.375	1	2	4	14.33	8.66
4	0.375	1	3	1	14.33	6.90
5	0.375	2	2	3	14.35	8.65
6	0.375	1	2	3	14.39	6.93
7	0.375	3	1	4	14.68	6.91
8	0.25	2	3	3	15.51	6.45
9	0.25	3	2	4	15.81	5.91
10	0.25	1	2	4	15.91	5.06
11	0.25	1	3	1	15.92	3.65
12	0.25	2	2	3	15.93	5.88
13	0.25	1	2	3	16.00	5.04
14	0.25	3	1	4	16.38	4.13
15	0.125	2	3	3	19.81	2.68
16	0.125	3	2	4	20.33	2.54
17	0.125	1	2	4	20.50	2.18
18	0.125	1	3	1	20.52	1.57
19	0.125	2	2	3	20.58	2.53
20	0.125	1	2	3	20.84	2.18
21	0.125	3	1	4	22.43	1.72

Analysis of obtained values of total deformations

As expected, the total deformation varies significantly with different lamina thicknesses and number of laminates. The minimum total deformation values were obtained for 0.375 mm lamina thickness, whereas the maximum values were obtained for 0.125 mm lamina thickness. The absolute minimum value of the total deformation was 14.04 mm for 0.375 mm lamina thickness, at design point (DP) 1, as presented in Figure 4.12. The minimum values of the total deformation for the three different lamina thickness were obtained on DPs 1, 8, and 15 when the number of the laminates were 2, 3 and 3 for the formers/vertical rib, stringers, and main frame/rectangular floor, respectively. On the other hand, when the number of the laminates were increased to 3 for the frames/vertical, and to 4 for main frame/rectangular floor, but decreased to 1 for the stringers, the total deformation was increased to the maximum value for all the lamina thicknesses, as shown in DPs 7, 14, and 21 in Table 4.2. This is expected because in reality stringers carry most of the tail structure loads. The maximum value of the total deformation is 22.43 mm at DP 21, with lamina thickness 0.125 mm and number of laminates 3, 1 and 4 attached to the formers/vertical rib, stringers, and main frame/rectangular floor, respectively (Figure 4.13).

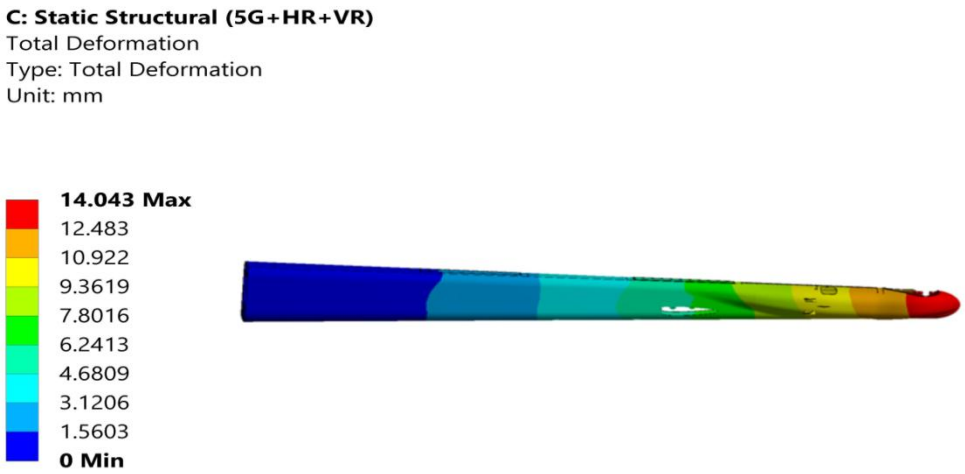

Figure 4.12 Minimum total deformation (design point 1) obtained in the 1st stage of optimization.

On the other hand, Table 4.2 shows that design points 2 and 6 have the same number of laminates applied on stringers (2). Here, similar maximum total deformations were obtained for these two DPs (14.27 mm and 14.39 mm respectively), where DP 6 has fewer total laminates than DP 2. This implies that reducing the number of laminates (two less on formers, vertical rib, and one less on main frame and floor) deformation is increasing by 0.84% only, which is negligible. This implies that reducing the thickness for formers, vertical rib, main frame, and floor do not make significant influence on tail boom structure deformation. The maximum obtained value of deformation was 22.43 mm (Figure 4.13) for DP 21 where lamina thickness was 0.125 mm, and the number of laminates 3, 1 and 4 for the formers/vertical rib, stringers, and main frame/rectangular floor respectively. However, it is obvious from Table 4.2 that maximum values of deformation have been obtained when only 1 laminate was used on stringers (DPs 7, 14 and 21). Comparing the total deformation obtained on DPs 15 and 21 which have same lamina thickness (0.125 mm), DP 15 has total deformation equal to 19.81 mm and DP 21 has total deformation equal to 22.43 mm for the same lamina thickness, and the difference in deformation for design points 15 and 21 is about 13%. This difference can be considered as a

significant and implies that stringers are more important for overall stability of the tail boom than the other elements. Also, decreasing the number of laminates on formers and vertical rib produces higher deformation than reducing the number of laminates on the main frame (see design points 9, 10 and 11). It is important to emphasize that all deformations shown in Table 4.2 are well below maximum allowed deformation limit of 110 mm, defined for this type of light aircraft.

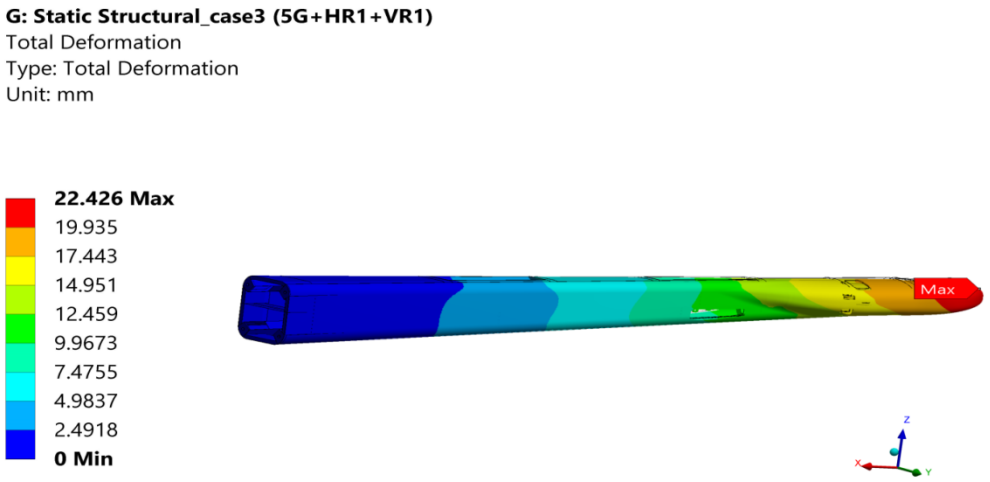

Figure 4.13 Maximum total deformation (design point 21) obtained in the 1st stage of optimization.

Analysis of obtained values of SF_{TW}

Obtained values of safety factors (SF_{TW}) are presented in Table 4.2. The minimum value of SF_{TW} was 1.57 obtained at DP 18 **with lamina thickness of 0.125** mm and number of laminates 1, 3 and 1 for the formers/vertical rib, stringers, and main frame/rectangular floor respectively.

For all considered lamina thicknesses (0.375mm, 0,25mm and 0.125mm) the minimum values of SF_{TW} were obtained at DPs 4, 11 and 18 when the number of laminates on the formers/vertical rib, stringers, and main frame/rectangular floor is 1, 3 and 1 respectively. This was expected since the number of laminates for the main frame was reduced to the minimum value (one laminate), and the stress on the main frame was expected to be high.

The maximum obtained value for SF_{TW} was 10.56 at DP 1 when the number of the laminates was 2, 3 and 3 on the formers/vertical rib, stringers, and main frame/rectangular floor respectively, **with lamina thickness equal to 0.375 mm** (Table 4.2). This was expected too, because when stringers have maximum number of the laminates (3) and main frame has 3 laminates with lamina thickness at maximum considered value (0.375 mm), the safety factor (strength) should increase to the maximum value since stringers and main frame are thicker than the other parts.

On the other hand, Table 4.2 shows that almost the same values of safety factor (8.66, and 8.65) were obtained for DPs 3 and 5, where DP 5 has 1 laminate less on mainframe and 1 laminate more on frames than the DP 3. The difference between safety factors of these DPs is negligible. Therefore, in this case by reducing the number of laminates (mainframe/floor) strength of the tail boom structure will not change significantly. However, it is obvious from Table 4.2 that minimum values of SF_{TW} have

been obtained when only 1 laminate was applied on main frame (design points 4, 11 and 18). Thus, comparing the safety factor values obtained at DPs 15 and 18 (which have number of laminates 2, 3 and 3, and 1, 3, and 1 on formers/vertical rib, stringers, and main frame/rectangular floor respectively), DP 15 has the maximum value of safety factor (SF_{TW} =2.68) for DPs when the lamina thickness is 0.125mm. However, DP 18 has fewer laminates (two less on formers, vertical rib, and main frame/rectangular floor, but they have the same laminates on stringers) with safety factor of 1.57. Difference in safety factors between DPs 15 and 18 is about 41% and is significant, indicating that the mainframe thicknesses play important role in distribution of the strength on the tail structure.

Comparing the safety factor values obtained at DPs 2 and 7 (with the number of laminates 3, 2, and 4, and 3, 1, and 4 on formers /vertical rib, stringers, and main frame/rectangular floor respectively) we can see that DP 7 contains less laminates than DP 2 (one laminate less on stringers) and that DP 2 has safety factor equal to 10.06, while DP 7 has safety factor value equal to 6.91. Difference in safety factor value between DPs 2 and 7 is about 30%, and this implies that thickness of stringers is important factor for strength of the tail structure. However, higher value of strength is more desirable.

From Table 4.2 the safety factor at DPs from 15 to 21, which have 0.125 mm lamina thickness have low values of safety factors (strength) when compared to the other DPs.

- **The choice of optimal thickness values for the tail boom structure**

Results from the previous FE analysis are presented in Table 4.2. The effect of changing the lamina thickness of different structure parts on the structure strength is obvious.

By comparing DPs 3 and 6, where latter has less laminates than former DP (one laminate less on the mainframe and floor) the safety factor differ by almost 20%. This is significant and implies that the thickness reduction on mainframe and floor is significantly influence the strength of the tail boom structure. Similar might be concluded about DPs 2 and 7, where DP 7 has less laminates than the other DP (one laminate less on stringers): difference in safety factor is about 31%, giving us the idea on how stringers' thicknesses effect the strength of the tail structure.

From the above summary, it can be concluded that stringers have bigger overall impact on the structure deformation than the other elements. In general, stringers, main frame, and rectangular floor have bigger impact, on the strength than frames and vertical rib have. **Thus, the thickness of stringers, main frame and rectangular floor have to be greater than the thickness of formers and vertical rib** (from this point of view).

Results presented in Table 4.2 show that design points from 15 to 21 with lamina thickness 0.125 mm have the minimum values of the safety factor less than other DPs with lamina thicknesses 0.250 mm and 0.375mm. The maximum safety factor of DPs (from 1 to 7) which have lamina thickness 0.375mm was (10.56) that is high and the structure will be safe due to the reduction in the strength due to some load disturbance (e.g. thermal load). Whereas, the maximum safety factor of DPs (from 8 to 14) which have lamina thickness 0.250mm was (6.17) which is still high enough to stand the decrease in the strength due to some load disturbance. While, the maximum safety factor for the DPs (from 15 to 21) which have lamina thickness 0.125mm was (2.68) which can be considered as low value suggesting that failure of structure under some external load disturbance (e.g. thermal load) could be easily reached.

Thus, DPs with lamina thickness 0.125 mm must be eliminated, because the structure may fail due to low strength under some external disturbance such as themperature load condition, probably causing fatal decrease of the structure strength.

Results in Table 4.2 also show that design points 1 and 8 have minimum values of total deformation and maximum safety factors (strength) for lamina thicknesses 0.375 mm and 0.250 mm. The maximum safety factor values of 10.56 and 6.17 were obtained for the DPs 1 and 8 which have the same number of laminates (2, 3 and 3) on formers /vertical rib, stringers, and main frame/rectangular floor respectively, but different lamina thicknesses: 0.375 mm and 0.250 mm. **Thus, these design points have been chosen as the best candidates for the definition of the tail structure**. Since, deformation and stress values were below design limits and high safety factor, the optimum design point should have the lowest weight, since reduced mass of the structure contributes to better aircraft performance. The mass of all parts (formers, vertical rib, stringers, main frame, and rectangular floor) have been calculated using Ansys Workbench for defined thicknesses and properties of laminas and are presented (with other values) in Table 4.3.

Table 4.3 Frame optimum laminate thickness properties for the tail boom

Design point		Number of laminates			Orientation angles $[0/+45/90/-45/0]_s$		
	Lamina thickness (mm)	Frames and vertical rib	Stringers	Mainframe and floor	Mass (kg)	Maximum total deformation (mm)	Safety factor SF_{TW}
1	0.375	2	3	3	18.33	14.04	10.56
8	0.250	2	3	3	12.25	15.51	6.45

Results in Table 4.3 shows that design point 1 has the minimum values of total deformation, and maximum safety factor value for the two lamina thickness, while DP 8 has total deformation higher than DP 1 by 1.47 mm only and significant value of safety factor ($SF_{TW} = 6.45$) sugesting that "reserve of strength" is considerable high. Besides that, in DP 8 the total mass of the tail boom structure (without skin) was evaluated to 12.25 kg, while in DP 1 the total mass is 18.33 kg, which is difference in the mass of 6.08 kg (almost 50%). **So, DP 8 with 2, 3 and 3 laminates on formers/vertical rib, stringers, and main frame/rectangular floor respectively, with lamina thickness 0.250 mm, can be considered as an optimum solution for the tail boom structure** in this stage. Actual thicknesses of all structure parts can be calculated as follow: since the lamina thickness is 0.250 mm, number of plies at each laminate 10, the number of laminates 2, 3 and 3 for the formers, vertical rib, stringers, main frame, and rectangular floor respectively, the thicknesses are 5.00 mm, 7.50 mm, and 7.50 mm for the formers/vertical rib, stringers, and main frame/rectangular floor respectively.

Thus, thickness of stringers and main frame, as the most loaded elements, is higher than the other elements, as expected from previous analyses and conclusions. Expected reactions of the structure during the flight are: maximum total deformation of 15.51mm (Figure 4.14) and 6.17 as reference value of SF_{TW} which represents considerable "reserve of strength" for considered structure.

Figure 4.14 Total deformation for the optimum laminate configuration (DP 8).

4.2 Optimization of tail boom skin

As mentioned earlier in this chapter, the second stage of defining the tail structure properties is the definition of the skin laminate properties. In this section, the similar FE procedure (presented in previous section) is used. As a reminder, the whole FE model was divided into 4 segments (according to required thicknesses) and first three segments have been analysed (and dimensioned) in so-called stage one; the fourth segment, the skin structure (Figure 4.8), will be defined in this section - stage two. The geometry model of the tail boom skin, along with the FE mesh, is shown in Figures 4.1 and 4.2.

In this stage, the lamina thickness and the number of the plies are varied for segment 4 (Figure 4.8), with previously adopted group of the orientation angles $[0,+45,90,-45,0]_s$. The thickness of the outer skin is expected to be less than the other parts of the tail boom since the other parts are carrying the main loads; anyhow, it is the fact that the skin is exposed to some load and must be dimensioned in accordance with that. In this stage the thicknesses of tail boom structural parts are fixed, and defined in Section 4.1 (2, 3 and 3 on formers/vertical rib, stringers, and main frame/rectangular floor).

In this stage, the same FEA procedure was used, as described in previous section. The analysis was carried out and results, total deformation, safety factor (SF_{TW}), are extracted from the solution database. All results (deformations and safety factors), for different thicknesses of the skin (0.125mm, 0.25mm and 0.375mm) are sorted and presented in Table 4.4. where total number of defined design points, having different number of laminates (1,2 or 3) was 9.

Analysis of obtained values of total deformations

The total deformation varies significantly with different lamina thicknesses and number of laminates as expected (see Table 4.4). The total deformation increases with reduced thickness and decreases with increasing number of laminates: this is something absolutely logical.

Table 4.4 shows that the minimum total deformation values were obtained for lamina thickness 0.375 mm, whereas the maximum values were obtained for lamina thickness 0.125 mm. The minimum value of the total deformation was 12.72 mm (Figure 4.15) for lamina thickness 0.375 mm, at design point one. The minimum values of the total deformation, for the three different lamina thicknesses, were recorded for design points 1, 2, 3 and 4 where the number of laminates was 2, and 3, and the lamina thickness was 0.375mm and 0.250mm.

However, when the number of laminates decreases to 1, total deformation increases to the maximum values for all lamina thickness, as can be seen on DPs 6, 8 and 9. This is expected since when the number of laminates decreases the total thickness decreases and the deformation increases. The maximum value of the total deformation is 17.85 mm at DP 9 with lamina thickness 0.125 mm and number of laminates equal to 1 (Figure 4.16).

Table 4.4 The tail boom skin thickness optimization through the definition of design points

Design point		Number of laminates	Orientation angles $[0/+45/90/-45/0]_s$	
	Lamina thickness (mm)	Skin	Maximum total deformation (mm)	Safety factor SF_{TW}
1	0.375	3	12.72	9.98
2	0.375	2	13.21	9.17
3	0.250	3	13.37	9.00
4	0.250	2	13.87	8.56
5	0.125	3	14.47	7.88
6	0.375	1	14.47	7.81
7	0.125	2	15.51	6.49
8	0.250	1	15.51	6.45
9	0.125	1	17.85	4.15

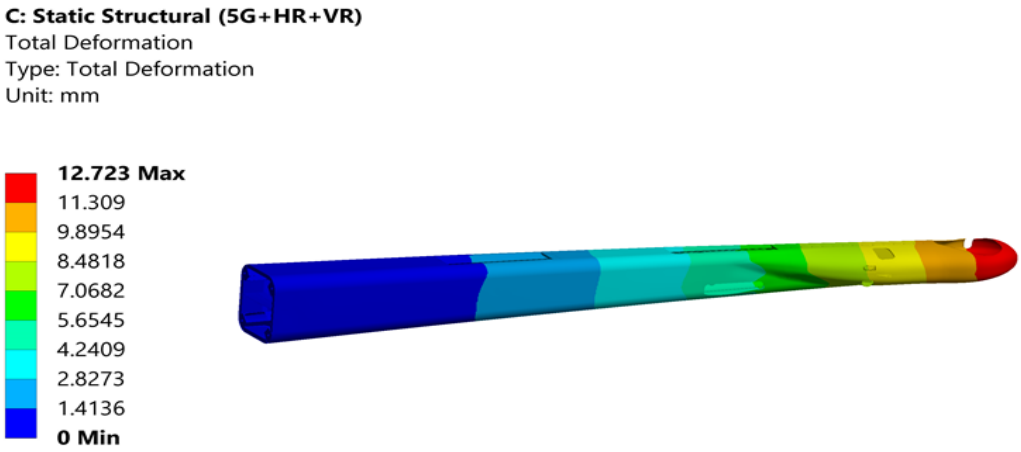

Figure 4.15 Minimum total deformation (design point 1) obtained in the 2nd stage of optimization; lamina thickness 0.375 mm

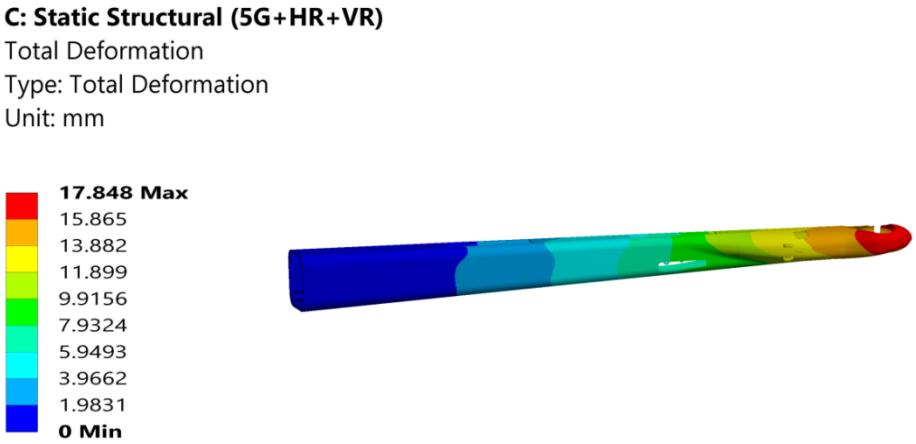

Figure 4.16 Maximum total deformation (design point 9) obtained in the 2nd stage of optimization; lamina thickness 0.125 mm

On the other hand, to quantify the effect of the skin laminates number reduction on the total deformation, comparing DPs 1 and 2 , which both have the same lamina thickness 0.375 mm , we can see that DP 1 shows the total deformation of 12.72 mm (Figure 4.15), while DP 2 shows 13.21 mm (Figure 4.17). Since DP 2 has less laminates than other DP (one laminate less), the difference in total deformation is increasing by 4% which is not a significant considering the absolute values of both deformations.

However, when DPs have the same number of laminates but different lamina thicknesses (0.375 mm and 0.250 mm) like DP 2 and DP 4 in Table 4.4, DP 2 shows total deformation of 13.21 mm

(Figure 4.17), while DP 4 gives total deformation of 13.87 mm (Figure 4.18). The total deformation increases by 5% which is again not significant increase but implies that reduction of the lamina thickness play some role in structure deformation.

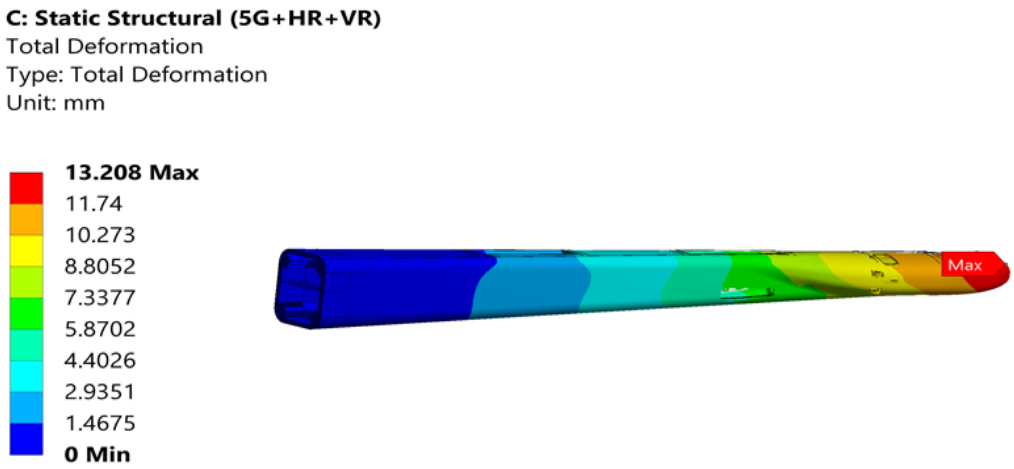

Figure 4.17 Total deformation (design point 2) obtained in the 2nd stage of optimization; lamina thickness 0.375 mm

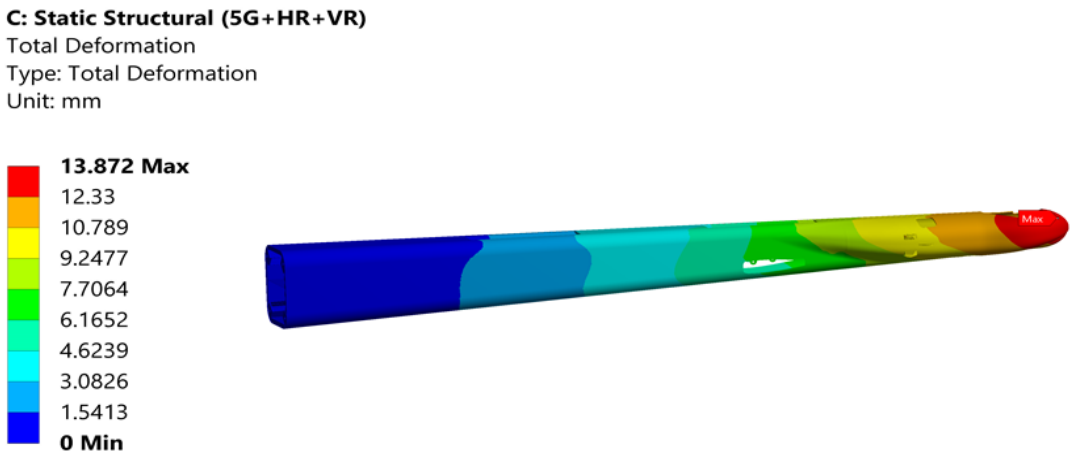

Figure 4.18 Total deformation (design point 4) obtained in the 2nd stage of optimization; lamina thickness 0.250 mm

The maximum obtained value of deformation was 17.85 mm (Figure 4.16) at design point 9 where lamina thickness was 0.125 mm and the number of laminates 1. Comparing DPs 1 and 9 which show the minimum and maximum total deformation, we can see that this difference comes from different number of laminates (1 against 3), i.e. different thicknesses. The change in deformation is about 40% which is significant value and confirms that reduction of the number of laminates to just 1 –

along with reduction of the lamina thickness to just 0.125 mm, leads to bigger structure deformation (but still acceptable). At the same time, reducing the number of laminates from 2 to 1 for the same lamina thickness (0.250 mm), the total deformation is increasing by 12% (when we compare deformations for DP 4 and DP 8: from 13.87 mm to 15.51 mm). This might be considered as a significant change, but, again, the absolute values of deformations are well below maximum allowed deformation (110 mm).

Analysis of obtained values of SF_{TW}

Results presented in Table 4.4 show that for all lamina thicknesses minimum values of safety factor appeared when only 1 laminate was applied on the skin (DPs 6, 8 and 9), whereas the maximum values of safety factor were obtained when 3 laminates were applied on the skin (DPs 1, 3 and 5). Thus the strength increases with increasing skin thickness. On the other hand, Table 4.4 also shows that almost the same values of safety factor 9.17 and 9.00 were obtained for DPs 2 and 3, where DP 3 has less laminates than the other DP (1 laminate less), and they have the same laminate thickness 0.75 mm. The safety factor (strength) increases by 2% only between DP 2 and DP 3. This is not significant and implies that with reduction of the number of laminates (one laminate less on the skin) but have different lamina thickness 0.250 mm and 0.375 mm and same laminate thickness 0.75 mm, the value of strength changes negligibly.

To evaluate the effect of the reduction of the number of skin laminates on safety factor values on the tail boom, let us compare the safety factor values obtained at DPs 5 and 9, which have different number of laminates (3 and 1) but the same lamina thickness (0.125 mm). DP 5 has the safety factor value of 7.88, while DP 9 has the value of safety factor 4.15. But in a case of DP 9 number of laminates is less than in the other DP (two less laminates) and the difference in safety factor is about 47%, which means that a lamina thickness 0.125 mm and 1 layer of laminates is reduces the structure strength.

To evaluate the effect of the reduction of the skin lamina thickness on the safety factor values on the tail boom, three DPs with the same number of laminates (2), but with different lamina thicknesses can be analysed (DPs 2, 4 and 7 with lamina thicknesses 0.375 mm, 0.250 mm, and 0.125 mm respectively). DP 2 shows the absolute safety factor of 9.17, while DP 4 gives 8.56. DP 7 has safety factor value 6.49. Comparing safety factor values for DP 4 and DP 7 it is easy to see that the difference is about 28% , while the difference between DP 5 and DP 8 is 24%. This implies that reducing lamina thickness from 0.250 mm to 0.125 mm influences safety factor more than reducing lamina thickness from 0.375 mm to 0.250 mm. This makes sense because when lamina thickness is reduced from 0.375 mm to 0.250 mm total skin thickness decreases from 7.5 mm to 5.00 mm. But, when the lamina thickness is reduced to 0.125 mm, the total skin thickness decreases from 5.00 mm to 2.50 mm, so the structure is thin enough to influence strength on the tail boom structure.

However, as shown above, changes in the safety factor values are not significant, so it is recommendable to use a smaller number of laminates to decrease the structural weight of the tail boom. But, using lamina thickness 0.125 mm and one laminate reduces the safety factor to 4.15 at DP 9, which is still safe for the structure because the safety factor is high enough to stand the reduction on the strength due to some unexpected loads such as thermal load (case when plane is operating at low environmental temperatures).

- **The choice of the optimal skin thickness for the tail boom structure**

From results presented in Table 4.4 and the analysis of results presented on previous pages, some final conclusions can be drawn, and the optimal skin thickness can be selected. For all lamina thicknesses **the maximum deformations, minimum values of safety factor appear when only 1**

laminate is used on the skin, with lamina thickness 0.125 mm. DP 9 shows the lowest safety factor of 4.15 which is high enough to secure high level of "reserve of strength".

Since all deformations are far below the limit (110 mm) let us focus our attention on the values of safety factors. If we compare DP 8 and DP 9 which have 1 laminate only, but DP 8 has lamina thickness 0.250 mm while DP 9 has 0.125 mm, we can see that deformations differ by 13%, while safety factor differ by almost 36%.

As mentioned before due to the fact that mass of the tail boom play important role in aircrafts' performance, it is important to define skin laminate properties having minimal possible mass. Calculated tail boom skin masses of different design points are presented in Table 4.5.

According to Table 4.5, the maximum evaluated skin mass is 55.692 kg (DP 1), whereas the minimum mass is 6.188 kg (DP 9), which makes a huge difference. Since all deformations are well below defined limits and levels of safety factors (strength) are sugesting high level of "reserve of strength", the optimum DP will be the one with minimum mass. Since differences between obtained values of deformation are small, and all safety factors are high enough, **the optimum design point must be DP 9 since it has the lowest mass and enough** high value of SF_{TW}. Thus, the skin will have the thickness of 1.250mm, since the lamina thickness is 0.125 mm, the number of laminas (plies) in one laminate is 10, and the number of laminates is 1.

Table 4.5 The tail boom skin masses of different design points

Design Point	Lamina thickness (mm)	Number of laminates	Orientation angles $[0/+45/90/-45/0]_s$		
			Skin mass (kg)	Maximum total def. (mm)	Safety factor SF_{TW}
1	0.375	3	55.692	12.72	9.98
2	0.375	2	37.128	13.21	9.17
3	0.250	3	37.128	13.37	9.00
4	0.250	2	24.752	13.87	8.56
5	0.125	3	18.564	14.47	7.88
6	0.375	1	18.564	14.47	7.81
7	0.125	2	12.376	15.51	6.49
8	0.250	1	12.376	15.51	6.45
9	0.125	1	6.188	17.85	4.15

4.3 Definition of the optimum laminate orientation angles and stacking sequences

After defining optimal thicknesses of the tail boom structural parts for fixed stacking sequence and orientation angles in the laminate, in this section results of the analysis of the influence of different stacking sequences on deformation and values of SF_{TW} will be presented briefly, along with the choice of the optimum orientation angles and stacking sequences.

Again, the finite element method has been used for this analysis and more or less the same procedure (as described in previous sections) has been used. Here, the lamina thickness for the main structural parts frames/vertical rib, stringers, main frame/rectangular floor (0.250 mm), for skin (0.125mm) and the number of plies in the modelling group (10) for all structural parts were fixed, as well as optimal thickness obtained earlier; thus, thicknesses of structural parts were 5.00 mm, 7.50 mm, 7.50 mm and 1.250 mm for the frames/vertical rib, stringers, main frame/rectangular floor, and skin respectively. On the contrary, in this section, the orientation angles (ply angles) and stacking sequences were varied. Outputs from the analysis were, as before, maximum total deformations and safety factor. Values obtained are shown in Table 4.6.

- **Results**

In total, six different design points have been defined, and the maximum total deformation and values of SF_{TW} for all DPs were as follows:

Table 4.6 Deformations and values of SF_{TW} for different orientation angles and stacking sequences

Design Point	Ply angles	Maximum total deformation (mm)	SF_{TW}
1	$[0/+45/-45/90/0]_s$	17.90	4.08
2	$[0/+30/90/-45/0]_s$	17.96	3.92
3	$[0/+60/90/-60/0]_s$	18.75	3.37
4	$[0/+30/90/-30/0]_s$	18.03	3.85
5	$[0/+30/90/+30/0]_s$	18.09	3.81
6	$[0/+45/90/-45/0]_s$	17.85	4.15

From results presented on table 4.6, it can be seen that **maximum total deformation of the tail boom structure is not influenced by considered orientation angles and considered stacking sequences changes** since their values change negligibly (maximum difference is about 4%). On the other hand, the safety factor changes significantly. Graph in Figure 4.19 shows variations of the safety factor through different design points. The maximum value of safety factor is 4.15 (plies orientation $[0/+45/90/-45/0]_s$), whereas the minimum value of the safety factor is 3.37 (plies orientation $[0/+60/90/-60/0]_s$) under given loads.

Thus, it is clear that lower values of the maximum total deformation were obtained for design point 4, with orientation angles and stacking sequence $[0/+60/90/-60/0]_s$, and the minimum values were obtained on design points 1, 2 and 6 with orientation angles and stacking sequences, $[0/+45/-45/90/0]_s$, $[0/+30/90/-45/0]_s$ and $[0/+45/90/-45/0]_s$.

The highest value of the safety factor was obtained for design point 6 with orientation angles and stacking sequence $[0/+45/90/-45/0]_s$. Finally, the lowest value was 3.37 obtained for design point 4, with orientation angles and stacking sequences $[0/+60/90/-60/0]_s$. Since the difference between the total deformation values for all the DPs were small, but the safety factor significantly changes between the DPs, the safety factor must be used as design criterion. It is clear that DP 6 has the highest safety factor value, so the DP 6 can be chosen as a better laminate choice in the current stage.

Thus, according to the above-mentioned results DP 6 with orientation angles $[0/+45/90/-45/0]_s$, has considered as optimum orientation angles and stacking sequence for the tail boom structure.

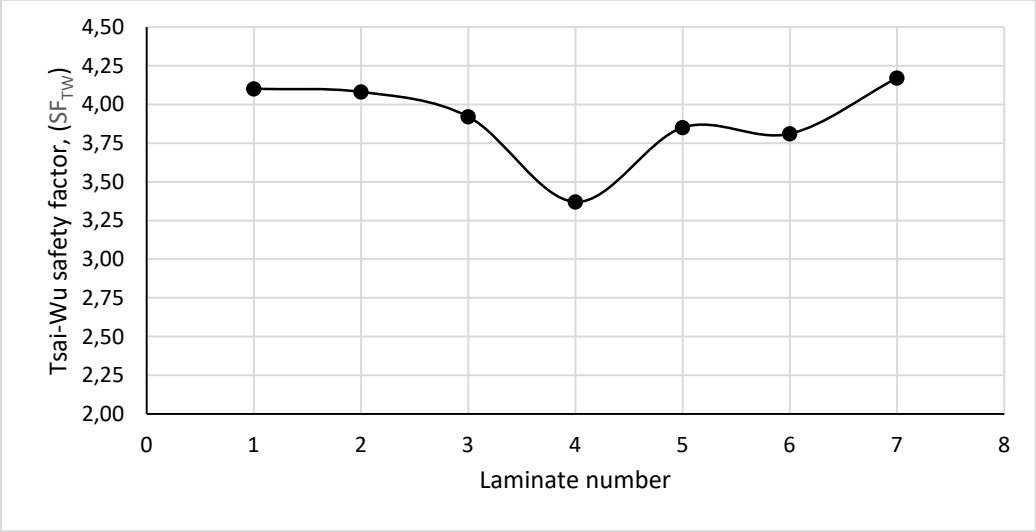

Figure 4.19 Safety factor for the different orientation angles

CHAPTER FIVE

5 Thermal stresses generated in the laminated composite structure

In laminated composite structures, during manufacturing, the sources of thermal loads include cooling down from processing temperatures. Stresses generated as a result of curing during the manufacturing process are called residual stresses. The mismatch of the coefficient of thermal expansion in different directions is the main cause of arising of residual stresses after the manufacturing process is finished. The second source of thermal loads appears to be the environment (extreme operating temperatures) resulting in the appearance of the so-called thermal stresses. To investigate possible thermal effects, the thermal stress analysis of carbon-epoxy fibre composite (CFC), subjected to different low temperatures (below 0°C) stress analysis, should be performed. This analysis can be done analytically – using CLT (Classical Lamination Theory) or numerically – using the finite element method (FEM), as the most suitable for such an analysis.

After defining the optimum laminate for the structure of tail boom, for applied aerodynamical loads, in this section, focus is on the influence of extreme operating temperatures on the strength of carbon fibre composite laminated structure, since the temperature change could reduce its strength. Aircraft starts from the ground where temperatures might be as high as 50^0C and then, in short period of time, temperatures might drop to -50 degrees at altitude of 8000 meters, for example. This is why it is necessary to check the integrity of composite structure when exposed to high temperature gradients.

5.1 Analytical and numerical modelling

In this section the FEM, besides analytical methods will use for studying the effect of external applied temperature loads on the strength of laminated carbon-epoxy fiber composite structure. The composite material laminates are modeled as a 3D continuum using FEM and first-order hexahedral elements. The material is modeled as orthotropic linear elastic and local coordinate system orientation is assigned to each element using Euler angles according to lamina orientation and element position in the model. The properties of material used in the analyses are presented in Table 5.1.

To assess the contribution of thermally induced stresses to the reduction of laminate load-carrying capacity, Tsai-Hill (TH) failure criterion, presented with Equation (2.17), is used. Out-of-plane stresses are negligible far from free edges and thus aren't considered.

1. Model validation – plate

For validating the numerical model, a simple case of an unconstrained carbon fiber-epoxy $[0/90_2]_S$ laminated plate (6 x 6 mm) is exposed to temperature of $-40℃$. Since there are no other external loads, such as external forces and moments, the plate is considered to be stress free at room temperature of $20℃$. In this case temperature change which induce thermal loads is: $\Delta T = -60℃$. The size of the numerically modeled plate is large enough so that the free-edges effects are negligible at the center of the plate Figure 5.1.

Numerically obtained thermal stresses, measured throughout the laminate thickness at the center of the plate, are in excellent agreement with the results obtained analytically (Section 2.1.5) as presented in Table 5.2. Out-of-plane stresses are negligible far from free edges and thus are not considered. Values of strength reserve (*RS*) for each lamina, calculated by using Equation (2.18), are also presented in Table 5.2.

Table 5.1 Mechanical properties of used material in the analyses (from [35])

Description	value	Units	Description	value	Units
Young's Modulus E_1	1.42E+05	MPa	Thermal expansion in direction (1) α_1	-1.8×10^{-6}	K^{-1}
Young's Modulus E_2	1.03E+04	MPa	Thermal expansion in direction (2) α_2	2.7×10^{-5}	K^{-1}
Young's Modulus E_3	1.03E+04	MPa	Thermal expansion in direction (3) α_3	2.7×10^{-5}	K^{-1}
Shear modulus G_{12}	7.67E+3	MPa	Ultimate longitudinal tensile strength (X_{1T})	1500	MPa
Shear modulus G_{23}	2.5E+3	MPa	Ultimate longitudinal compression strength (X_{1C})	1500	MPa
Shear modulus G_{31}	7.67E+3	MPa	Ultimate transverse tensile strength (Y_T)	40	MPa
Poisons ratio (v_{12})	0.27		Ultimate transverse compression strength (Y_C)	246	MPa
Poisons ratio (v_{23})	0.37		Ultimate in-plane shear strength (S)	68	MPa
Poisons ratio (v_{31})	0.37				

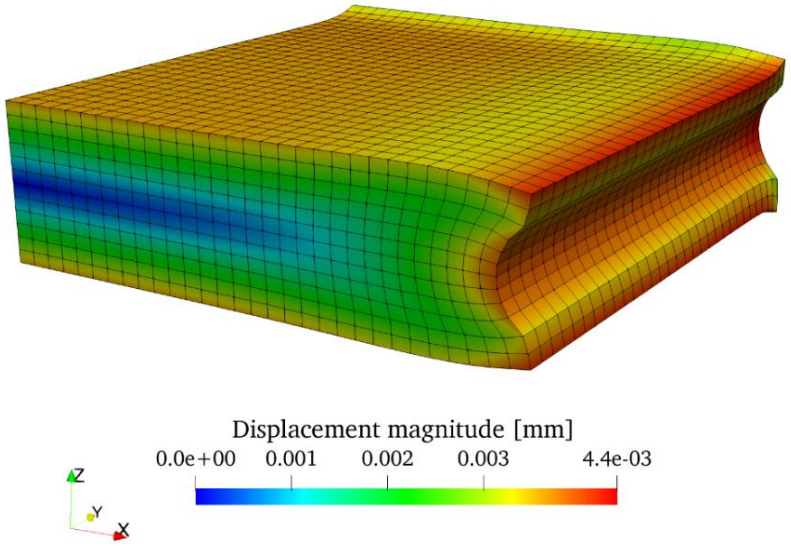

Figure 5.1: Deformed shape of thermally loaded plate (50x displacement scale factor, ¼ of the model)

Table 5.2 Stresses and values of RS of each lamina in thermally loaded plate ($\Delta T = -60$℃).

		σ_x	σ_y	τ_{xy}	RS
0° lamina	analytical	-30.250 MPa	16.313 MPa	0 MPa	0.8330
	numerical	-29.818 MPa	16.310 MPa	0 (-0.002) MPa	0.8331
	relative error	1.43%	0.02%	/	0.01%
90° lamina	analytical	15.125 MPa	-8.254 MPa	0 MPa	0.9573
	numerical	15.139 MPa	-8.206 MPa	0 (-0.006) MPa	0.9578
	relative error	-0.10%	0.58%	/	0.05%

2. Analysis of a mechanically and thermally loaded cylinder

A carbon fiber-epoxy laminated cylinder (80 mm in diameter and 80 mm long), representing a part of a more complex structure, is considered here. The laminate is symmetric $[0/+45/-45/90]_S$ and each lamina is 0.25 mm thick. Thickness $t = 0$ mm, corresponds to the inner surface, while $t = 2$ mm corresponds to the outer surface of the cylinder (Figure 5.2).

All nodes at lower end of the cylinder are fixed – Figure 5.3. At the right end, displacements along the axial direction and all relative displacements of the nodes are constrained, allowing only uniform rotation of the upper end. Two load cases are considered:

- Load case A – no mechanical loads and temperature differences $\Delta T = (0, -20, -40, -60)$ ℃;
- Load case B – torque of 2500 Nm resulting in 0.64° rotation of the upper end and temperature differences $\Delta T = (0, -20, -40, -60)$ ℃.

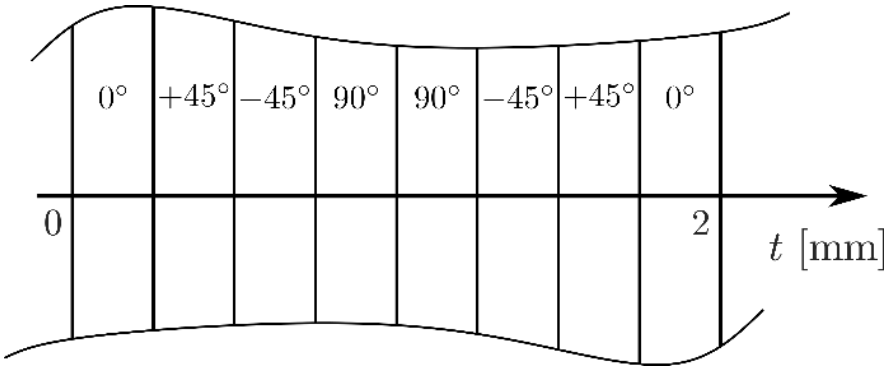

Figure 5.2: laminate orientations for the cylinder

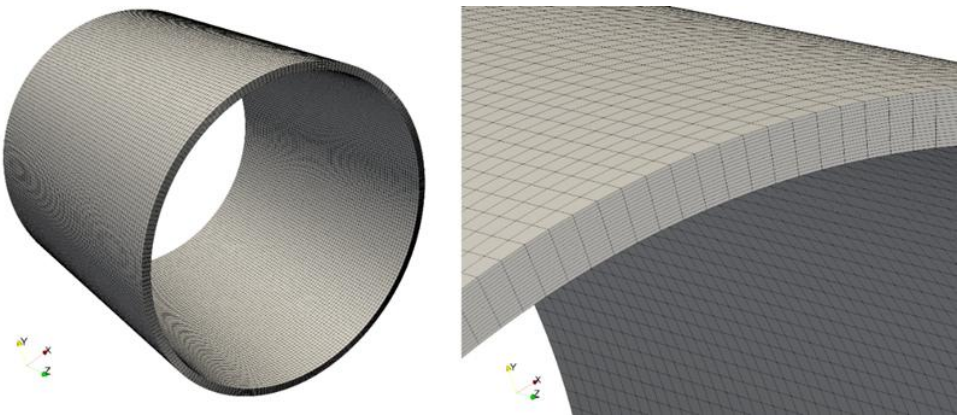

Figure 5.3: Finite element mesh for the cylinder

In load case A, it has been shown that temperature difference of $\Delta T = -60℃$ reduces the strength (load-carrying capacity) of the modeled structure by 21.3% ($+45°$ oriented inner lamina), as shown on Figure 5.4.

As it can be seen, the rise of the failure criterion value with respect to an increase in negative temperature difference is exponential.

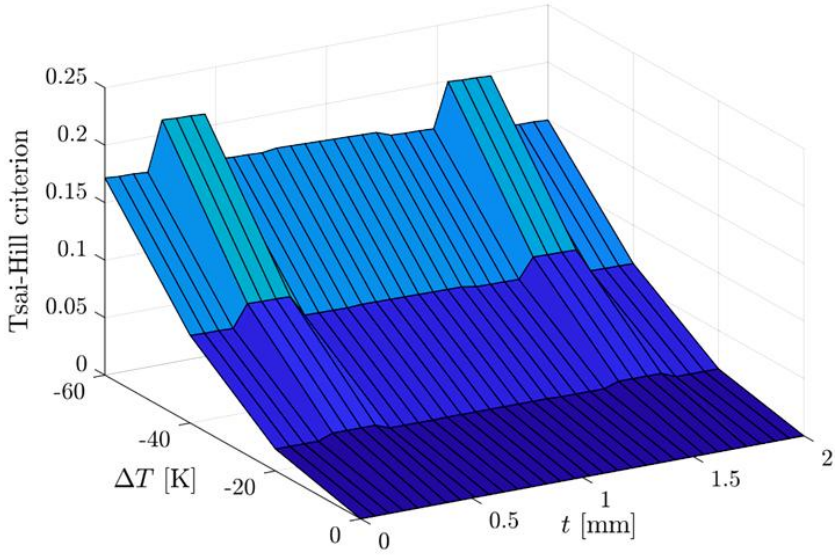

Figure 5.4: Tsai-Hill failure criterion values (load case A)

In load case B, the initial mechanical load reduces the strength by 41.4%, as shown on Figure 5.5. By including a temperature difference of $\Delta T = -60℃$, the value of *RS* is dramatically reduced from 0.5857 (state of no thermal stresses) to 0.0685 (state with thermal stresses). As shown in Figure 5.5, values of *RS* in other laminae are either not so significantly decreased or even slightly increased.

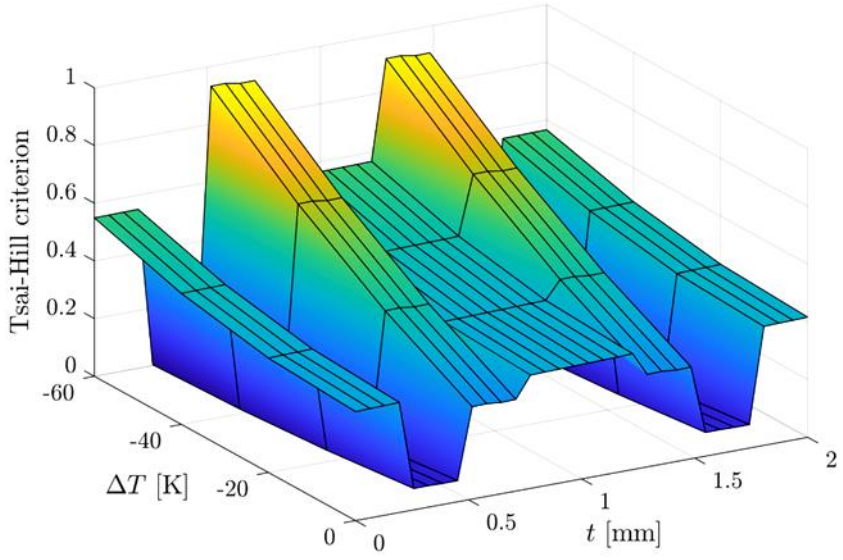

Figure 5.5: mTH failure criterion values (load case B)

Numerically obtained values of *RS* presented in Tables 5.3 and 5.4, suggest the fact that linearly added temperature loads result in a nonlinear reduction of *RS* as shown on Figures 5.4 and 5.5. That can be attributed to the complex interaction of stresses: $\sigma_1, \sigma_2,$ and τ_{12} , as well as the quadratic form of the TH failure criteria (Equations 2.17 and 2.18).

Table 5.3 Minimum *RS* values in each lamina for load case A.

	0°	+45°	-45°	90°	90_s°	-45_s°	$+45_s$°	0_s°
0°C	1	1	1	1	1	1	1	1
-20°C	0.9809	0.9764	0.9812	0.9812	0.9813	0.9820	0.9779	0.9832
-40°C	0.9238	0.9054	0.9247	0.9246	0.9253	0.9279	0.9114	0.9327
-60°C	0.8285	0.7872	0.8306	0.8304	0.8319	0.8377	0.8007	0.8486

Table 5.4 Minimum RS values in each lamina for load case B.

	0°	+45°	-45°	90°	90_s°	-45_s°	$+45_s$°	0_s°
0°C	0.6185	0.9257	0.6788	0.6037	0.5988	0.6782	0.9177	0.5857
-20°C	0.5997	0.9599	0.5129	0.5850	0.5802	0.5162	0.9528	0.5671
-40°C	0.5432	0.9836	0.3095	0.5289	0.5246	0.3183	0.9782	0.5172
-60°C	0.4491	0.9969	0.0685	0.4353	0.4319	0.0845	0.9939	0.4314

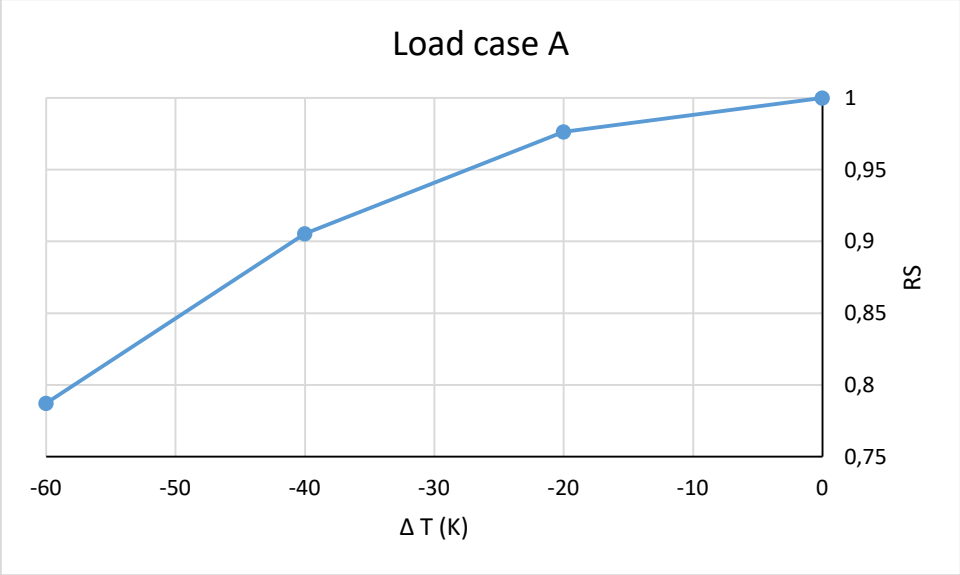

Figure 5.6 Minimum RS values in the laminate for load case A

From results presented in Table 5.4 it can be concluded that in case of further increase of temperature load, failure of -45^0 oriented inner lamina is expected to occur. This means that for considered mechanical and temperature loads "first ply failure" of laminate is expected at -45° oriented inner ply.

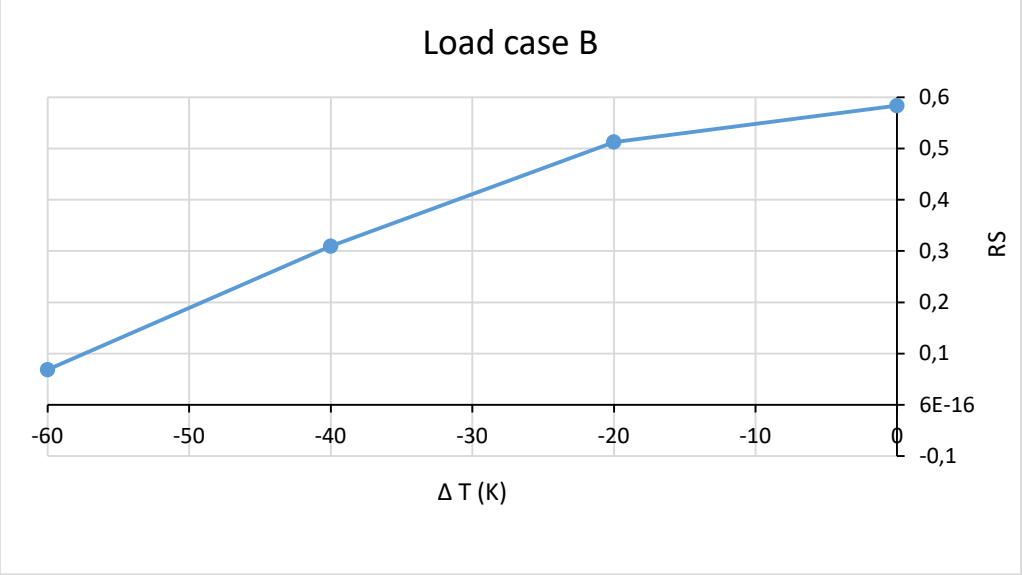

Figure 5.7 Minimum RS values in the laminate for load case B

Thus, it was shown that, compared to a structure subjected to temperature change only, the decrease of laminate strength due to thermal stresses is significantly greater in a mechanically loaded structure.

5.2 Numerical evaluation of thermal stresses generated in the tail boom structure

After obtaining the optimal laminate structural properties (Section 4.3), in the following sections a numerical approach (FEM) is used for the analysis of the tail boom structure under additional load (thermal load). For that purpose numerical finite element model of the structure has been built using the optimal laminate properties defined in Section 4.3. In order to determine strength under extreme working conditions, the tail boom structure is analyzed under applied loads and defined thermal conditions.

The FE model of the tail boom created and described earlier (Section 4) with carbon fiber-epoxy composite material of the properties presented in Table 5.5. The orientation angles of the optimum laminate layup obtained in Section 4.3 were $[0/+45/90/-45/0]_s$. The analysis has been performed under six different temperatures (+50°C, +40°C, +20°C, 0°C, -40°C, and -50°C) which assumed to be possible working temperatures for the aircraft on the ground and at the flight altitude. Thus, different changes in environmental temperature have been considered, with theoretically maximum difference of: $|\Delta T| = +20^0\mathrm{C} - (-50^0\mathrm{C}) = 70^0\mathrm{C}$ .The other applied loads were as presented in Table 3.4.

1. Numerical modelling

In the numerical modelling of the tail boom, composite material laminates have been modelled as a 3D continuum using FEM and first-order hexahedral elements. The material is modelled as orthotropic linear elastic and local coordinate system orientation is assigned to each element using the orientation angles sets according to the optimum laminate configuration. The properties of the material used in the analyses are presented in Table 5.5.

Table 5.5 The Mechanical properties of the carbon fiber composite material

Description	value	Units	Description	value	Units
Young's Modulus E_1	1.20E+05	MPa	Thermal expansion in direction (3) α_3	$2.7\mathrm{E}-05$	K^{-1}
Young's Modulus E_2	9.94E+03	MPa	Ultimate longitudinal tensile strength (X_{1T})	2.1291E+03	MPa
Shear modulus G_{12}	3.17E+03	MPa	Ultimate longitudinal compression strength ($X_{1\mathrm{C}}$)	2.10E+03	MPa
Poisons ratio (v_{12})	0.30		Ultimate transverse tensile strength (Y_T)	7.4221E+02	MPa
Thermal expansion in direction (1) α_1	$-1.8\mathrm{E}-06$	K^{-1}	Ultimate transverse compression strength (Y_{C})	4.0611E+02	MPa
Thermal expansion in direction (2) α_2	$2.7\mathrm{E}-05$	K^{-1}	Ultimate in-plane shear strength (S)	8.00 E+01	MPa

2. Creating the tail boom structure

The FE model of the carbon fibre composite structure of the tail boom was based on the optimum laminate structure identified in Section 4.3. In Section 4.3 the mainframe structure of the tail boom has been defined for mainframe structural parts (10 plies of lamina having thickness of 0.250 mm) with orientation angles of [0/+45/90/-45/0]s. As mentioned before, mainframe structure consists of parts which are formers, vertical ribs, stringers, mainframe, and rectangular floor with thicknesses 5.00 mm, 5.00 mm, 7.50 mm, 7.50 mm, and 7.50 mm, respectively.

The optimum laminates for the outer surface (skin) for the tail boom have also been defined earlier in Section 4.3. The number of the plies was 10, lamina thickness was 0.125 mm with orientation angles of [0/+45/90/-45/0]s. The geometry model of laminated tail boom structure is shown in Figure 5.8. The model was meshed using face sizing of 4 mm, and the meshed model with 379,132 nodes is presented in Figure 5.9.

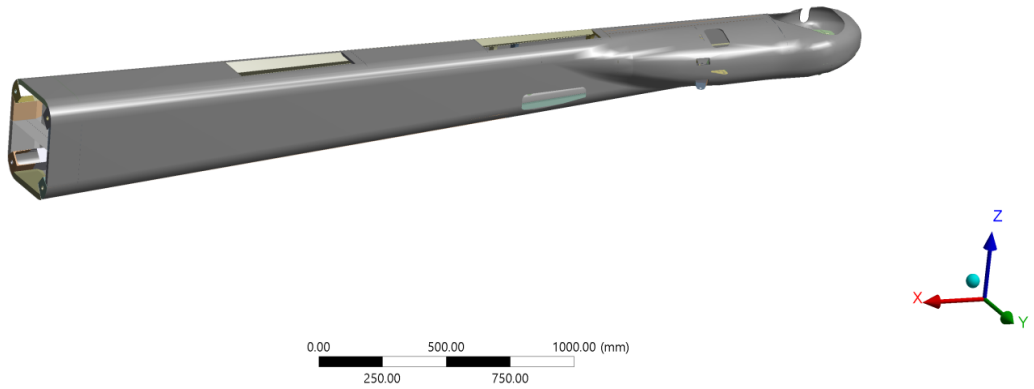

Figure 5.8: The final optimized tail boom geometry created in Ansys Workbench.

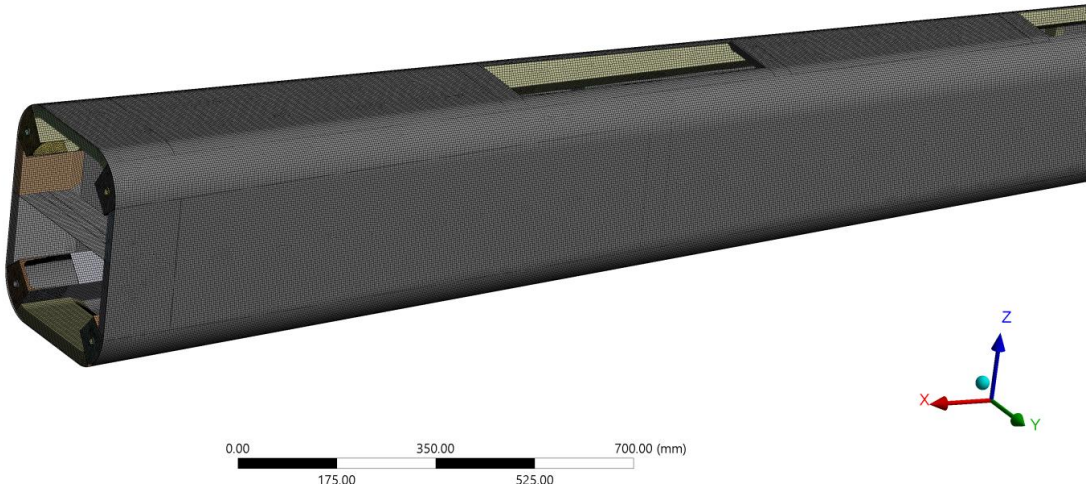

Figure 5.9: Tail boom FE model mesh (379,132 nodes).

3. Boundary conditions and loads

The boundary conditions used in this FE analysis have been defined before (see Section 3): fixed supports were applied on the connecting joints (Figure 4.10) along with aerodynamical loads on the tail boom model as presented in Table 3.4, and shown in Figure 3.2. Furthermore, six different temperatures (+50°C, +40°C, +20°C, 0°C, -40°C, and -50°C) were introduced as additional load on FE model with initial temperature set to +20°C. For estimating composite structure strength on all tail boom structure laminated parts Tsai-Wu safety factor (SF_{TW}) were used. Tsai-Wu safety factor (SF_{TW}) was calculated using Equation (2.23) – Section 2.1.4.

4. Results of numerical simulations

Obtained values of SF_{TW} of the tail boom structure when exposed to different external temperatures and aerodynamical loads are presented in Table 5.6.

Table 5.6 Tsai-Wu safety factor (SF_{TW}) of the tail boom structure when exposed to different external temperatures and aerodynamical loads.

Temperature (°C)	Tsai-Wu safety factor (SF_{TW})
+50	3.27
+40	3.54
+20	4.15
0	3.49
- 40	3.02
- 50	2.85

Results presented in Table 5.6 show that the maximum value of SF_{TW} was 4.15 (Figure 5.10) at **the reference environmental temperature +20°C**, while the minimum value was 2.85 (Figure 5.10) at the temperature -50°C. Therefore value of SF_{TW} at the temperature +20°C should be used as a reference for the analysis of the influence of temperature change.

When comparing obtained values, we can see that the difference in obtained values of SF_{TW} between the case when temperature is set to +20°C, and the case when temperature is set to -50°C is about 31%. This is indicating significant decrease due to low temperature thermal conditions.

The values of SF_{TW} obtained under different environmental temperatures are shown in the Figure 5.10. Value of SF_{TW} obtained at the maximum temperature of +50°C was 3.27 result in decrease by 22. % when compared to safety factor at the reference temperature.

Recapping the findings presented in this section the following conclusions can be drawn: safety factor values on the tail boom decreased by maximum 31.3% due to expected thermal load by exposing tail boom at $-50\ °C$, which representing reduction of its' strength by 31.3% . Furthermore, raching the safety factor value of 2.85**,** in the practice**, is theoretically reachable** only in areas of

extreme cold temperatures (Arctik circle, Syberia, etc.) since the maximum required flight altitude of this type of aircraft is 7000 m where average temperature of the air is around -30 °C.

By analysing obtained values of SF_{TW} presented in Table 5.6 it can be concluded that minimum safety value will never be lower than 3.02 (value at -40 °C) implying that safety factor will be at least $SF_{TW} = 3.02$ suggesting the structure still has good level of strength.

From the results that have been obtained, the change in the temperature significaly influences the strength of the carbon fibre composite material by increasing the thermal stresses which directly reduces the strength. This is the reason why the thermal stresses must be taken into account in the design of the carbon fibre composite structures when exposed to extreme temperatures. The safety factor value 4.15 at temperature (+20°C) obtained in this section is equal to safety factor value obtained in Section 4.2, calculated at normal environmental conditions.

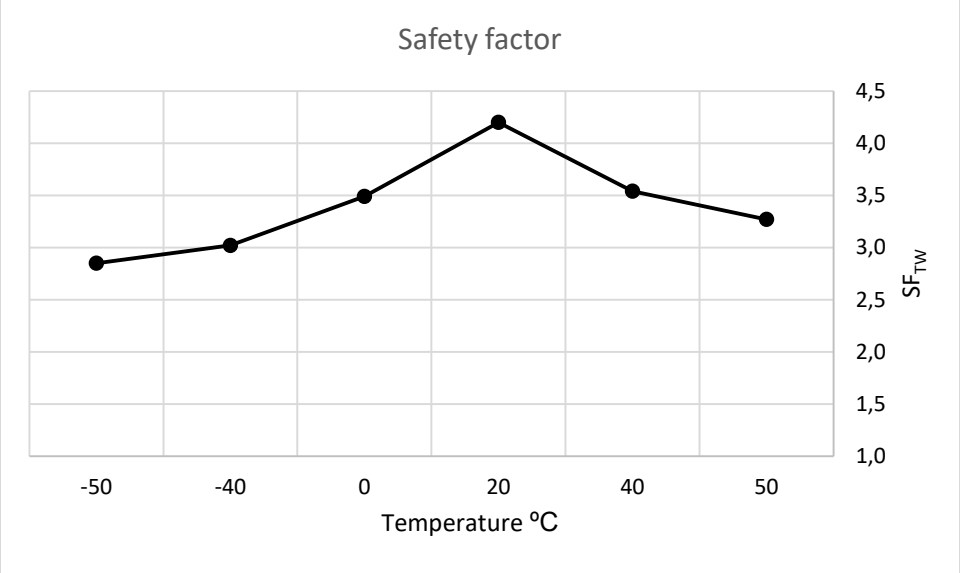

Figure 5.10 Tsai-Wu safety factor under different environmental temperatures.

CHAPTER SIX

6 Manufacturing of the Tail boom

After finishing the defining of the tail boom final structure and performing it under the applied loads and thermal conditions, the tail boom has been manufactured according to the design results which have been done in this thesis. The mechanical properties of the material used as presented in Table 2.2 the thickness of the different parts of the structure, and the stacking sequences, as shown in Table 6.1.

Table 6.1 The configuration of the different parts for the Tail boom structure

Part name	Thickness (mm)	Orientation angles
Stringers	7.50	$[0/+45/90/-45/0]_s$
Vertical ribs	5.00	$[0/+45/90/-45/0]_s$
Rectangular floor	7.50	$[0/+45/90/-45/0]_s$
Mainframe	7.50	$[0/+45/90/-45/0]_s$
Formers	5.00	$[0/+45/90/-45/0]_s$
Outer skin	1.25	$[0/+45/90/-45/0]_s$

6.1 Manufacturing methods

There are two general methods of manufacturing composites, which are open molding and closed molding. Open molding describes processes with materials being exposed to the atmosphere during the manufacturing process, whereas closed molding processes use two-sided mold sets or vacuum bags. The open molding process can be done by using Hand lay-up, Spray lay-up, and Filament winding [37]. In **Hand lay-up** method, composite layers are placed manually on a mold, and the resin is applied by pouring, brushing, or spraying. Layers are added to build laminate thickness. Disadvantages of hand lay-up method are low volume and labor-intensive. Advantages of hand lay-up method**:**

- Low tooling costs and minimum investments in equipment.
- Wide range of part sizes.
- Skilled operators allow good production rates and consistent quality.
- Complex geometry can be produced.
- Inserting holes and stiffeners are possible.
- The finished surface is moderate-good and the finished product quality is moderate.

6.2 Manufacturing steps

The tail boom structure has been manufactured by using open molding and hand lay-up methods, whereas the carbon fibre material has been used in the process as follows:

Preparing molds of the structure, as shown in Figure 6.1 and hand lay-up in the open mold method of the tail structure, as shown in Figure 6.2 and Figure 6.3, while Figure 6.4 shows the installation of the stringers and vertical rib on the tail boom structure.

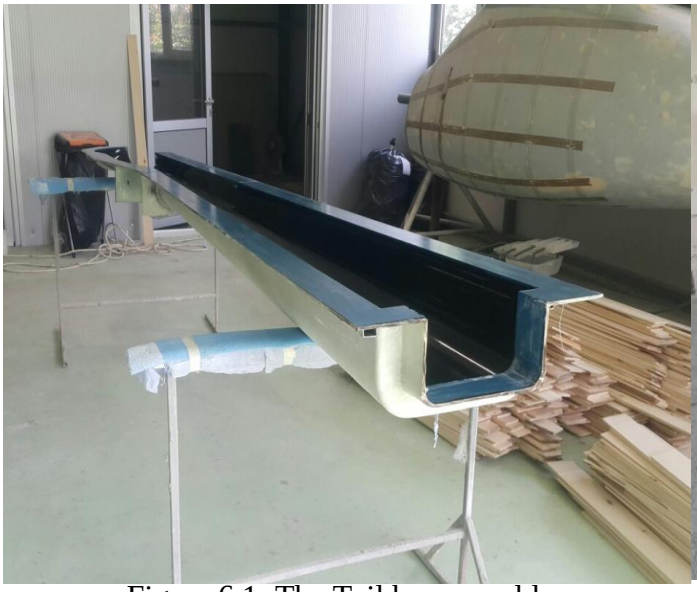

Figure 6.1: The Tail boom mold

Figure 6.2: Hand lay-up of the Tail boom structure

Figure 6.3: Hand lay-up of the carbon fiber composite material

Figure 6.4: Fixing of the stringers and vertical rib on the structure

Figure 6.5 shows the manufacturing of the upper and lower parts of the tail boom structure, while Figure 6.6 shows the placement of the tail boom structural parts; whereas Figure 6.7 shows the outer surface for the upper half of the Tail boom structure.

Figure 6.5: Manufacturing the upper and lower parts of the structure

Figure 6.6: Placement of the Tail boom structural parts

Figure 6.7: Outer shape of the Tail boom upper half

Figure 6.8 shows the outer surface shape of the two finished tail boom upper and lower halves, while Figure 6.9 shows the final tail boom assembled body.

Figure 6.8: The outer shape of the Tail boom two halves

Figure 6.9: The Tail boom structure assembly

After finishing the final stage of manufacturing and assembling processes of the Tail boom body, the final product has been attached to the aircraft thrust for flight testing, as presented in Figure 6.10.

Figure 6.10: The final assembled Tail boom body

CHAPTER SEVEN

7 Conclusions and future research

This thesis has aimed to obtain the methodology capable of optimizing composite structure of defined geometry with defined laminate layup, under given loading conditions, where the goal was to obtain the structure having high level of strength and minimal weight. Composite structure of defined geometry has chosen to be tail boom of a lightweight aircraft. In order to achieve predefined goals, tail boom of a lightweight aircraft was made of carbon fibre / epoxy composite material. Analytical and numerical methods have been used for estimating the strength and elastic constants of used carbon fibre / epoxy composite material.

The influence of porosity on material properties of carbon fibre composite material has been studied through finite element (FE) numerical analysis. The FE analysis has been applied to study the effect of micro-scale structural low-level porosity on the elastic properties of structural materials using the 3-D unit cell numerical model (UCNM).

In order to define optimal laminate layup of all structural parts of the tail boom, numerical FE model of the tail boom has been made. Coupling fluid/structure simulations have been used for the accurate prediction of the external aerodynamic loads acting on the tail boom structure. To obtain failure free laminate, the strength of each part of the tail boom structure has been checked by using the Tsai-Wu failure theory. The level of strength was estimated by pre-defined parameter, called safety factor (*SF*). An optimization procedure of the tail boom composite structure has been done through a FE modelling procedure with the following design variables: orientation angle, stacking sequence, lamina thickness, and the number of plies.

The effect of thermal load (extreme operating temperatures) on carbon fibre composite structure, which results in thermal stresses, has been studied as well. The thermal stress analysis of carbon fibre composite (CFC) structure, exposed to different levels of low and high temperatures, has been performed. This analysis has been done using the FE numerical analysis by applying different temperature ranges between (-50 and +50 °C).

7.1 Conclusions

The influence of material low-level porosity on elastic properties of the matrix, used as fiber binder in carbon fibre reinforced composite material, has been studied through numerical FE analysis. The conclusion that has been drawn is that the low-level porosity had noticeable influence on elastic properties of the composite material while the shape of porosity had a low level impact. For fixed volume fraction with changing the shape of pores, by increasing the aspect ratio (length to diameter ratio), values of E, G and ν slightly decreased. Therefore, the shape of pores had no significant influence on elastic properties. The volume fraction of porosity had a significant impact on material elastic properties. As it is evident from obtained results, with the increase in porosity content, compressive modulus significantly decreased. For example, porosity level of 10% leaded to a modulus of elasticity decrease of approximately 20%. Obtained values of compressive modulus of elasticity and shear modulus, for different values of void contents, predicted by multi-pore in the unit cell (MPUC) model were in excellent agreement with several sets of previously published experimental data presented in the literature [47].

In order to minimize the weight of the composite tail boom, without jeopardizing its' strength, analytical and numerical optimization procedures have been proposed. At the end of conducted optimization process, according to Tsai-Wu safety factor (SF_{TW}), which has been used as a key parameter in estimating structures' "reserve of strength", for different tail boom structural parts, different thicknesses have been defined. Different orientation angles and stacking sequences lead to different values of safety factors, which can be directly related to the remaining "reserve of strength". The proposed methodology showed that structure strength can be enhanced by choosing proper orientation angles and stacking sequences without increasing its weight.

The effect of temperature load on the strength of the carbon fiber composite materials has been analyzed by FEM. A carbon fiber-epoxy laminated cylinder (80 mm in diameter and 80 mm long), was examined in case when two load cases were applied: load case A – no mechanical loads and temperature differences $\Delta T = (0, -20, -40, -60)$ ℃ and load case B with a torque of 2500 Nm resulted in $0.64°$ rotation of the upper end and temperature differences $\Delta T = (0, -20, -40, -60)$ ℃. In load case A, it has been shown that temperature difference of $\Delta T = -60$℃ reduced the strength (load-carrying capacity) of the modeled cylinder by 21% while lowering the "reserve of strength" value, with respect to an increase in negative temperature difference, was exponential. In load case B, by including a temperature difference of $\Delta T = -60$℃, where the initial mechanical load reduces the strength by 41.4%, the strength reserve dramatically reduced from 0.5857 (a state of no thermal stresses) to 0.0685 (a state with thermal stresses). It has been shown that, compared to laminate subjected to temperature change only, the decrease of laminate strength due to thermal stresses is significantly greater in a mechanically loaded structure. Obtained results clearly suggested that the magnitude of thermal stresses generated at extremely low temperatures can be of the order of the mechanical ones. Extreme temperature ranges produce a considerable level of thermal stresses which can dramatically lower the strength of CFC structure. It has been shown that linear increase of mechanical or temperature load, as well as combination of them, contributed to the reduction of "reserve of strength" in a nonlinear manner. Therefore, thermal stresses must not be neglected and had to be involved in composite design regarding the strength of CFC structure.

7.2 Future research

In the current research the effect of thermal load (extreme operating temperatures) on carbon fibre composite (CFC) structure strength, has been studied by identifying two pre-defined parameters called "reserve of strength" (RS) - see Equation (2.18) and safety factor (SF_{TW}) - see Equations (2.19) – (2.23). As presented in Section 2, Equation (2.18) directly relies on Tsai-Hill failure theory. Implementation of the Tsai-Hill failure theory implies the following strengths of a single lamina as known outputs:

$(\sigma_1^T)_{ult}$ - Ultimate longitudinal (in direction along fiber axis) tensile strength,
$(\sigma_1^C)_{ult}$ - Ultimate longitudinal (in direction along fiber axis) compression strength,
$(\sigma_2^T)_{ult}$ - Ultimate transverse (in direction normal to fiber axis) tensile strength,
$(\sigma_2^C)_{ult}$ - Ultimate transverse (in direction normal to fiber axis) compression strength,
$(\tau_{12})_{ult}$ - Ultimate in-plane shear strength (in plane1-2).

Quoted strengths are usually obtained as a result of conducted experiments. Standard procedures condition that these experiments must be carried out at standard room temperature. Possible future research might involve low temperature conditions for experiments used for obtaining quoted strengths.

Potential changes in values of ultimate strengths might notably influence on the value of summary positioned on the left side of inequality presented in Equation (2.18) and therefore additionally reduce obtained values of reserve of strength. Therefore, it might be interesting to analyze how ultimate strength values, experimentally obtained at extremely low or extremely high temperatures, contribute to futher reduction of strength of CFC structures.

REFERENCES:

[1] Bouvet, Christophe, 'Mechanics of Aeronautical Composite Materials', first published by ISTE Ltd and John Wiley & Sons, Inc., 2017.

[2] M. Mehdikhani, L. Gorbatikh, I. Verpoest, and S. V. Lomov, 'Voids in Fiber-reinforced Polymer Composites: A Review on their Formation, Characteristics, and Effects on Mechanical Performance', Journal: Composite Materials, pages 1-91, 2018.

[3] X. Liu and F. Chen, 'A Review of Void formation and its Effects on the Mechanical Performance of Carbon Fiber Reinforced Plastic', Journal: Engineering Transactions, Volume 64, Issue1, pages 33–51, 2016.

[4] T. S. Mesogitis, A. A. Skordos, and A. C. Long, 'Uncertainty in the Manufacturing of Fibrous Thermosetting Composites: A review', Journal: Applied Sciences, Manufacturing and Materials, Volume 57, pages 67–75, 2014.

[5] M. de Almeida, M. Cerqueira, and M. Leali, 'The influence of Porosity on the Interlaminar Shear Strength of Carbon / Epoxy and Carbon / Bismaleimide Fabric Laminates', Journal: Composites Science and Technology, Volume 61, pages 2101–2108, 2001.

[6] M. Mehdikhani, L. Gorbatikh, and S. V Lomov, 'An overview of research on Voids in Fiber-reinforced Composites from formation to Mechanical Effects', KU Leuven, Materials Engineering Department (MTM), Belgium SIM M3 program, Volume 2, pages 2-30, June 2017.

[7] WWW.hexion.com, 'HEXION', 2019.

[8] **A.** Elmiladi, I. Balac, A. Grbovic, A. Sedmak, V. Petrovic. 'Numerical Evaluation of Thermal Stresses Generated in Laminated Composite Structure Operating at low Temperatures' Thermal Science, Volume 25, Issue 5 (Part B), pages 3847 – 3856, 2021.

[9] N. Chowdhury; J. Wang; W.K. Chiu and W. Yan, 'Residual Stresses Introduced to Composite Structures due to the Cure Regime: Effect of Environment Temperature and Moisture', Journal: Composites, Volume 2016, pages 1-13, 2016.

[10] A. Ondurucu; M. Topcu, 'Thermal Residual Stresses in Simply Supported Thermoplastic Laminated Plates under a Parabolic Temperature Distribution', Journal: Thermoplastic Composite Materials, Volume19, Issue 2, pages 155-171, 2006.

[11] H.T. Liu; L.Z Sun, 'Effects of Thermal Residual Stresses on Effective Elastoplastic Behavior of Metal Matrix Composites', International Journal: Solids and Structures, Volume 41, Issue 8, pages 2189-2203, 2004.

[12] S.S. Kim; et al., 'Study on the Curing Process for Carbon/Epoxy Composites to Reduce Thermal Residual Stress', Journal: Composites Part A: Applied Sciences and Manufacturing, Volume 43, Issue 8, pages 1197-1202, 2012.

[13] R. P. Tomić; A. S. Sedmak; D.M. Catic; M. V. Milos and Z. Stefanovic, 'Thermal Stress Analysis of a Fiber-Epoxy Composite Material', Journal: Thermal Science, Volume 15, Issue 2, pages 559-563, 2011.

[14] H. Ghiasi, K. Fayazbakhsh, D. Pasini, and L. Lessard, 'Optimum Stacking Sequence Design of Composite Materials Part II: Variable Stiffness Design', Journal: Composite Structures, Volume 93, Issue1, pages 1-13, 2010.

[15] F.K. Benra, H. J. Dohmen, J. Pei, S. Schuster, and B. Wan, 'A Comparison of One-Way and Two-Way Coupling Methods for Numerical Analysis of Fluid-Structure Interactions', Journal: Applied Mathematics, Volume 2011, pages 1-16, 2011.

[16] R. S. Raja, 'Coupled Fluid Structure Interaction Analysis on a Cylinder Exposed to Ocean Wave Loading', Chalmers University of Technology, Ph.D. Thesis, 2012.

[17] D. E. Raveh, 'Computational-fluid-Dynamics-Based Aeroelastic Analysis and Structural Design Optimization - A Researcher's Perspective', Journal: Computer Methods in Applied Mechanics and Engineering, Volume 194, Issue 30-33 SPEC. ISS., 2005, pages 3453–3471, 2005.

[18] F. Javed, S. Javed, T. Bilal, and V. Rastogi, 'Design of multiple airfoil HAWT blade using MATLAB programming', 2016 IEEE International Conference on Renewable Energy Research and Applications, ICRERA 2016, Volume 5, pages 425-430, 2016.

[19] M. Sudheer, P. K. R, S. Somayaji, and Xx, 'Analytical and Numerical Validation of Epoxy/Glass Structural Composites for Elastic Models', American Journal: Material Science, Volume 5, Issue 3C, pages 162–168, 2015.

[20] C. H. Chen and S. Cheng, 'Mechanical Properties of Fiber Reinforced Composites', Journal: Composite Materials, Volume 1, Issue 1, pages 30-41, 2015.

[21] T. Seshaiah, K. V. K. Reddy, 'Effect of Fiber Orientation on the Mechanical Behavior of E-glass Fiber Reinforced Epoxy Composite Materials', International Journal: Mechanical and Production Engineering Research and Development, Volume 8, Issue 4, pages 379-396, 2018.

[22] J. Thomsen, "Finite Element Analysis and optimization of Automotive Composite Drive Shaft" International Journal: Engineering Trends and Technology (IJETT), Volume 5, Issue 7, pages 346-351, 2013.

[23] M. Arian Nik, K. Fayazbakhsh, D. Pasini, and L. Lessard, 'Optimization of Variable Stiffness Composites with Embedded Defects Induced by Automated Fiber Placement', Journal: Composite Structures, Volume 107, Issue1, pages 160-166, 2014.

[24] S. Setoodeh, M. M. Abdalla, and Z. Gürdal, 'Design of Variable-stiffness Laminates using Lamination Parameters', Journal: Composites part B: Engineering, Volume 37, Issue 4-5, pages 301-309, 2006.

[25] C. M. Aceves, A. A. Skordos, and M. P. F. Sutcliffe, 'Design Selection Methodology for Composite Structures', Journal: Materials and Design, Volume 29, Issue 2, pages 418-426, 2007.

[26] S. Shrivastava, P. M. Mohite, and M. D. Limaye, 'Optimal design of fighter aircraft wing panels laminates under multi-load case environment by ply-drop and ply-migrations', Journal: Composite Structures, Volume. 207, pages. 909-922, 2019.

[27] P. E. Emmanuel Nicholas, K. P. Padmanaban, and A. Sathya Sofia, 'Optimization of Dispersed Laminated Composite Plate for Maximum Safety Factor using Genetic Algorithm and Various Failure Criteria', Journal: Procedia Engineering, Volume 38, pages 1209-1217, 2012.

[28] M. Akbulut and F. O. Sonmez, 'Optimum Design of Composite Laminates for Minimum Thickness', Journal: Computers and Structures, Volume 86, Issue 21-22, pages 1974-1982, 2008.

[29] J. Bruce Ralphin Rose, G. R. Jinu, and M. Manivel, 'Partly Coupled Fluid Structure Interaction Analysis of an Aircraft Wing at Subsonic Speeds', International Journal: Mechanical and Mechatronics Engineering, Volume 14, Issue 3, pages 22-29, 2014.

[30] H. Dang, Z. Yang, and Y. Li, 'Accelerated Loosely-coupled CFD/CSD Method for Nonlinear Static Aeroelasticity Analysis', Journal: Aerospace Science and Technology, Volume 14, Issue 4, pages 250-258, 2010.

[31] C. Wood, A. J. Gil, O. Hassan, and J. Bonet, 'Partitioned Block-Gauss-Seidel Coupling for Dynamic Fluid-Structure Interaction', Journal: Computers and Structures, Volume 88, Issue 23–24, pages 1367-1382, 2010.

[32] B. Landis, A. M. Goj, and G. Périgaud, 'Development of a Two-Way Fluid Structure Coupling for Studying Power Transformers Subjected to Internal Dynamic Over-Pressures', Proceedings of the ASME 2013, Pressure Vessels and Piping Conference PVP2013, July 14-18, 2013, Paris, France, pages 1-7, 2013.

[33] R.F. Gibson, Principles of Composite Materials Mechanics, 3rd Edition., CRC Press, 2012.

[34] R.M. Jones, Mechanics of Composite Materials, Taylor&Francis,1999.

[35] K. Kaw, Mechanics of Composite Materials, 2nd Edition, Taylor and Francis Group, 2006.

[36] T. Liaghat, F. Guibault, L. Allenbach, and B. Nennemann, 'Two-Way Fluid-Structure Coupling in Vibration and Damping Analysis of an Oscillating Hydrofoil', Journal: Dynamics Vibration and Control, Volume 4A, pages 1-95, 2014.

[37] M. M. Hasan, 'Design and Performance Analysis of Small Scale Horizontal Axis Wind Turbine for Nano Grid Application', 2017.

[38] B. Burnett, 'Coupled Fluid-Structure Interaction Modeling of a Parafoil', Aerospace Engineering, Dissertations and theses , page 144, 2016.

[39] M. Higaeg, 'Optimization of Composite Horizontal Axis Wind Turbine Blade on the Basis of Fluid-Structure Interaction Analysis', Ph.D. Thesis University of Belgrade, Faculity of Mechanical Engineering, 2020.

[40] Ansys Inc., 'ANSYS FLUENT Theory Guide, V18.2', August 2017, pages 870.

[41] H. Y. Zhu, D. H. Li, D. X. Zhang, B. C. Wu, and Y. Y. Chen, 'Influence of Voids on Interlaminar Shear Strength of Carbon/Epoxy Fabric Laminates', Journal: Transactions of Nonferrous Metals Society of China (English Edition), Volume 19, Issue SUPPL. 2, pages 470-475, 2009.

[42] W. V. Liebig, C. Leopold, and K. Schulte, 'Photoelastic Study of Stresses in the Vicinity of a Unique Void in a Fibre-Reinforced Model Composite under Compression', Journal: Composites Science and Technology, Volume 84, pages 72-77, 2013.

[43] S. Filipović, N. Obradović, S. Marković, A. Đorđević, I. Balać, A. Dapčević, J. Rogan, 'Physical Properties of Sintered Alumina Doped with Different Oxides', Journal: Science of Sintering, Volume 50, pages 409-419, 2018.

[44] T. Naganuma, K. Naito, J. Kyono, and Y. Kagawa, 'Influence of Prepreg Conditions on the Void Occurrence and Tensile Properties of Woven Glass Fiber-reinforced Polyimide Composites', Journal: Composites Science and Technology, Volume 69, Issue 14, pages 2428–2433, 2009.

[45] A. Elmiladi, I. Balać, K. Čolić, A. Grbović, M. Milovancević, M. Jelić. 'Numerical Modeling of the Matrix Porosity Influence on the Elastic Properties of Sintered Materials' Journal: Science of Sintering, Volume 51, pages 153-161, 2019.

[46] I. Balac, K. Colic, M. Milovancevic, P. Uskokovic, 'Modeling of the Matrix Porosity Influence on the Elastic Properties of Particulate Biocomposites, Journal: FME Transactions', Volume 40, Issue 2, pages 81-86, 2012.

[47] L. Wang, K. K. Tseng, 'A multi-scale framework for effective elastic properties of porous materials' Journal of Material Science, Volume 38, Issue 14, pages 3019-3027, 2003.

Прилог 1.

Изјава о ауторству

Име и презиме аутора: Абдулразаг Абдалах Елмилади

Број индекса: D11/2016

Изјављујем

да је докторска дисертација под насловом

НАПОНСКА АНАЛИЗА И ОПТИМИЗАЦИЈА СЛАГАЊА ЛАМИНА КОМПОЗИТНЕ КОНСТРУКЦИЈЕ ДЕФИНИСАНЕ ГЕОМЕТРИЈЕ ЗА ЗАДАТЕ УСЛОВЕ ОПТЕРЕЋЕЊА

(STRESS ANALYSIS AND OPTIMIZATION OF LAMINATE LAYUP OF DEFINED COMPOSITE STRUCTURE GEOMETRY UNDER GIVEN LOADING CONDITIONS)

- резултат сопственог истраживачког рада;
- да дисертација у целини ни у деловима није била предложена за стицање друге дипломе према студијским програмима других високошколских установа;
- да су резултати коректно наведени и
- да нисам кршио/ла ауторска права и користио/ла интелектуалну својину других лица.

Потпис аутора

У Београду, 01.12.2021.

Прилог 2.

Изјава о истоветности штампане и електронске верзије докторског рада

Име и презиме аутора : Абдулразаг Абдалах Елмилади

Број индекса: D11/2016

Студијски програм: докторске студије

Наслов рада

НАПОНСКА АНАЛИЗА И ОПТИМИЗАЦИЈА СЛАГАЊА ЛАМИНА КОМПОЗИТНЕ КОНСТРУКЦИЈЕ ДЕФИНИСАНЕ ГЕОМЕТРИЈЕ ЗА ЗАДАТЕ УСЛОВЕ ОПТЕРЕЋЕЊА

(STRESS ANALYSIS AND OPTIMIZATION OF LAMINATE LAYUP OF DEFINED COMPOSITE STRUCTURE GEOMETRY UNDER GIVEN LOADING CONDITIONS)

Ментор : Проф. др Игор Балаћ

Изјављујем да је штампана верзија мог докторског рада истоветна електронској верзији коју сам предао/ла ради похрањена у **Дигиталном репозиторијуму Универзитета у Београду.**

Дозвољавам да се објаве моји лични подаци везани за добијање академског назива доктора наука, као што су име и презиме, година и место рођења и датум одбране рада.

Ови лични подаци могу се објавити на мрежним страницама дигиталне библиотеке, у електронском каталогу и у публикацијама Универзитета у Београду.

Потпис аутора

У Београду, 01.12.2021.

Прилог 3.

Изјава о коришћењу

Овлашћујем Универзитетску библиотеку „Светозар Марковић“ да у Дигитални репозиторијум Универзитета у Београду унесе моју докторску дисертацију под насловом:

НАПОНСКА АНАЛИЗА И ОПТИМИЗАЦИЈА СЛАГАЊА ЛАМИНА КОМПОЗИТНЕ КОНСТРУКЦИЈЕ ДЕФИНИСАНЕ ГЕОМЕТРИЈЕ ЗА ЗАДАТЕ УСЛОВЕ ОПТЕРЕЋЕЊА

STRESS ANALYSIS AND OPTIMIZATION OF LAMINATE LAYUP OF DEFINED COMPOSITE STRUCTURE GEOMETRY UNDER GIVEN LOADING CONDITIONS

која је моје ауторско дело.

Дисертацију са свим прилозима предао/ла сам у електронском формату погодном за трајно архивирање.

Моју докторску дисертацију похрањену у Дигиталном репозиторијуму Универзитета у Београду и доступну у отвореном приступу могу да користе сви који поштују одредбе садржане у одабраном типу лиценце Креативне заједнице (Creative Commons) за коју сам се одлучио/ла.

1. Ауторство (CC BY)

2. Ауторство – некомерцијално (CC BY-NC)

3. Ауторство – некомерцијално – без прерада (CC BY-NC-ND)

4. Ауторство – некомерцијално – делити под истим условима (CC BY-NC-SA)

5. Ауторство – без прерада (CC BY-ND)

6. Ауторство – делити под истим условима (CC BY-SA)

(Молимо да заокружите само једну од шест понуђених лиценци.
Кратак опис лиценци је саставни део ове изјаве).

Потпис аутора

У Београду, 01.12.2021.